"MULTI RESPONSE OPTIMIZATION OF WIRE ELECTRICAL DISCHARGE MACHINING OF NITRONIC-30 BY USING COATED WIRE MATERIAL FOR AUTOMOTIVE APPLICATION"

A Thesis Submitted to

VISVESVARAYA TECHNOLOGICAL UNIVERSITY
BELAGAVI

For the award of degree of

Doctor of Philosophy

in

Mechanical Engineering and Science

By

NILESH TANAJI MOHITE
(USN: 2BL18PME01)

Research Guide
Dr. Geetanjali V. Patil
Professor

DEPARTMENT OF MECHANICAL ENGINEERING

B.L.D.E.A's V.P. Dr. P.G. Halakatti College of Engineering and Technology
VIJAYAPUR- 586103, KARNATAKA, INDIA

2024

B.L.D.E.A's V.P. Dr. P.G. Halakatti College of Engineering and Technology
Vijayapur- 586103, Karnataka, India

Certificate

Certified that **Mr. Nilesh T. Mohite**, bearing **USN: 2BL18PME01**, a bonafide student of **B.L.D.E. A's V.P. Dr. P.G. Halakatti College of Engineering and Technology,** Vijayapur, Karnataka, India, is working on his thesis entitled **"MULTI RESPONSE OPTIMIZATION OF WIRE ELECTRICAL DISCHARGE MACHINING OF NITRONIC-30 BY USING COATED WIRE MATERIAL FOR AUTOMOTIVE APPLICATION."** To the best of my knowledge, the work described in this thesis has not been submitted for a degree elsewhere and is not a repeat of work done by others.

Dr. G.V. Patil
Research Supervisor

Dr. R.N.Jeeragal
Head of the Department

Dr. V.G.Sangam
Principal

PRINCIPAL
B.L.D.E.A's. V.P. Dr. P.G.H
College of Engg. & Tech
VIJAYAPUR.

DECLARATION

I solemnly affirm that the research work presented in this thesis is my original contribution to the field of Mechanical Enginnering. The ideas, methodologies, and findings presented herein are the result of my independent investigation and scholarly endeavors. All sources consulted during the course of this study have been duly acknowledged and referenced. I further declare that this thesis has not been previously submitted, in part or in whole, for the award of any academic degree or diploma. Additionally, it has not been concurrently submitted to any other institution for examination. I bear full responsibility for the accuracy and integrity of the content presented in this thesis.

Place: Vijayapur
Date: 25/01/2024

Nilesh T. Mohite
Research Scholar
(USN: 2BL18PME01)

ACKNOWLEDGEMENT

I seize this moment to express my sincere appreciation and profound gratitude to Dr. Geetanjali V. Patil, Professor in the Mechanical Engineering Department at BLDEA's V. P. Dr. P. G. Halakatti College of Engineering and Technology, Vijayapur. Her steadfast guidance, insightful suggestions, engaging discussions, and unwavering inspiration have been instrumental in shaping the trajectory of this research endeavor. It has truly been a privilege for me to experience numerous invaluable moments under the mentorship of this consummate professional. The culmination of the present work stands as a testament to her enthusiasm, inspiration, and heartfelt personal commitment throughout the progression of this thesis.

I am grateful to Dr. R.N.Jeergal, Associate Professor and Head, Mechanical Engineering Department, BLDEA's V. P. Dr. P. G. Halakatti College of Engineering and Technology, Vijayapur for his timely guidance, support and encouragement during the research work. I am thankful Dr. Anupama N. Kallol, Professor, Gogte Institute of technology, Belagavi, Karnataka for providing valuable suggestions concerning the research work. I am also thankful Dr. Basavaraj M. Angadi, Associate Professor, BLDEA's V. P. Dr. P. G. Halakatti College of Engineering and Technology, Vijayapur for providing valuable suggestions. I am thankful to Dr.S.J.Raykar, Professor, D.Y.Patil College of Engineering and Technology, Kolhapur, Maharashtra for providing valuable inputs, suggestions and guidance.

I am very much grateful to Mr.Vishwas Patil, Owner, Able Tools Ltd., Gokul Shirgaon, M.I.D.C., Kolhapur, Maharashtra for providing the necessary facilities and technical assistance to conduct the experimental work.

I acknowledge the services of the staff of BLDEA's V. P. Dr. P. G. Halakatti College of Engineering and Technology, Vijayapur with sincere thanks.

I express deep gratitude to my parents for their unwavering support and belief in my potential, providing a solid foundation for my journey. Special thanks to my wife, Poonam, whose enduring love and understanding have been my anchor through challenges. I am also grateful for my daughter, Manasvi, whose presence brings joy and motivation. Their collective encouragement is the driving force behind my pursuit of excellence, and I feel fortunate to have such a supportive and loving family by my side.

Finally, I am grateful to God for providing guidance and strength throughout my journey. His unwavering presence has been a source of comfort and inspiration, shaping my path with divine grace.

Nilesh Tanaji Mohite

ABSTRACT

In order to make the machining process sustainable, uninterrupted machining is crucial to minimize cutting time and energy requirements. It is essential to understand the reasons and mechanisms influencing wire failure in order to save machining time, conserve resources, and enhance sustainability. Different electrode materials perform differently due to variations in conductivity, composition, and tensile strength. Thus, a thorough comparative investigation was conducted to understand the impact of zinc-coated wire, diffused wire, and gamma-coated wire during WEDM of Nitronic-30. The investigation involved measuring the material removal rate (MRR) and surface roughness (SR) for different input parameters like pulse on time (Ton), pulse off time (Toff), peak current (IP), and servo voltage (SV). Surface morphology analysis, recast layer thickness analysis were performed to compare and comprehend the performance of wire electrode materials. The findings revealed that zinc-coated wire material was not suitable for machining due to multiple wire breakage incidents. Gamma-coated wire emerged as the ideal candidate, exhibiting a significant improvement in MRR, with 28.84% more compared to diffused wire. However, diffused wire showed promising results in terms of surface roughness. Furthermore, economic justification indicated an 18.87% cost saving with the use of gamma-coated wire. Surface morphology analysis showed minimal surface defects for diffused wire, while the defects gradually increased for zinc-coated wire and gamma-coated wire. The mathematical model developed by response surface methodology shows very good prediction of output responses. Also, the finite element thermal modeling of the process has been done by considering important aspects such as energy distribution factor, Gaussian heat distribution and latent heat of fusion to predict thermal behavior as well as material removal mechanism in WEDM process. Validation of model MRR with experimental MRR shows very good agreement.

Contents

List of Figures

List of Tables

LIST OF ABBREVIATIONS

A

Adaptive Network Based Fuzzy Inference System: ANFIS · 19

B

Back Propagation Neural Network: BPNN · 19
BOX BEHNKEN DESIGN: BBD · 50

C

CENTRAL COMPOSITE DESIGN: CCD · 49
Computational Fluid Dynamics: CFD · 20

D

Dimensional Deviation: DD · 11

F

finite element model: (FEM) · 20
Flushing Pressure: FP · 32

G

General Regression Neural Networks: GRNN · 19
Grey Relational Analysis: GRA · 24
Grey Relational Coefficient: GRC · 73
Grey Relational Grade: GRG · 69
Grey Wolf Optimization: GWO · 19

H

Heat Affected Zone: HAZ · 61

K

Kerf Width: KW · 11

M

Material Removal Rate: MRR · 24

P

Particle swarm optimization: PSO · 19
peak current: IP · 11
Pulse off time: Toff · 11
pulse on time: Ton · 11

R

Response Surface Methodology: RSM · 24
Roughness average: Ra · 35

S

scanning electron microscope: SEM · 66
Servo Voltage: SV · 11
Surface Roughness: SR · 11

T

Teaching-learning based optimization: TLBO · 19

W

Wire Electrical Discharge Machining: (WEDM) · 1
Wire Feed: WF · 11
Wire Tension: WT · 11
Wire Wear Rate: WWR · 11
work coordinate system: WCS · 37

Chapter 1 INTRODUCTION

1.1 INTRODUCTION OF WEDM PROCESS

WEDM is an essential machining technique for producing intricate shaped parts from hard materials. The demand for high-speed cutting along with high precision machining is increasing so as to improve productivity and achieve high quality machining.

The harder materials are preferred for the engineering components to increase the service life of the components. But the machining of these steels is very difficult using the conventional process. The WEDM has been successfully used for machining different types of steels, aluminium alloys, titanium alloys, shape memory alloy and nickel-based superalloys as shown in figure 1.1.

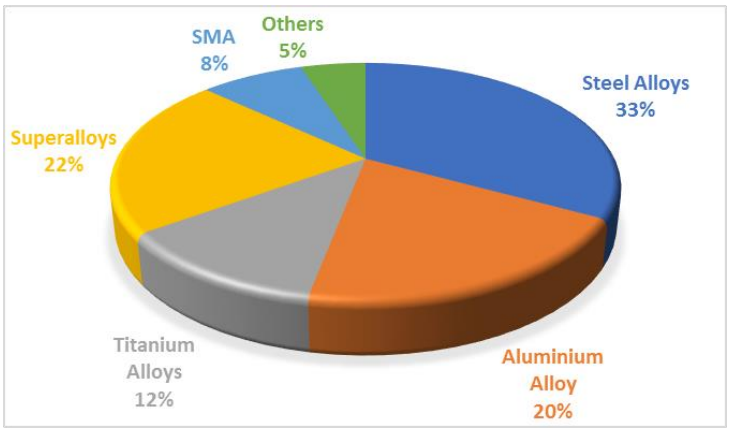

Figure 1.1 Types of materials used in WEDM process

The non-conventional machining process is introduced for processing complex parts to solve this problem. Among the non-conventional machining process, the small heat affected zone and improved accuracy of machining can be achieved using WEDM process. WEDM is widely used for machining the high corrosion resistant materials like super alloys in the automotive, aerospace, marine, and high temperature applications. (K. Natarajan et al.) [1]

In recent years both industry and academia have shown an increasing interest in the WEDM process. The development and advances of WEDM machines in the last 20 years have been impressive, and this now constitutes a key technology for advanced sectors such as the aerospace, automotive, and biomedical industries, and is also important for traditional fields such as tool and die manufacturers. Therefore,

researchers are concentrating on enhancing the quality and efficiency of machining. (J. Wang et al.) [2]

Presently, the machining of nickel-iron based super alloys has become an important area of research because of the growing demands of these materials in automotive applications.

New materials with progressively greater strengths and capacities are continuously being developed, and response characteristics depend not only on the machining parameters but also on the workpiece materials. Nitronic-30 is a Nickel Iron based super alloy. This alloy has huge potential in automotive applications. It has high strength to weight ratio therefore the cost reduction can be accomplished using lighter gauges for manufacturing. Moreover, this superalloy possesses good mechanical strength (approx. 655 Mpa), toughness, better fabricability. It also offers excellent fatigue and wear resistant as compared to other grades of steels which makes it ideal material for automotive applications. Conventional machining of Nitronic-30 superalloy exhibits poor machinability due to high temperature resistance, low thermal conductivity (25.5 W/mK), and intricate shapes of automotive components. It requires resulfurized lubricant and slow speeds during conventional machining. Furthermore, because of the tough texture of the chips, the breakers and curlers are essential.

Considering the competitive economic conditions and increase in demand for machining of advanced materials for challenging applications, WEDM is a very good option while machining these types of materials. Manufacturing of automotive parts requires enhanced dimensional accuracy and high precision. Majority of the automotive parts come with complex shape profile. Therefore, there is a scope to improve existing WDEM technology for automotive applications.

During the WEDM process, wire breakage is a dominant and time-consuming problem. Once broken; the rethreading time is a non-value-adding activity while background activities consume a considerable amount of energy. Manual rethreading time is approximately 5 minutes. This causes a waste of 1.7 kWh electrical energy which is over 23 % of total machining energy and an average 15 minutes of machining time is lost which accounts for approximately 30% of total machining time.(J. Gamage and A. Desilva) [3] For wire breakage, complex contour of workpieces, supply energy fluctuations, higher values of current and wire electrode material are very much responsible. The wire breakage is also dependent on the proper selection of input process parameter levels. The parameter levels of pulse on time (>125μs), pulse off

time (<20μs), peak current (>200A), spark gap voltage (<40V), wire feed (>4m/min) and wire tension (<8grams) are responsible for wire breakage (A. Kumar et al.) [4]. Wire electrode material is the key elements of the WEDM system. Zinc coated brass wire electrodes are used mainly as a tool for WEDM process. However, due to broad variety of applications of WEDM in manufacturing sector, the requirement for a wire electrode material superior than the conventional wire electrode is very much essential.

1.2 IMPORTANCE OF WEDM IN MANUFACTURING INDUSTRY

The WEDM technology has witnessed significant growth and development over last three decades. In 1974, D.H. Dulebohn introduced the optical-line follower system to automatically control the profile of the objects machined using WEDM. In the late 1970s, the Computer Numerical Control (CNC) system was integrated into WEDM, leading to a significant revolution of the machining process.

Because of the wide capabilities, WEDM has found applications in different industries, including production, aerospace, automotive, and almost all fields involving machining of conductive material. This is because WEDM offers the optimal or sometimes the only solution for machining conductive, high-strength, and temperature-resistant materials, enabling the machining of complex profiles and shapes. WEDM possesses significant potential in the metal cutting industry, enabling to achieve high dimensional precision, superior surface finish, and the generation of intricate contours for various products or components.

1.3 BASIC WORKING PRINCIPLE OF WIRE ELCTRICAL DISCHARGE MACHINING (WEDM) PROCESS

The WEDM machine is composed of a main worktable where the workpiece is securely fastened, along with an additional table and a wire drive mechanism. The main table is driven by the D.C servo motor along the X and Y-axis. The traveling wire is uninterruptedly supplied from a wire feed spool and wound onto a take-up spool. It remains under tension and is guided by a pair of wire guides. The lower wire guide remains stationary, while the upper wire guide, which is supported by the U-V table, can be moved transversely in coordination with the U and V axes, relative to the lower wire guide. The upper wire guide's vertical position along the Z-axis can also be adjusted by manipulating the quill.

A sequence of electrical pulses produced by the pulse generator unit is applied between the workpiece and travelling wire electrode, to cause the electro erosion of the workpiece. During the WEDM process, the X-Y controller moves the worktable carrying the workpiece in a transverse direction. The path of the traveling wire is preprogrammed in the controller. The nozzles are provided on both the sides of the workpiece which provides the deionized water in the machining region to remove the debris generated during the process. Water is used as a dielectric medium and hence it is essential that it should not ionize. If water decompose into oxygen and hydrogen gases, then it forms the gas bubbles and may affect the debris removal and can affect the overall efficiency of the process. Therefore, an ion exchange resin is used to prevent the ionization of water.

The wire electrode is tilted to produce taper cuts. To achieve this, the position of upper wire guide along the U-V axis is adjusted relative to the lower wire guide. The simultaneous control of the X-Y table and U-V table movements occurs along their predefined paths stored in the controller to achieve the desired taper angle. The NC program which consists of linear and circular motions is communicated to both the tables via a controller to perform the specified motions. Figure 1.2 shows a schematic diagram illustrating the fundamental principle of the WEDM process. Figure 1.3 provides a closer look at the WEDM cutting gap's specific details.

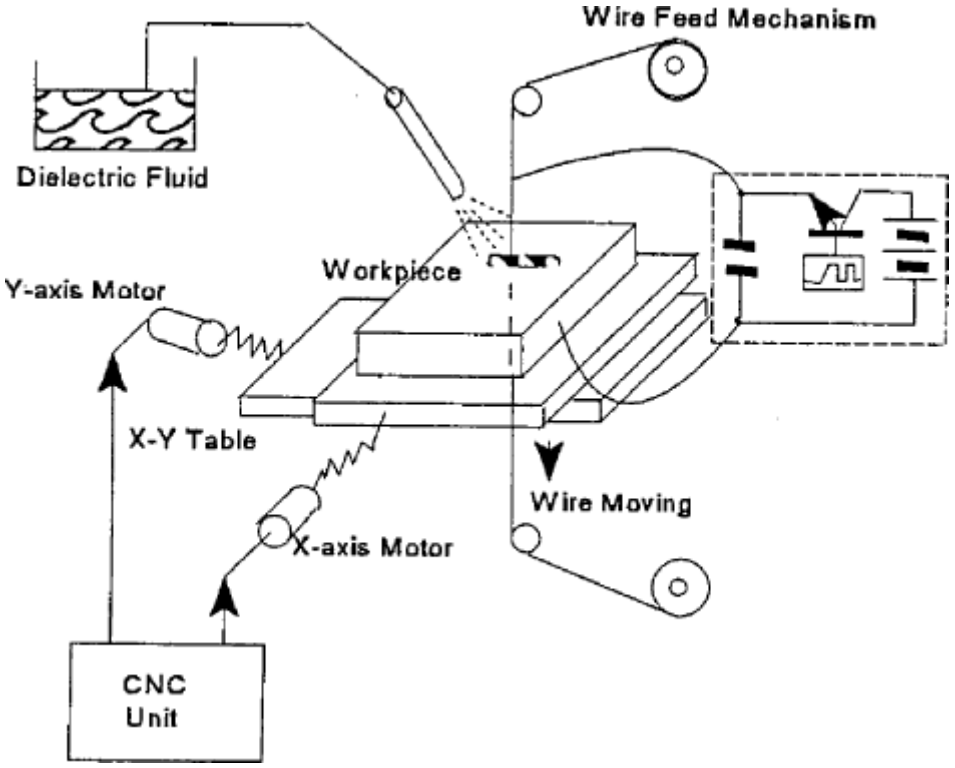

Figure 1.2 Basic Working Principle of WEDM Process (S. Saha et al.) [5]

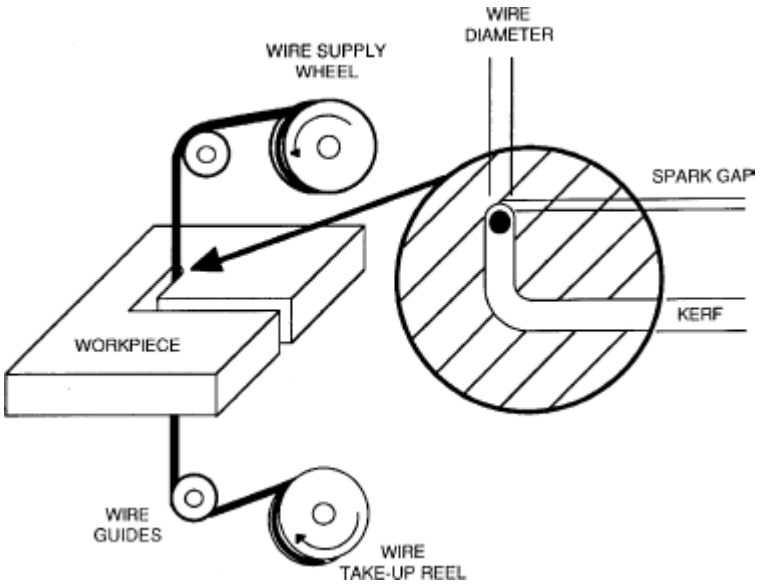

Figure 1.3 Detail of WEDM Cutting Gap (N. Tosun et al.) [6]

1.4 DEVELOPMENT OF WIRE ELECTRODE MATERIAL

The initial EDM wire was copper wire. At that time, it was expected that copper wire would be the best EDM wire due to its great electrical conductivity. However, copper wire has a low tensile strength of 234 to 413 N/mm^2. Brass wires quickly took the place of copper wire. Brass wire is an alloy which consists of Cu (63–65 %) and Zn (35– 37 %). The zinc present in the brass wire vaporizes during cutting, helps cooling of the wire and supply more energy for the work area. Zinc addition significantly increases tensile strength offsetting relative conductivity losses. Additionally, some zinc particles are present in the space between the electrode and workpiece to help in the ionization process. This leads to improved cutting rate of brass wire as compared to copper wire. Molybdenum wire is used where extremely high tensile strength is needed. Molybdenum wire is difficult to thread automatically and is extremely tough on power feeds and wire guides. Also, molybdenum wire is very costly. Coated wires were developed in an attempt to coat the wire with zinc while maintaining a drawable core material since it's not possible to manufacture a plain brass wire with an alloy fraction of greater than 40% zinc. Re-draw wire (0.9mm) is plated or hot-dipped, then drawn to the desired size to create coated wires. The zinc-coated brass wire was developed first by adding extra zinc onto the core of the wire material. This wire is made from common brass alloys used in WEDM with a thin (around 5 microns) zinc coating on top. The Zn

in the coating reduces melting point of the brass wire, this reduction in melting point increases the spark formation and also decreases ionization-time. Coating of zinc over the brass wire provides more tensile strength to wire. The higher tensile strength and uniform discharge characteristics leads to improved MRR compared to regular brass wires. (I. Maher et al.) [7]

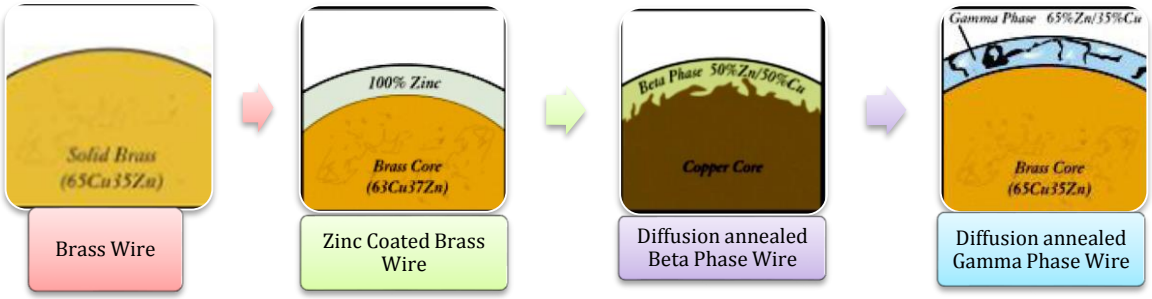

Figure 1.4 Development of Wire Electrode Material (I. Maher et al.) [7]

As zinc is having a low melting point, the high temperature discharges try to blast the zinc from the wire core. So, to achieve adequate adhesion to the wire core, the coating should have a high zinc concentration and a higher melting point.

The zinc-coated wire can be heated to achieve all these things (at 0.9 mm diameter). The name of this procedure is diffusion annealing. Diffusion will occur under the correct circumstances, at a regulated elevated temperature, and in an environment with inert gas. Atoms move through the process of diffusion from densely populated areas to less densely populated places. In this example, atoms of Copper from Brass diffuse into atoms of Zinc, whereas the Zinc atoms diffuse into the Brass. The zinc coating is changed by the diffusion process into a high-zinc alloy brass that is metallurgically bound to the core material, and is zinc rich. The diffusion annealed beta phase wire (Diffused wire here onwards) consists Zn in the range of 40 to 53%. The Gamma coated wire consists of approximately 57 to 70 % Zn in the coating. (I. Maher et al.) [7] The higher zinc content in the coating results in lowering the volumetric heat of sublimation for the coating significantly. It therefore causes the wire to flush efficiently while surviving the erosion process. With increase in Zn content, the tensile strength also increases rapidly with improves the wire's ability to resist the tension applied leading to make a vertically straight cut. The melting point of gamma phase coating is about 800 ^{0}C and for diffused wire it is approximately 825 ^{0}C which is greater than the pure zinc coating (approximately 420 ^{0}C) in zinc-coated wire. This enables the wire

electrode to operate at high levels of currents which are responsible for improved cutting rate. (I. Maher et al.) [7]

Also, as the gamma phase brass is extremely brittle; the gamma coating's thickness is usually limited to 5 microns. These thicker coatings will crack and peel off after the last drawing process. Due to its brittleness, brass in the Gamma phase completely breaks during the last drawing process, leaving a surface that is very uneven. This uneven surface provides the benefit of accelerating cutting by increasing flush as the wire passes through into the cut, increasing water flow, and eliminating waste from the gap. Contrary to other zinc-coated wires, the irregular surface has the disadvantage of being a little bit dirtier. (I. Maher et al.) [7]

1.5 ADVANTAGES OF WEDM PROCESS

1. WEDM is able to achieve extremely high accuracy of the order of ±0.025 to ±0.127mm for machined parts. (R. Rajendran and S.Vendan) [8]
2. WEDM is able to produce intricate shaped parts with tight tolerances which are challenging to produce using conventional machining processes.
3. WEDM effectively machines the variety of materials like hard metals, heat resistant alloys, superalloys which are difficult to cut using traditional processes.
4. WEDM is an automated process which improves productivity with reduced labor costs.

1.6 DISADVANTAGES OF WEDM PROCESS

1. WEDM is a slower machining process possessing volumetric material removal rate of 0.1 to 10 mm^3/min., therefore it is not suitable for mass production. (R. Rajendran and S.Vendan) [8]
2. The process is prone to wire breakage issue which interrupts the machining process and consequently leads to lowered production rate.
3. WEDM can only be applied to machine electrically conductive materials.
4. The debris generated during the machining process requires proper disposal of recycling as it’s harmful to environment.

1.7 APPLICATIONS OF WEDM PROCESS IN AUTOMOTIVE APPLICATIONS

WEDM founds the variety of applications ranging from aerospace to jewelry industry. The applications of the WEDM process includes aerospace, automotive, mold, tool, and die-making industries, optical, medical, dental, and jewelry industries.

WEDM has numerous applications in automotive industry because the capability of producing highly precise and intricate shaped components. Some of the important applications are as follows

1. **Fuel injection components:** WEDM is used to manufacture nozzles, injector body which require tight tolerance.
2. **Gear Manufacturing:** Gears with precise tooth profile are manufactured using WEDM which are the integral part of automotive transmission system, differential and engine.
3. **Engine components:** Engine components like valve seats, valve guides and cylinder head components are produced using WEDM.
4. **Fuel system parts:** WEDM is used to manufacture parts like pump components, pressure relief valves and sensor housing of fuel delivery system.
5. **Turbocharger components:** WEDM is used to manufacture the turbocharger components like turbine wheels, compressor wheels and housing.

1.8 REQUIREMENT OF MATERIAL FOR AUTOMOTIVE APPLICATIONS

The materials used in the automotive applications should possess the desired properties for a particular application. The table 1.1 gives the type of materials used for manufacturing the different automotive components.

Table 1.1 Types of materials used for different automotive applications

Automotive Application	Components	Materials
Fuel Injection Components	Injector Body [9]	Stainless steel, high-strength alloys
	Injector Nozzle [9]	Stainless steel, hardened alloys
Gear Manufacturing	Gears [10] (R. Panchal and P. Umrigar)	Alloy steel, stainless steel, carbon steel, brass/bronze
Engine Components	Cylinder Block [11] (L. Alvarez et al.)	Grey Cast iron, aluminum alloy

	Crankshaft [12] (A. Ktari et al.)	Alloy steel
	Camshaft [13] (M. Bassey et al.)	Cast iron, alloy steel, sintered metal
	Connecting Rods [14] (C. Juarez et al.)	Forged steel, aluminum alloy
Fuel System Parts	Fuel Pump Housing [15]	Aluminum or steel alloy (housing), stainless steel (internal
Turbocharger Components	Turbine Housing [16] (R. Couturier and C.	Stainless steel, Inconel
	Compressor Housing [17]	Aluminum alloys, reinforced plastics
	Turbine Wheel and Compressor Wheel [18] (S. Krawiec and L. Krawczyk)	Inconel 713c, titanium, aluminum alloys

The following table 1.2 shows the common materials used for the different applications and the important considerations while selecting the material.

Table 1.2 Important material properties

Component	**Common Materials**	**Key Considerations**
Injector Body [9]	Stainless steel	Corrosion resistance, machining properties
Injector Nozzle [9]	Heat-resistant alloys, stainless steel	High-temperature and pressure resistance, precision
Gears [10] (R. Panchal and P. Umrigar)	4130 Alloy steels with heat treatment	Strength, wear resistance, application-specific materials
Cylinder Block [11] (L. Alvarez et al.)	Grey Cast iron	Strength, thermal conductivity
Crankshaft [12] (A. Ktari et al.)	4130 Alloy steels	High strength, durability, proper heat treatment
Camshaft [13] (M. Bassey et al.)	4130 alloy steel	Wear resistance, strength
Connecting Rods [14] (C. Juarez et al.)	4340 Alloy steel	High strength, fatigue resistance
Fuel Pump housing [15]	Stainless steel	Corrosion resistance, thermal properties
Turbine Housing [16] (R. Couturier and C. Escaravage)	Inconel 713 C	Withstand high exhaust gas temperatures, Tensile strength at elevated temp.
Compressor Housing [17]	Aluminium Alloy	Corrosion resistance, thermal properties

Turbine Wheel [18] (S. Krawiec and L. Krawczyk)	Inconel 713 C	Endure extreme temperatures, Tensile strength at elevated temp.
Compressor Wheel	Inconel 713 C	Endure extreme temperatures, Tensile strength at elevated temp.

The following table 1.3 shows the comparison of Nitronic-30 properties with respect to different components with the material that is normally used. From the table 1.3, it is seen that the Nitronic-30 possesses very good properties to replace the existing materials. Therefore, it is inferred that the Nitronic-30 has a very good potential for the use in automotive applications.

Table 1.3 Comparison of Nitronic-30 properties with Existing materials

Component	**Common Materials**	**Key Considerations**		**Nitronic-30** [19]	**Unit**	**Remark**	**Potential of Nitronic-30 as a substitute**
Injector Body	Stainless steel	Corrosion resistance	0.01 [19]	**0.04**	Inches per year	**Value <0.05 is desired.**	**Yes**
Injector Nozzle	stainless steel	High-temperature resistance	72 [20]	**187**	Mpa (at 1000 ^{0}F)		**Yes**
Gears	4130 Alloy steels	wear resistance	3.8 [19]	**1.9**	(mg/1000 cycles at 25rpm)		**Yes**
Cylinder Block	Grey Cast iron	Strength thermal conductivity	450 **40** [21]	**758** 25.5	Mpa W/mk		Partially Yes
Crankshaft	4130 Alloy steels	High strength	560 [22]	**758**	Mpa		**Yes**
Camshaft	4130 alloy steel	Wear resistance	3.8 [19]	**1.9**	(mg/1000 cycles at 25rpm)		**Yes**
Connecting Rods	4340 Alloy steel	High strength	745 [23]	**758**	Mpa		**Yes**
Fuel Pump housing	Stainless steel	Corrosion resistance	0.01 [19]	**0.04**	Inches per year	**Value <0.05 is desired.**	**Yes**
Turbine Housing, Turbine Wheel, Compressor Wheel	Inconel 713 C	Tensile strength at elevated temp.	**704** [24]	187	Mpa (at 1000 ^{0}F)		No
Compressor Housing	Aluminium Alloy	Thermal Conductivity	**152**	25.5	W/mk		No

Chapter 2 LITERATURE SURVEY

2.1 REVIEW OF LITERATURE

A thorough literature review has been conducted considering different aspects such as influence of input process parameters, wire breakage issue, materials and methods used during WEDM process, and modeling and simulation.

2.1.1 Influence of input process parameters

The researchers have investigated the impact of different parameters like pulse on time (Ton), peak current (IP), Pulse off time (Toff), Servo Voltage (SV), Wire Tension (WT), Wire Feed (WF) on different quality characteristics such as MRR, Surface Roughness (SR), Dimensional Deviation (DD), Kerf Width (KW), Wire Wear Rate (WWR), corner error etc. Most of the research is focused on the effect of input parameters on MRR and SR as these are the key output requirements for industry.

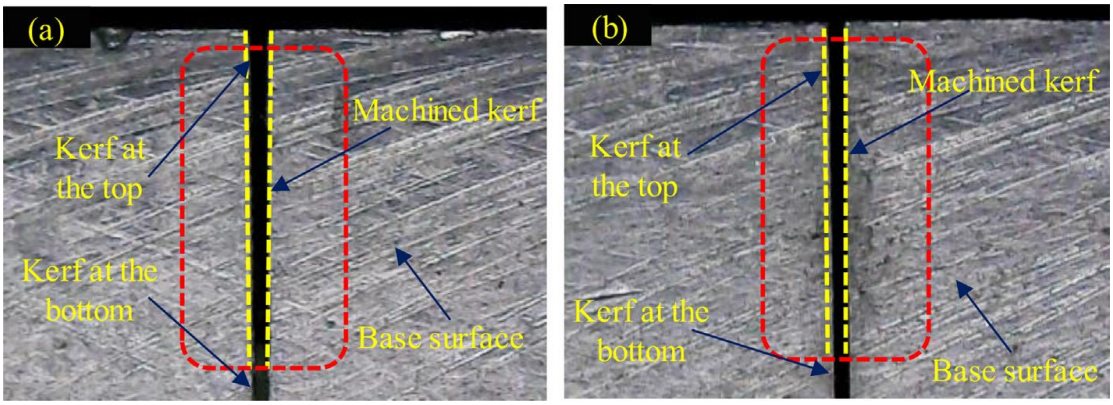

Figure 2.1 Micrograph to illustrate the machined kerf at top and bottom face. (K. Ishfaq et al.) [42]

The two most key machining process parameter that influence the quality characteristics are peak current and pulse on time. A.Yadav [25], D. Mahto and N. Singh [26], A. Kumar et al. [27], G. Lakshmikanth et al. [28], S. Kumar et al. [29], U. Dabade and S. Karidkar [30], Ashish Goyal [31], D. Kashid and S. Bhatwadekar [32], R. Chalisgaonkar and J. Kumar [33] have reported that, the material removal accelerates when pulse on time and peak current are increased because they increase the quantity of electrons that strike the workpiece surface during a single discharge, which removes extra material from the workpiece surface every discharge. U. Dabade and S. Karidkar [30], D. Kashid and S. Bhatwadekar [32] have reported that, given a constant peak

current and pulse on time, MRR falls with increased spark gap voltage and pulse off time. Long pulse-off times cause the workpiece's temperature to drop before the next spark ignites, which lowers MRR. The high peak current values produce high discharge energy which increases the MRR. As wire tension is increased, it facilitates the quick and easy removal of eroded material from the spark gap, leading to increased MRR. G. Lakshmikanth et al. [28], S. Kumar et al. [29], Ashish Goyal [31], R. Chalisgaonkar and J. Kumar [33], B. Lodhi and S. Agarwal [34], Kausar et al. [35] have observed that, when peak current and pulse on time increase, the surface roughness also increases.

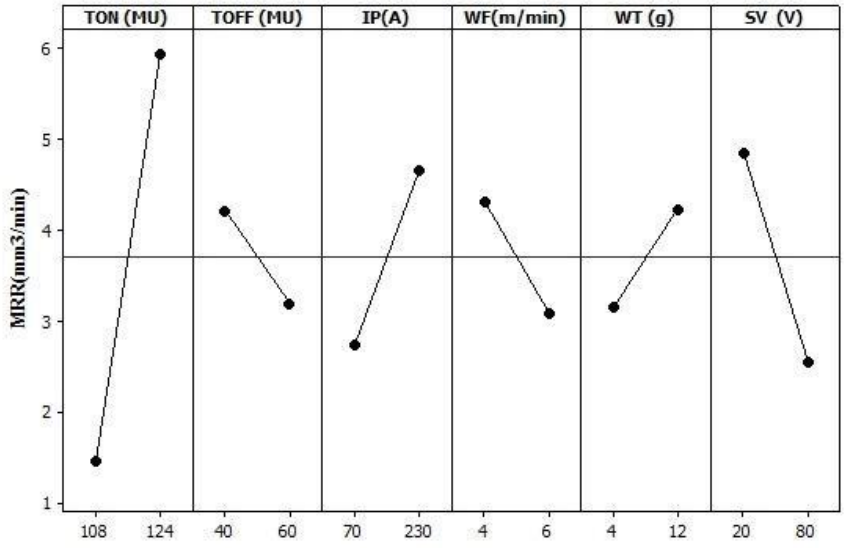

Figure 2.2 Effect of various parameters on MRR (U. Dabade and S. Karidkar) [30]

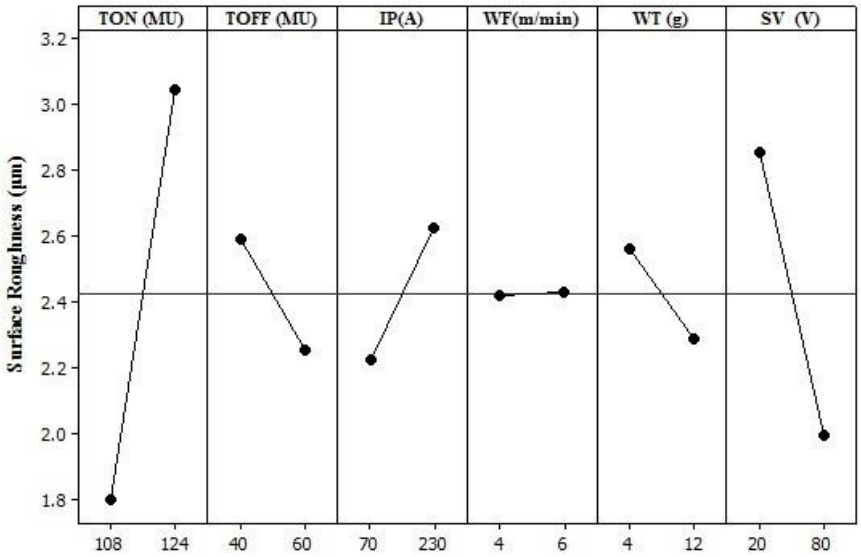

Figure 2.3 Effect of various parameters on SR (U. Dabade and S. Karidkar) [30]

A. Kumar et al. [27], S. Kumar et al. [29], J. Saedon et al. [36], S. Sherdual and S. Dahake [37], Mandal et al. [38] have found that Pulse-off time as the important machining parameter. Very few researchers like Mandal et al. [38], T. Choudhary et al. [39], K. Ishfaq et al. [40] have reported wire tension and voltage as the significant machining parameter. Few studies viz. U. Dabade and S. Karidkar [30], D. Kashid and S. Bhatwadekar [32], T. Muthuramalingam et al. [41] and Kumar et al. [4] also indicates that servo voltage, wire feed, and wire tension don't have a large influence on the MRR.

Comparatively few investigations have reported for Wire Wear Rate (WWR) and corner error or angular error. K. Ishfaq et al. [42] had reported that the corner errors values are significantly different for top and bottom face as these faces experience different discharge characteristics because of wire lag and wire vibrations.

N. Tosun and C. Cogun [43] investigated that the Wire Wear Rate (WWR) increases with increase in pulse duration and open circuit voltage whereas the increasing wire speed and pressure of dielectric fluid decrease the WWR. The high WWR is always associated with high MRR and high Ra values. K. Ishfaq et al. [42] found that the angular error at the top face is mainly affected by pulse off-time, wire tension, and flushing pressure. Whereas, for bottom surface, the angular error is largely influenced by wire feed, pulse on time, and flushing pressure. Higher magnitude of corner error for top face is noticed because of the higher magnitude of wire tension.

2.1.2 Wire Breakage

According to J. Gamage and A. Desilva [3], during the WEDM process, wire breakage is a crucial and time-consuming issue. Once a wire has been broken, rethreading is no longer beneficial, while background activities consume a lot of power. Wire breaking is largely influenced by complex workpiece forms, energy supply changes, high peak current values, and the wire electrode materials. Wire breakage has been attributed to longer machining times and poorer-quality machined surfaces. W. Dekeyser et al. [44] noticed that it is fairly typical for wire electrodes to rupture during an operation, which makes the entire process unstable and is viewed as a serious issue.

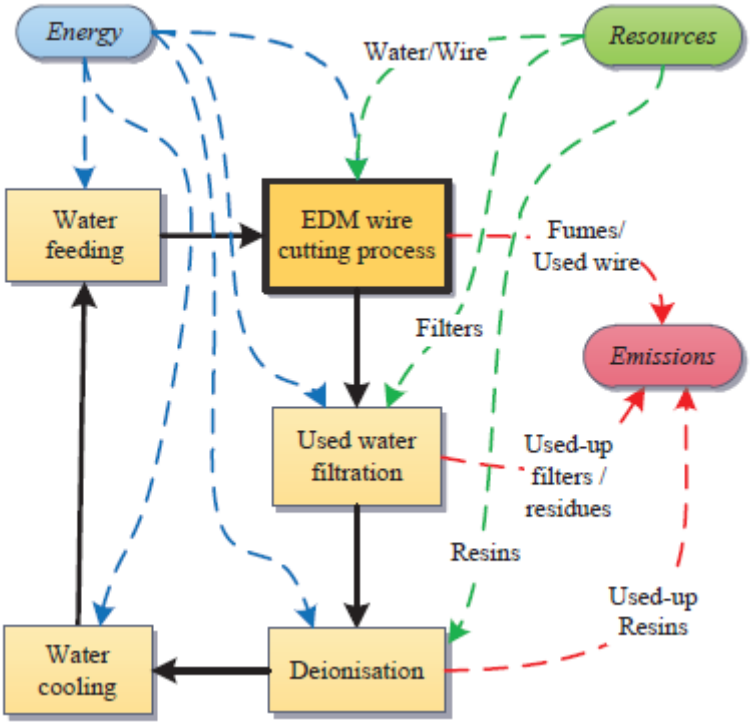

Figure 2.4 Trace of impact sources of WEDM process (J. Gamage and A. Desilva) [3]

J. Gamage and A. Desilva [3] reported that, the WEDM process uses a significant amount of thermal energy, its environmental effects are crucial. From the study of environmental impact, it was discovered that wire failure significantly increased (48%) the energy consumption. Since most of the WEDM machine's sub units continue to use energy, plenty of time and energy is wasted while rethreading the wire. The pump, water coolers and chillers used the most energy, which is depend on the machining variables and the machine tool.

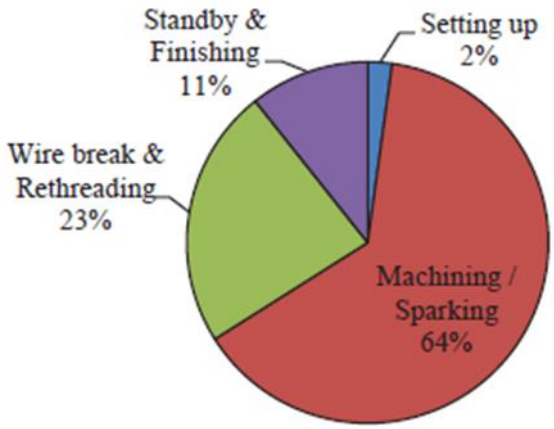

Figure 2.5 Process energy utilization during each phase of machining (J. Gamage and A. Desilva) [3]

A. Pramanik and A. Basak [45] explained the phenomenon of wire breakage in detail. They stated that wire failure issue has negative effects on sustainability and production economics since it affects the productivity and have a bigger environmental impact as well. In order to increase productivity while maintaining sustainable production in WEDM, knowledge of wire breakage/ failure issue and its prevention is crucial. The wire breakage occurs in three stages. In stage 1, the cross section of the wire starts to change from circular to oval shape where the diameter in one direction is bigger than the diameter in other direction. This is the outcome of the simultaneous effect of motion of the wire, wire tension and high temperature during WEDM process. In stage 2, the cross section of the wire remains oval in shape but the diameter of the cross section decreases. In stage 3, the sudden elongation of wire takes place as the induced stress in the wire becomes more than that of the strength of the wire which ultimately leads to the wire failure.

Also, B. Ranganath [46] found that, in the WEDM process, wire failure occurs because of severe wire wear rate, which is dependent on discharge current and discharge

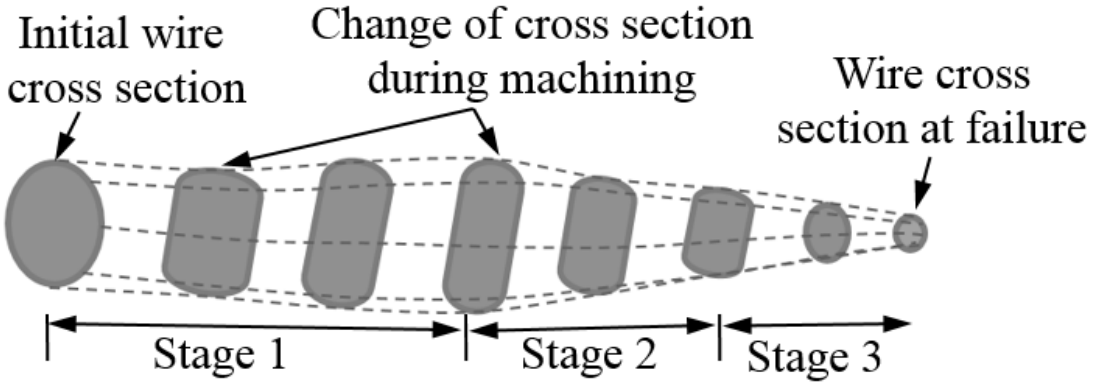

Figure 2.6 Schematic diagram of the deformation of wire electrode cross-section leading to wire failure. (A. Pramanik and A. Basak) [45]

duration. M. Selvam and P. Kumar [47] reported different observations regarding the causes of wire breakages and different parameter settings to reduce the incidences of wire breakage. Wire feed should be set to its highest setting. This will reduce wire breakage, enhance machining stability, and slightly boost cutting speed. Inadequate tension adjustment leads to wire failure and imprecise work. R. Bobbili et al. [48] found that greater voltages can be applied without bothering about wire breakage as workpiece thickness increases. This allows the energy to be distributed across a larger area when thickness is more. Wire breakage can be decreased by increasing the wire feed. Brass wire breaks very often as input energy causes an increase in its rate of wear.

S. Shahane and S. Pande [49] noted that, to avoid localized high temperatures and, consequently, wire breakage, axial speed (wire feed rate) is crucial. T. Ebisu et al. [50] reported that the wire often breaks easily while cutting corners, therefore the surface quality tends to deteriorate. The wire is experiencing explosive forces throughout the operation, electrostatic forces from the introduction of open voltage, and hydrodynamic forces from jet cleansing. After that, the wire deflects in a direction opposite to the cutting direction. Similarly, wire breakage is because of severe debris accumulation in the small machined kerf primarily brought on by discharge concentrations at the same location. To remove debris from the machined kerf, the dielectric fluid jet cleaning with nozzles is used. High flow rates may encourage significant wire vibration and deflection, which reduces shape accuracy and results in wire breakage.

J. Wang et al. [2] investigated that the local accumulation of discharges is attributed to the impossibility of effectively removing the debris generated by one or several previous discharges. This can be related to causes such as too short Toff, which prevents debris removal and wire cooling. Thus, local conductivity in a region close to the previous discharges then increases and the probability of a new discharge occurring in that region increases. The hypothesis is that, if discharge accumulation in a region is sufficiently high, the local thermal load on the wire increases resulting in the reduction of the active load bearing section of the wire. If this reduction is sufficiently high, the section of wire cannot withstand the axial force, and, consequently, ductile wire failure occurs.

D. Sudhakara and G. Prasanthi [51] also highlighted the fact that there haven't been many studies done to use coated wire electrodes and create novel electrode materials to prevent wire breaks.

2.1.3 Materials and methods used

A great deal of the work has been undertaken on various materials, including Inconel, tool steel, hybrid metal, polycrystalline diamond, and shape memory alloy, to examine the effect of cutting parameters. Different types of wires are used by the researchers for experimentation work. From the table 2.1, it is clear that most of the researchers have used brass wire and zinc coated brass wire is used by some researchers.

Table 2.1 Types of wire used by researchers

Sr.No.	Type of Wire	Name of the researcher
1	Brass Wire	J. Gamage and A. Desilva [3], D. Kashid and S. Bhatwadekar [32], Kausar et al. [35], J. Saedon et al. [36], S. Sherdual and S. Dahake [37], T. Muthuramalingam et al. [41], A. Kumar et al. [4], R. Bobbili et al. [48], K. Zakaria et al. [52], M. Selvam and P. Kumar [47], J. Saliya [53], A. Goswami and J. Kumar [54], N. Sharma et al. [55], N. Sharma et al. [56], A. Conde et al. [57], N. Sharma et al. [58], J. Liu et al. [59], M. Galindo et al. [60], Y. Zhu et al. [61], Z. Chen et al. [62], P. Singh et al. [63], T. Ebisu et al. [50], K. Mohapatra et al. [64], F. Vogeler et al. [65], O. Guven et al. [66], R. Ramakrishnan and L. Karunamoorthy [67], M. Sadeghi et al. [68], K. Manikandan et al. [69], M Singh et al. [70], H. Majumder et al. [71], T. Sibalija et al. [72], V. Sharma et al. [73], S. Wang et al. [74]
2	Zinc Coated Brass Wire	S. Kumar et al. [29], U. Dabade and S. Karidkar [30], Ashish Goyal [31], R. Chalisgaonkar and J. Kumar [33], R. Ravi et al. [75], S. Jarin et al. [76], C. Cao et al. [77], S. Karidkar and U. Dabade [78], M. Priyadarshini et al. [79], A. Mori et al. [80], P. Rao et al. [81], A. Takale and N. Chougule [82], P. Reddy et al. [83], R. Abdallah et al. [84], L. Prasad et al. [85], V. Aggarwal et al. [86]
3	Molybdenum Wire	T. Chaudhary et al. [39], C.He [87], C. Naresh et al. [88], R. Chaudhari et al. [89]
4	Tungsten Wire	T. Kamei et al. [90]
5	Copper Wire	M. Hewidy et al. [91]

Different techniques like Taguchi, ANOVA, Response Surface Methodology, desirability approach and Grey Relational Analysis are used by the researchers to analyze and optimize the response characteristics which are summarized in the following table.

Table 2.2 Techniques used by the researchers

Sr.No.	Technique used	Name of the researcher
1	Taguchi	A.Yadav [25], G. Lakshmikanth et al. [28], U. Dabade and S. Karidkar [30], Ashish Goyal [31], D. Kashid and S. Bhatwadekar [32], B. Lodhi and S. Agarwal [34], Kausar et al. [35], J. Saedon et al. [36], S. Sherdual and S. Dahake [37], A. Kumar et al. [4], K. Ishfaq et al. [42], J. Saliya [53], A. Goswami and J. Kumar [54], P. Singh et al. [63], M. Sadeghi et al. [68], M. Priyadarshini et al. [79], P. Rao et al. [81], A. Takale and N. Chougule [82], S. Datta and S. Mahapatra [92]
2	Analysis of Variance (ANOVA)	A.Yadav [25], U. Dabade and S. Karidkar [30], A. Goyal [31], D. Kashid and S. Bhatwadekar. [32], B. Lodhi and S. Agarwal [34], F. Kausar et al. [35], S. Sherdual and S. Dahake [37], K. Ishfaq et al. [42], D. Sudhakara and G. Prasanthi [51], J. Saliya [53], P. Singh et al. [63], R. Ramakrishnan and L. Karunamoorthy [67], M. Sadeghi et al. [68], M. Priyadarshini et al. [79], P. Rao et al. [81], L. Prasad et al. [85], J. Oberholzer et al. [93], K. Raju et al. [94]
3	Response Surface Methodology (RSM)	N. Sharma et al. [55], N. Sharma et al. [56], N. Sharma et al. [58], S. Wang et al. [74], R. Ravi et al. [75], M. Hewidy et al. [91], V. Shukla et al. [95]
4	Desirability approach	A. Kumar et al. [27], R. Soundararajan et al. [96]
5	Grey Relational Analysis	K. Natarajan et al. [1], S. Kumar et al. [29], J. Saedon et al. [36], T. Muthuramalingam et al. [41], A. Goswami and J. Kumar [54], A. Takale and N. Chougule [82], S. Datta and S. Mahapatra [92], Y. Kuo et al. [97], V. Kavimani et al. [98], A. Raj et al. [99]

2.1.4 Modeling & Simulation

O. Guven et al. [66], R. Ramakrishnan and L. Karunamoorthy [67], H. Majumder et al. [71], P.Reddy et al. [83], A. Goyal et al. [100] have used models like General Regression Neural Networks (GRNN) and Back Propagation Neural Network (BPNN) to establish the relationship between input parameters and performance characteristics. Both the models are capable of predicting the WEDM performance with reasonable accuracy. However, BPNN has better learning ability for the WEDM process than the GRNN model. Also, the BPNN model has better generalization ability. The average errors reported for BPNN network are less as compared to the errors obtained using GRNN networks.

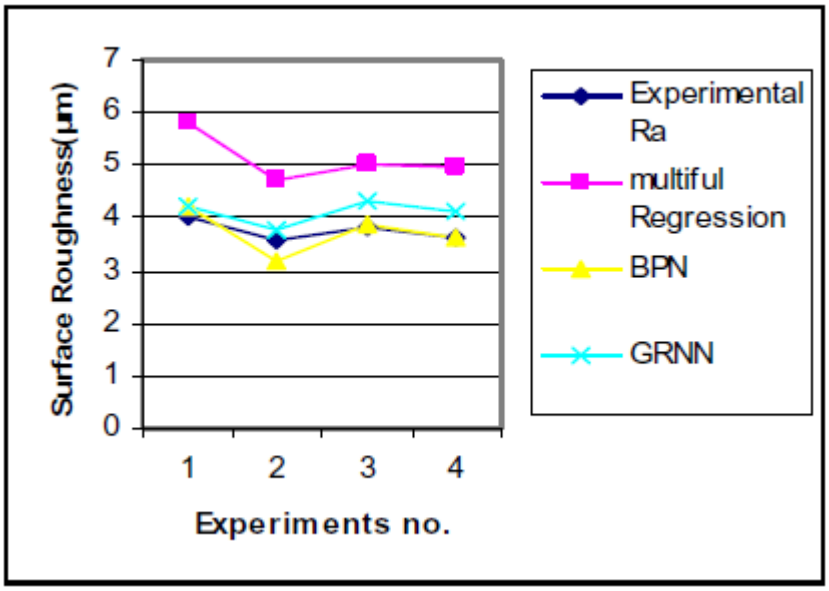

Figure 2.7 comparison between actual and predicted results for different ANN models (P. Reddy et al.) [83]

S.Kumar et al. [29], C. Naresh et al. [88] have used Adaptive Network Based Fuzzy Inference System (ANFIS) model and the findings reveals that this model delivers more precise and useful soft computing approach as compared to ANN model.

T. Sibalija et al. [72], S. Singh Nain et al. [101] used different evolutionary algorithms such as Support Vector Machines (SVM), Gaussian Process (GP), Particle swarm optimization (PSO), Teaching-learning based optimization (TLBO), Grey Wolf Optimization (GWO), Jaya algorithm, Bayesian regularized artificial neural network to find the optimal machining conditions. PSO algorithm exhibited the fastest convergence, followed by GWO and TLBO. The TLBO and Jaya algorithms are

recommended as they exhibited excellent accuracy, fast convergence (TLBO) and minimal computational time (Java algorithm), and they do not need a specific algorithm's tuning.

R. Bobbili et al. [48], M. Selvam and P. Kumar [47], N. Sharma et al. [55] used genetic Algorithm (GA), Buckingham pi theorem and Multilayer perceptron (MLP) to model and predict the output responses.

Some efforts have also taken by researchers to model and simulate WEDM process using different analysis software's like ANSYS, CFD etc. A 3-D single spark finite element thermal model was developed using ANSYS software where model MRR shows an excellent agreement with the experimental MRR with some deviation.

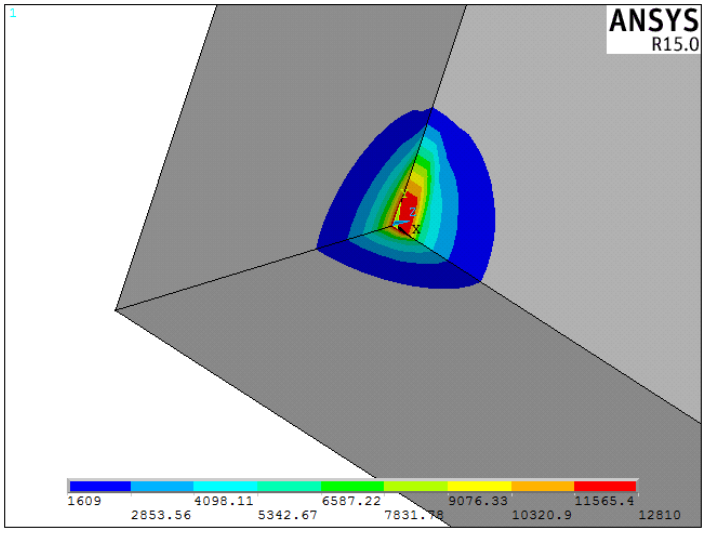

Figure 2.8 Temperature distribution profile for a single spark (S. Karidkar and U. Dabade) [78]

S. Karidkar and U. Dabade [78] developed two-dimensional model and transient thermo-physical finite element model (FEM) shows that the temperature is maximum towards the contact region of the workpiece than noncontact region. Similarly, it is also evident that the stress produced in the wire is maximum at the center. Based on Computational Fluid Dynamics (CFD) analysis, by changing the cutting direction at the corner, the pressure field and flow field around the wire also changes significantly with the use of jet flushing. (K. Mohapatra et al.) [64]

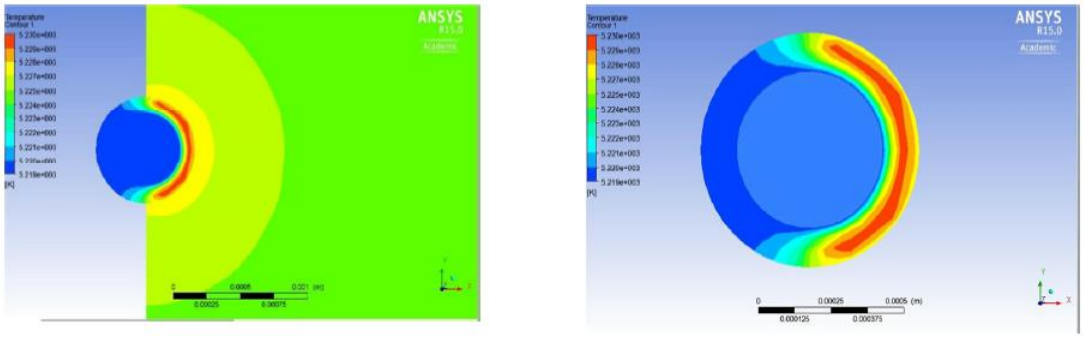

Figure 2.9 Temperature distribution of the wire for a 2D model using ANSYS Fluent (K. Mohapatra et al.) [64]

2.2 LITERATURE FINDINGS:

1. Only a small number of researchers have attempted to identify the reasons for wire breaking, their effects, and the potential solutions.
2. Different types of wire material can be used for machining on a particular material and optimum parameters can be obtained.
3. Parameters like the type of dielectric used, flushing pressure, duty cycle, and electrode material can be varied, and as a result, their effects can be studied. (A.Yadav) [25]
4. The Taguchi method is suitable for the optimization of a single performance characteristic. The GRA procedure can be employed to optimize the process performance involving number of output responses. (Y. Kuo et al.) [97]
5. Most of the researchers have used brass wire as a wire electrode material.
6. Steel, composites, titanium alloys, aluminium alloys, Inconel materials and low-grade stainless steels are employed in most studies.

2.3 LITERATURE GAPS

Following gaps were observed after a comprehensive literature study.

1. No work has been reported to choose appropriate wire electrode material to prevent wire breakage.
2. Very few researchers have investigated the use of different coated wire electrodes for improving the WEDM process performance.

3. Optimization of WEDM process parameters using Nitronic-30 material is a potential area of research.
4. No significant work has been reported to carry out machining of high grade austenitic stainless steel and nickel based super alloys.
5. To understand the economic feasibility of suitable wire electrode material, economic aspect needs to be discussed as this issue has not been highlighted by researchers.

2.4 STATEMENT OF THE PROBLEM

Wire electrode breakage during the operation is very common which makes the entire process unstable and considered as a main problem. The wire failures are not only reducing the cutting rate and gives poor quality output, but also cause increased energy consumption which is detrimental to production economics and sustainability.

2.5 OBJECTIVES OF THE RESEARCH WORK

1) To determine the parameters which affects the WEDM performance like pulse on time, peak current, pulse off time, spark gap voltage, wire tension and wire feed.

Justification: Identification of influence of input process parameters will help to select few important parameters for optimizing the WEDM performance.

2) To investigate the WEDM process performance using different wire electrode materials.

Justification: As wire electrode material comes with different compositions of wire coatings. Investigating the WEDM process performance will help to choose the appropriate electrode material.

3) To optimize the WEDM performance for the parameters affecting the process using suitable coated wire electrode material by Grey Relational Analysis (GRA) method.

Justification: The Taguchi method is only suitable for the optimization of a single performance characteristic. The GRA procedure can be employed to optimize the process performance involving number of output responses.

4) To develop a mathematical correlation between input parameters and response characteristics using Response Surface Methodology (RSM).

Justification: RSM is a mathematical and statistical technique which is effective for analysis and modeling of responses that are influenced by several variables. Also, RSM can effectively predict the output responses with reasonable accuracy.

5) To develop a thermal model for WEDM using ANSYS software to achieve more precise temperature distribution profile and the Material Removal Rate (MRR).
Justification: Developed thermal model will be able to predict the MRR which may eliminate the need of performing the experiments.

Chapter 3 EXPERIMENTATION WORK

3.1 METHODOLOGY FOLLOWED

The following flowchart represents the methodology followed to complete the research work.

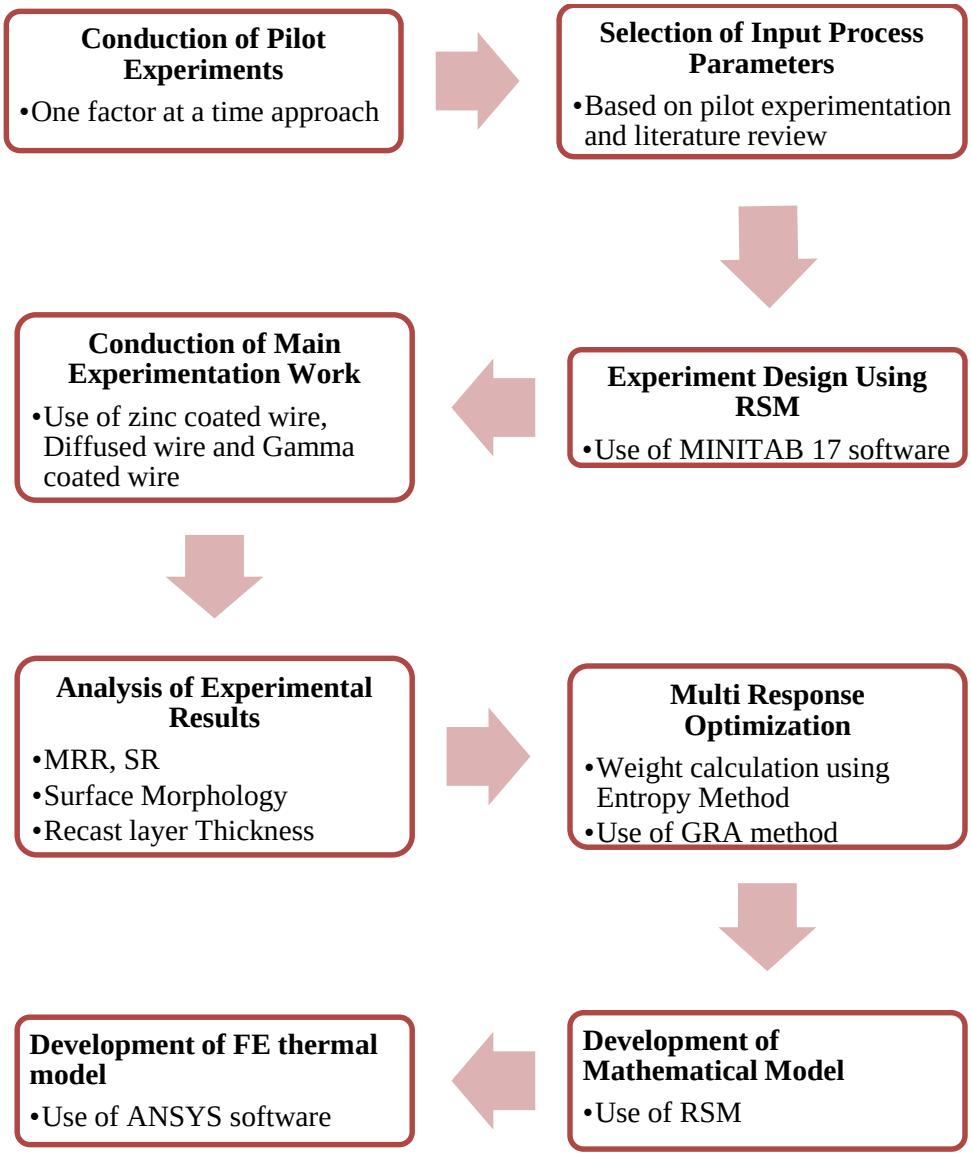

3.2 MACHINE TOOL

A WEDM machine of Electronica Machine Tools Ltd. installed at Able Tools Pvt. Ltd. Gokul Shirgaon MIDC, Kolhapur, Maharashtra, India, is used to carry out the experimental work. Below are the specifications for the machine tool.

Design	:	Fixed column, moving table
Table size	:	440 x 650 mm
Max. workpiece height	:	200 mm
Max. workpiece weight	:	500 kg
Main table traverse (X, Y)	:	300, 400 mm

Auxiliary table traverse (u, v)	:	80, 80 mm
Wire electrode diameter	:	0.25 mm (Standard) 0.15, 0.20 mm (Optional)
Generator	:	ELPULS-40 A DLX
Controlled axes	:	X Y, U, V simultaneous/independent
Interpolation	:	Linear & Circular
Least input increment	:	0.0001mm
Least command input	:	0.0005mm
Input Power supply	:	3 phase, AC 415 V, 50 Hz
Connected load	:	10 kVA
Average power consumption	:	6 to 7 kVA

3.3 WORKPIECE MATERIAL

The Nitronic-30 plate of 5 mm thickness is used as a workpiece material. Nitronic- 30 is nitrogen-strengthened stainless steel which offers higher yield strength (≅655 Mpa) than other types of stainless steel (≅505 Mpa) and, therefore, may allow lighter gauges to further reduce costs. Nitronic-30 is difficult to cut using conventional machining as it possesses high hardness. It requires the use of resulfurized lubricant and slow speeds during conventional machining. Also, breakers and curlers are necessary because of the tough texture of the chips. WEDM is a very good option while machining these types of materials.

The workpiece was procured as a rectangular plate with dimensions of 300 mm in length, 300 mm in breadth, and 5 mm in thickness. The chemical composition of Nitronic -30 is mentioned in Table 3.1. The dielectric media used was deionized water.

Table 3.1 Chemical Composition of Nitronic-30

Element	**C**	**Si**	**Mn**	**Cr**	**S**	**N**	**Ni**	**Fe**
% Composition	0.03 (max.)	0.2	15.52	15.90	0.005	0.18	2.9	Balance

3.4 MACHINE TOOL SETUP

Figure 3.1 shows the Nitronic-30 plate of 300 mm x 300 mm x 5 mm size mounted on the machine. Figure 3.2 shows the close-up view of the blank plate used for cutting and figure 3.3 shows the plate after cutting operation.

Figure 3.1 WEDM Machine Tool

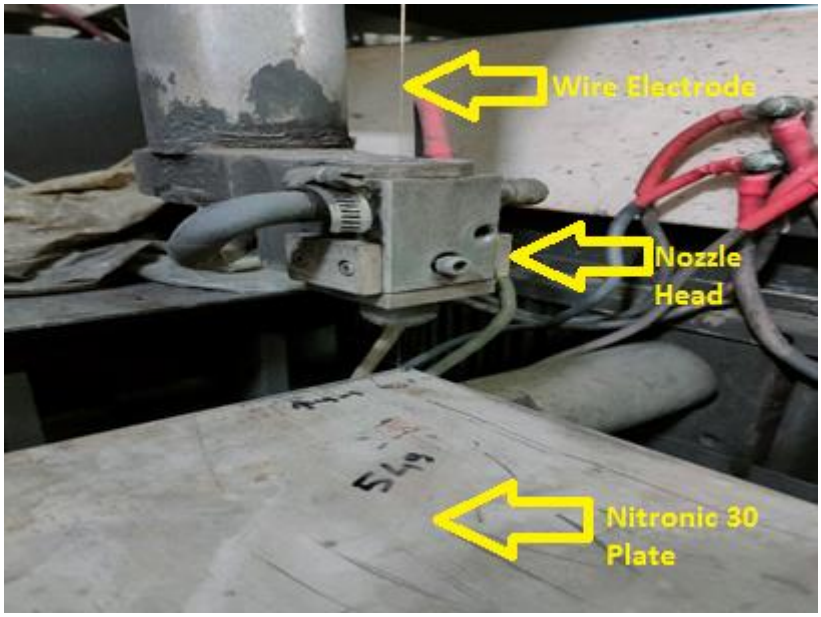

Figure 3.2 Blank Plate Mounted on WEDM Machine

Figure 3.3 Plate after cutting operation

Fig.3.4, 3.5, 3.6 shows the gamma coated wire, diffused wire and zinc-coated wire spool mounted to the machine.

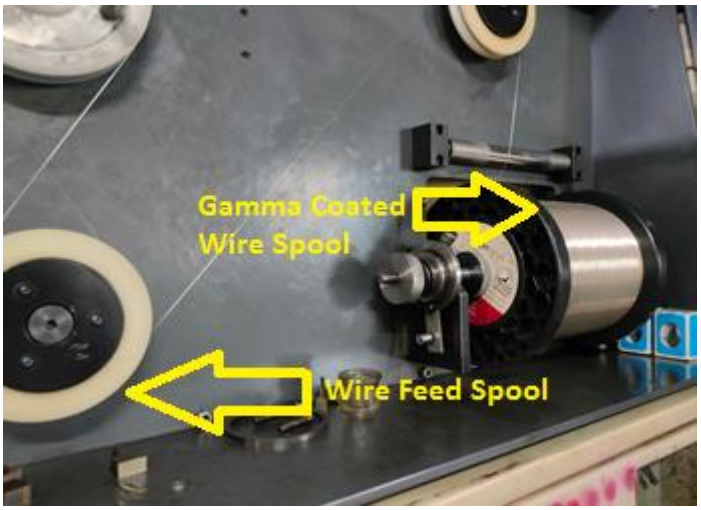

Figure 3.4 Use of Gamma coated wire

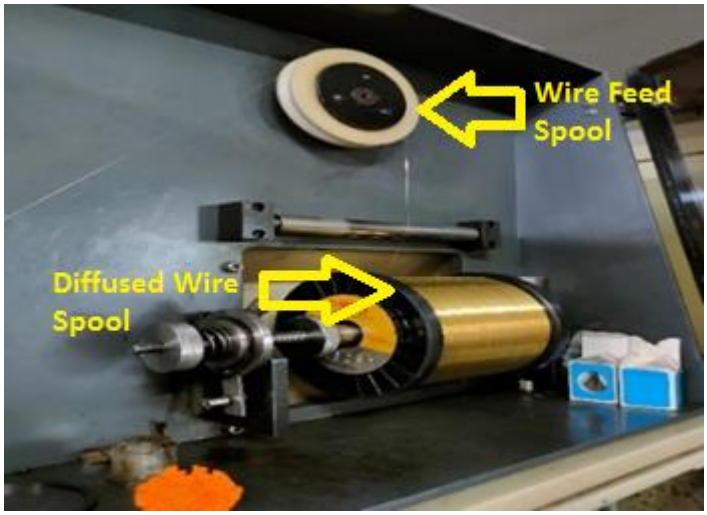

Figure 3.5 Use of Diffused wire

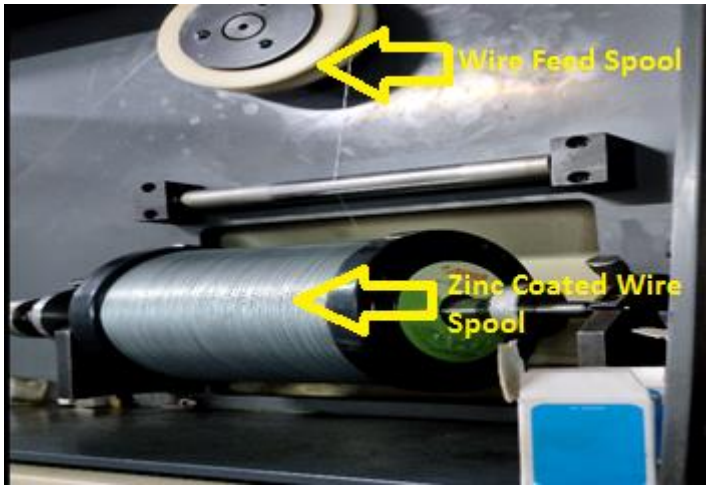

Figure 3.6 Use of Zinc-coated wire

3.5 PROCESS PARAMETER DEFINITIONS

An Ishikawa cause- effect diagram is prepared to identify the different input parameters like electrode parameters, electrical parameters, non-electrical parameters and workpiece parameters which may influence the WEDM performance characteristics and is represented in Figure 3.7.

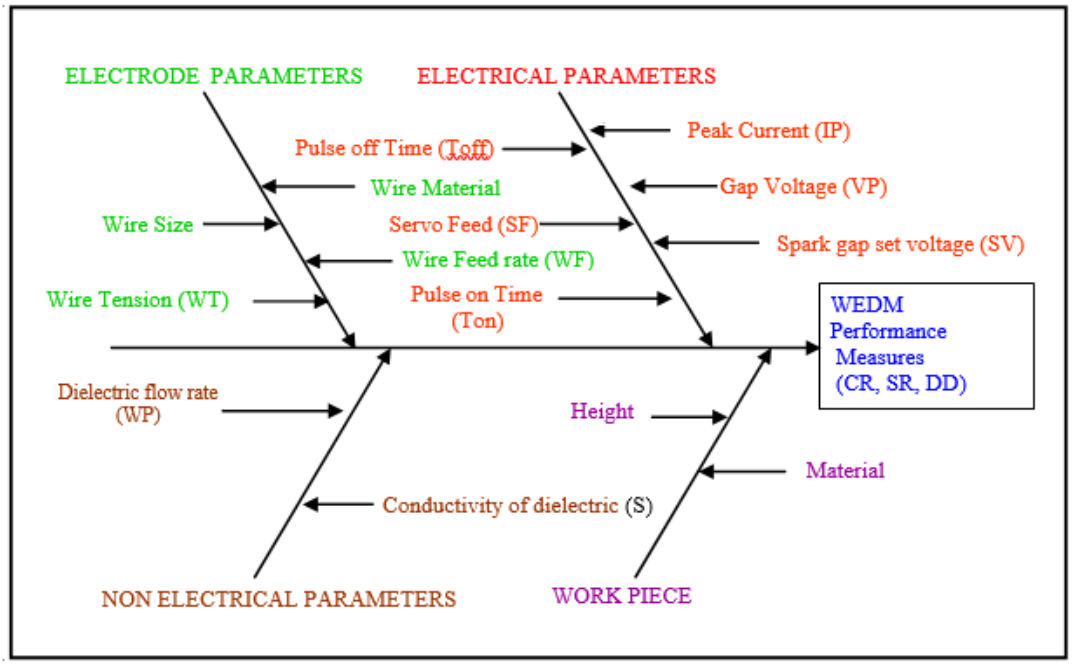

Figure 3.7 Ishikawa Cause - Effect Diagram

Figure 3.8 shows the different input process parameters and the performance characteristics for the WEDM process.

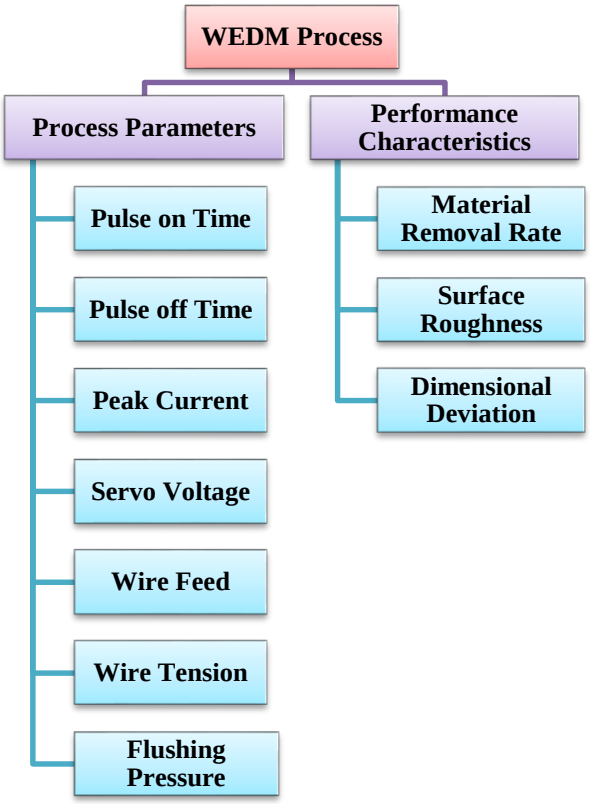

Figure 3.8 Process Parameters and Performance Characteristics of WEDM

3.5.1 Pulse on Time (Ton)

Ton represents the time duration (in microseconds) during which the current flows in each cycle. (Figure 3.9) During Ton, the voltage is applied across the positive and negative electrodes. The available range is 100-131 machine units in the increments of 1 unit. Increase in Ton period causes the discharge energy to increase which results in a higher cutting rate. However, the SR values tend to increase with higher levels of Ton. Also, the wire failure is observed at higher values of Ton where the wire material is exposed to high discharge energy as the pulse duration will be more.

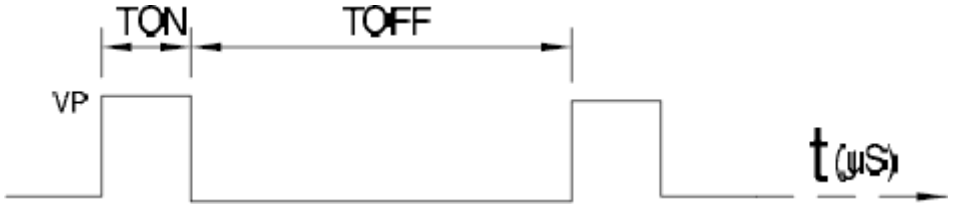

Figure 3.9 Series of Electrical Pulses

3.5.2 Pulse off Time (Toff)

Toff represents the time duration (in microseconds) between the two successive sparks. During this period, the voltage is not applied across the electrodes. The range for Toff is 00 – 63 machine units in the increments of 1 unit. With low level of Toff, there will be less gap between consecutive sparks, increasing the sparking rate ultimately which leads to improved MRR. With low Toff values, the efficient removal of the debris is not possible, also this won't provide enough time for wire to cool down. This phenomenon leads to wire failure and also reduce the MRR. Whereas, for higher levels of Toff, the gap between two successive sparks is more leading to reduction in the sparking rate which lowers the MRR. But, the efficient removal of debris from the spark gap is possible which promotes the better surface quality.

3.5.3 Peak Current (IP)

IP represents the highest value of the current passing through the electrodes for the given pulse. The setting for peak current is in the range of 10–230 ampere in the increments of 10 amperes. Higher peak current values increase the discharge energy. This leads to generation of very intense heat energy. This removes more amount of material from the workpiece material which increases the MRR.

3.5.4 Spark Gap Set Voltage (SV)

The gap between wire and the workpiece is represented by SV. As the SV increases, the spark gap between wire and workpiece increases. The SV range available is 00 - 99 volts in the step of 1volt.

3.5.5 Wire Feed (WF)

WF represents the rate at which the wire electrode travels along the wire guide path and is fed continuously for sparking. The range for WF available on the machine is 1–15 m/min in the increments of 1m/min. Wire feed should set to maximum value in order to avoid wire breakages, to provide improved machining stability and for improved cutting speed.

3.5.6 Wire Tension (WT)

WT controls the amount by which the wire electrode is kept under tension between lower and upper wire guides. For ensuring straight cutting, it's important that the wire should be fed continuously under tension between the two guides. Larger WT values are preferred while cutting jobs with higher thickness. Inappropriate setting of WT may lead to wire failure and inaccuracy in cutting. The range available for WT is 1-15 units in the increments of 1.

3.5.7 Flushing Pressure (FP)

FP represents the pressure at which the dielectric fluid flushes out the debris generated in the machining process. The setting for WP on the machine is either (High) 1 or (low) 0. FP should be set at high when cutting larger thickness workpiece with high discharge energy. Whereas, FP should be low, when cutting thin workpiece with low discharge energy.

3.6 MEASUREMENT OF RESPONSE CHARACTERISTICS

The following section explains measurement of WEDM experimental parameters e.g., Material removal rate, surface roughness, and dimensional accuracy.

3.6.1 Measurement of Material Removal Rate (MRR)

For WEDM, the MRR is an important output characteristic which should be as high as possible to reduce the machining or cutting time and improve the efficiency of WEDM process. Cutting speed is a measure of workpiece cutting that is displayed on the machine screen and is given quantitatively in mm/min. (Figure 3.10)

The term "kerf width" refers to the measurement of a cut slot formed during material removal during machining, whereas "cutting length" refers to the distance an electrode wire travels while machining a workpiece's dimensions. An optical profile projector is used to measure the kerf width. Figure 3.11 shows the optical profile projector showing the plate mounted on it. The magnified image of the kerf is visible on the screen. The kerf is aligned with the dotted line on the screen and readings are taken by setting the parameters on the digital display.

Due to poor flushing of debris, which causes varied voltage and consequently varying cutting speed, the values that were presented on the monitor somewhat deviate from a mean value. Therefore, cutting speed is computed by dividing the cutting length i.e.,40 mm by the time taken for cutting the slot. For each experiment, three measurements were taken on the machined slot, and the average of these 3 measurements is considered for calculation and analysis.

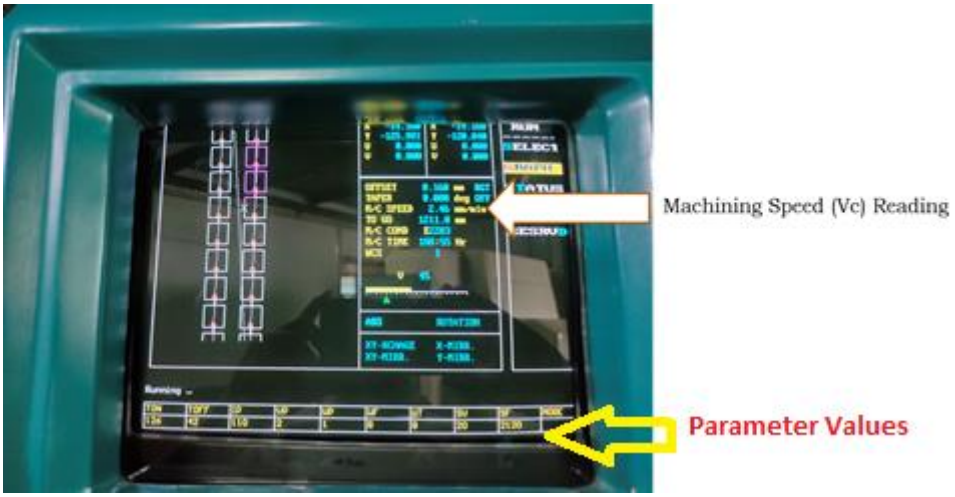

Figure 3.10 Machine Display Showing Cutting Speed Reading

Figure 3.11 shows the optical profile projector which is used to measure the kerf width and figure 3.12 shows the sample reading for kerf width.

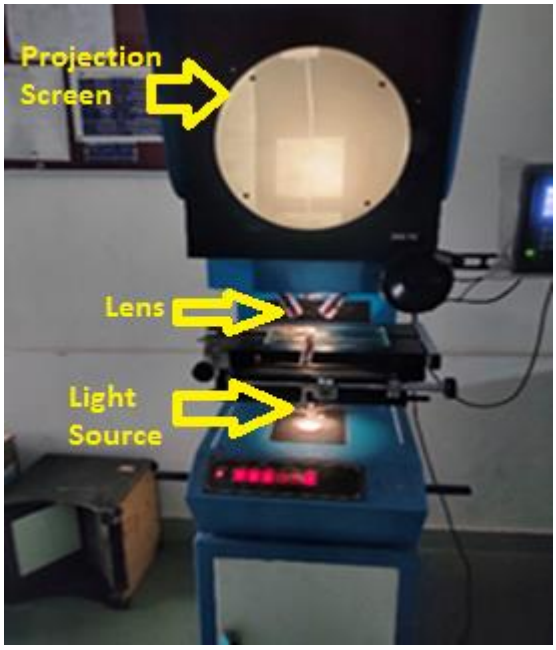

Figure 3.11 Optical Profile Projector

Figure 3.12 Kerf Width Reading

The MRR is calculated using the formula as shown below.

$$MRR = V_c * K_w * M_t \left(\frac{mm^3}{min}\right) \qquad 3.1$$

Where, V_c = m/c Speed (mm/min), K_w = Kerf width (mm), M_t = Material Thickness (mm)

3.6.2 Measurement of Surface Roughness (SR)

SR is a good evaluator for the surface quality of the mechanical component, as irregularities in the surface may lead to formation of nucleation sites for cracks or corrosion. The vertical deviations of the real surface from the ideal surface gives the readings for SR. The surface is considered to be rough if these deviations are large and smooth, if the deviations are small.

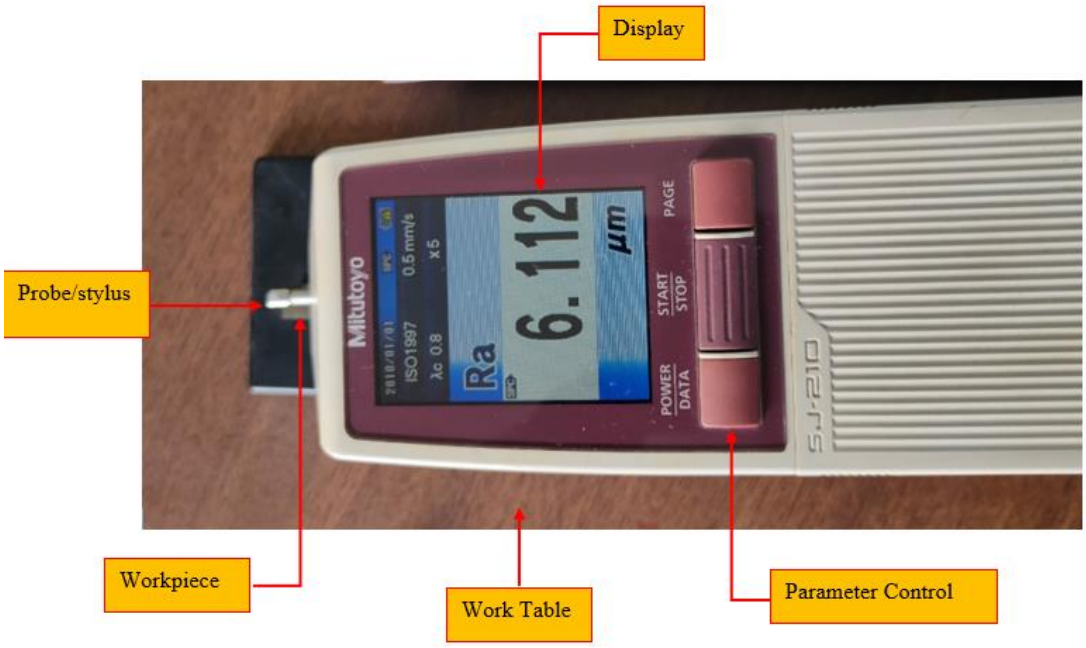

Figure 3.13 Surface Roughness Measurement Set Up

Roughness average (Ra) value is considered for measurement of surface roughness. It measures the distance of all peaks and valleys from the mean line and then averages over the cut off length. The length for which the stylus drags across the surface is called as cut off length. A longer cut off length means that there will be more number of points for measurement and will give more accurate average value, while a short cut off length gives a less accurate result over a shorter stretch of the surface.

The surface roughness tester of Mitutoyo (surftest SJ-210) is utilized for the measurement of the SR values shown in Figure 3.13. The specimen is placed such that the stylus of the detector unit just touches the surface of the specimen. When the stylus drags across the workpiece surface, the vertical displacements of the stylus are processed and displayed on the screen. The surf test has a resolution varying from .01 µm to 0.4 µm depending on the measurement range.

For each sample, 3 readings are taken on 3 different surfaces of the specimen and the average is reported for the further analysis.

3.6.3 Measurement of Dimensional Deviation:

Digital micrometer (Least count 0.001 mm) is used for the measurement of the specimen's cross section dimensions. (Figure 3.14) The dimensional deviation is calculated using the following expression.

$$\text{Dimensional Deviation } (\%) = \frac{\text{Observed Value} - \text{Actual Value}}{\text{Actual Value}} * 100 \qquad \textbf{3.2}$$

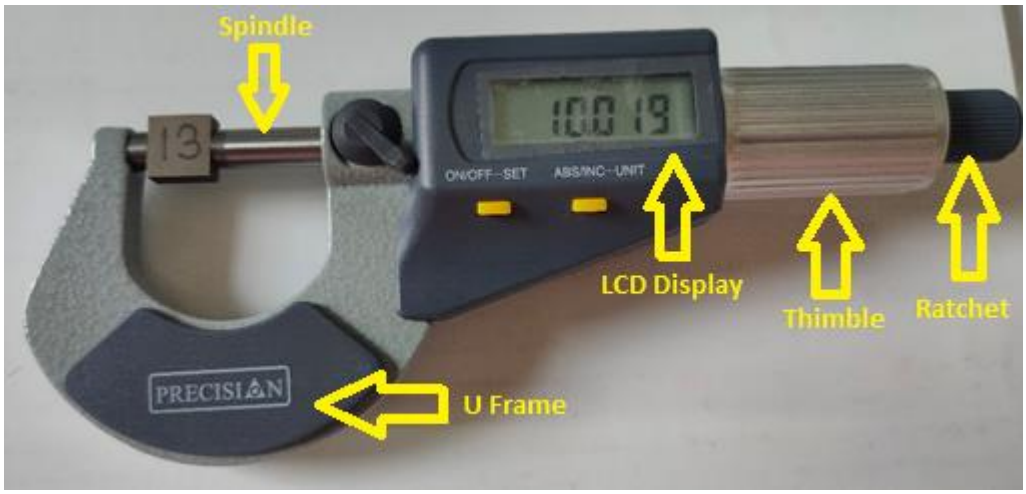

Figure 3.14 Digital Micrometer

3.7 CONDUCTION OF PILOT EXPERIMENTS

Pilot experiments are performed to examine the impact of process parameters such as pulse on time, pulse off time, peak current, servo voltage, wire feed, and wire tension on quality characteristics such as material removal rate, surface roughness and dimensional deviation. Similarly, it is necessary to ascertain the range of the input parameters for the main experimental work. One factor at a time approach is used to examine the effect of the input parameters on the quality characteristics.

During the experimentation work, following parameters were kept constant.

1.	Work Material	:	Nitronic-30
2.	Cutting Tool	:	Gamma Coated wire (0.25 mm diameter)
3.	Servo Feed	:	2120 unit
4.	Flushing Pressure	:	1 unit
5.	Dielectric Medium	:	Distilled water
6.	Workpiece Thickness	:	10 mm

3.7.1 Steps Followed During Experimentation

Electronica Supercut734 WEDM machine is employed to perform the experiments. During the experimentation process, following steps are followed

1. The workpiece is properly clamped on to the work table.
2. The wire spool is mounted on the wire spool unit.
3. The wire is then moved through the rollers of the wire spool unit and then taken out through the pair of nozzle heads.
4. A reference point on the workpiece is set for setting the work coordinate system (WCS).
5. The programming is done with the reference to the WCS.
6. The reference point is defined by the ground edges of the workpiece.
4. The program is prepared for a square profile of 10 mm in size.

The reading for cutting rate (mm/min) is noted from the machine's display screen. Mitutoyo's tester was used to get the SR values (μm). The measurements were taken on 3 different surfaces of the workpiece and average of three readings is considered for analysis. For measurement of dimensional deviation, the digital micrometer with 0.001 mm least count was used.

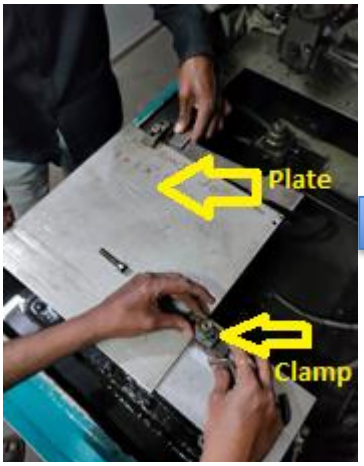

1. Mounting of Nitronic-30 plate on machine bed

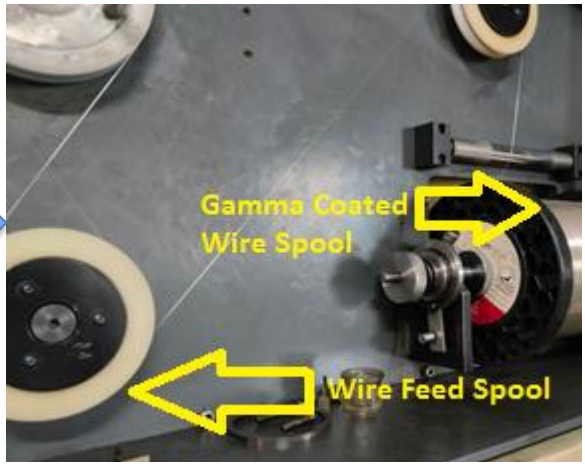

2. Mounting of Wire spool

3. Wire threading

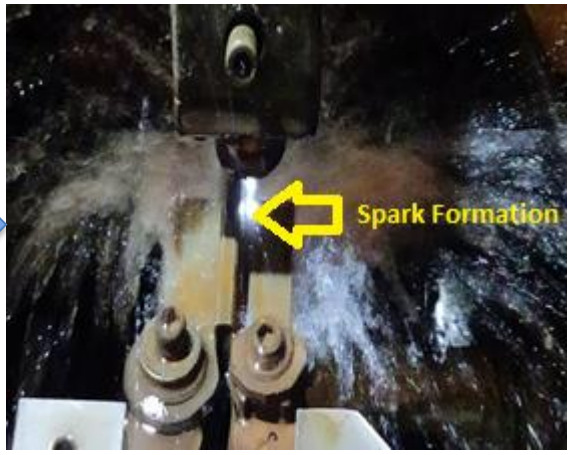

4. Workpiece machining

5. Noting down the cutting speed (vc) reading

6.Workpiece plate after cutting

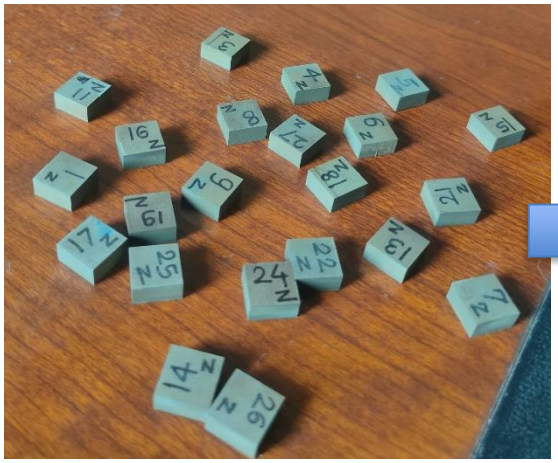

7. Specimens after machining process

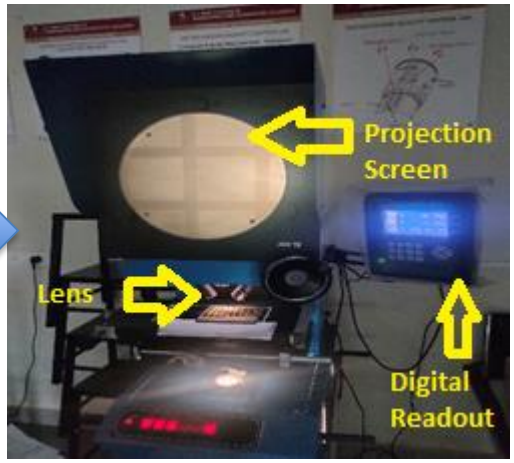

8. Measurement of kerf width using optical profile projector

9. Measurement of surface roughness using surface roughness tester

10. Measurement of dimensional deviation using digital micrometer

The following precautionary actions are taken while performing the experiments,

1. Every experiment is conducted twice (for gamma coated wire) to reduce the random error.
2. The experiments are replicated and performed in randomized order to avoid any bias in the experimental results.
3. Experiments are performed at controlled temperature range. (≈22 ^{0}C)

3.7.2 Influence of Pulse on Time on Performance Characteristics

Ton is changed from 105 units to 126 units in the increment of 3 units. The levels of remaining parameters are fixed as Toff = 42 units; IP = 230 ampere; WF = 8 m/min; WT = 8 units; SV = 20 volt. Table 3.2 represents the results for measurement of performance characteristics. Figure 3.15, 3.16 and 3.17 represents the scatter plots of pulse on-time versus different response characteristics. Figure 3.15 shows that with increment in Ton the MRR also increases in a following a linear curve. Figure 3.16

shows that with increment in Ton, the SR value also increases but rather with a wavy pattern. From figure 3.2 the dimensional deviation shows downward trend with respect to Ton up to 115 machine units and then it increases with increase in Ton.

Table 3.2 Performance Characteristics Measurement for Pulse on Time

Sr.No.	Pulse on Time (Machine Unit)	Material Removal Rate(mm^3/min)	Surface Roughness(µm)	Dimensional Deviation (%)
1	105	3.33	2.42	0.20
2	108	4.18	2.28	0.10
3	111	5.55	2.48	0.10
4	114	6.76	2.58	0.01
5	117	8.30	2.97	0.09
6	120	12.64	4.00	0.07
7	123	15.72	5.06	0.08
8	126	22.52	5.16	0.14

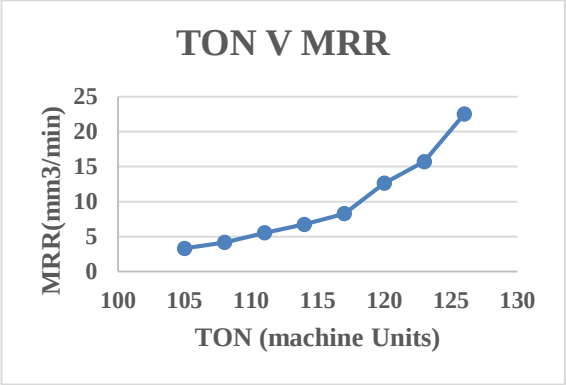

Figure 3.15 Ton Vs MRR

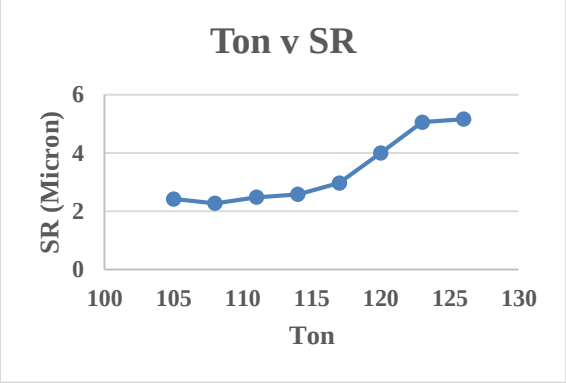

Figure 3.16 Ton Vs SR

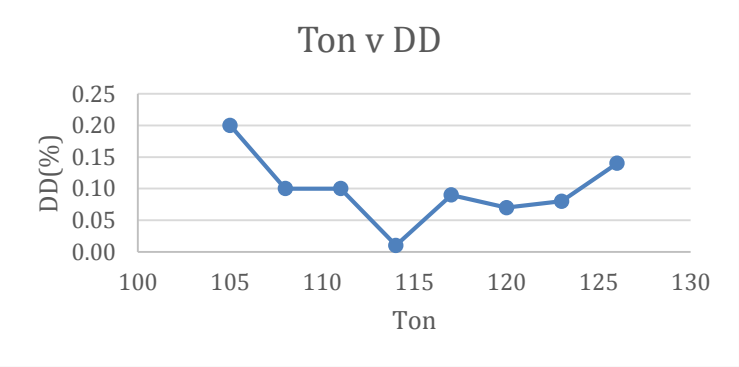

Figure 3.17 Ton Vs DD

3.7.3 Influence of Pulse off Time on Performance Characteristics

Toff is varied from 39 units to 63 units with an increment of 3 units. The levels of remaining parameters are fixed as Ton = 126 units; IP = 230 ampere; WF = 8 m/min; WT = 8 units; SV = 20 Volt. Table 3.3 represents the results for measurement of performance characteristics. Figure 3.18, 3.19 and 3.20 represents the scatter plots of pulse off time versus different response characteristics. Figure 3.18 shows that with increment in Toff, the MRR decreases linearly. For SR, the curve shows increasing trend up to 48 units and after this point it follows a wavy pattern (figure 3.19) The dimensional deviation almost remains same for different values of pulse Toff as depicted in figure 3.20.

Table 3.3 Performance Characteristics Measurement for Pulse off Time

Sr.No.	Pulse off Time (Machine Unit)	Material Removal Rate(mm^3/min)	Surface Roughness(µm)	Dimensional Deviation (%)
1	39	16.22	3.71	0.03
2	42	14.96	3.73	0.9
3	45	14.06	3.93	0.05
4	48	13.70	4.73	0.07
5	51	13.05	4.06	0.10
6	54	12.21	5.56	0.10
7	57	11.00	4.07	0.17
8	60	11.86	5.05	0.20
9	63	8.94	4.15	0.22

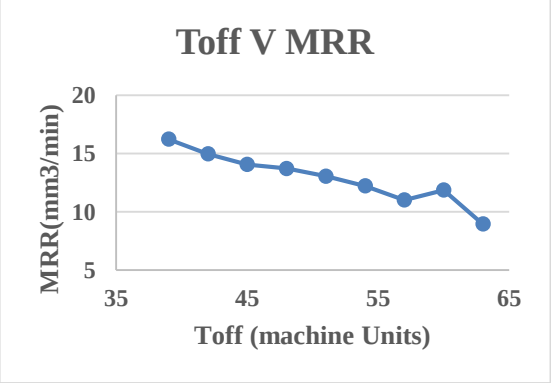

Figure 3.18 Toff vs MRR

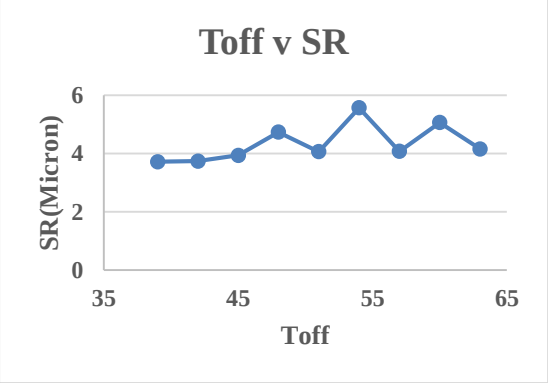

Figure 3.19 Toff vs SR

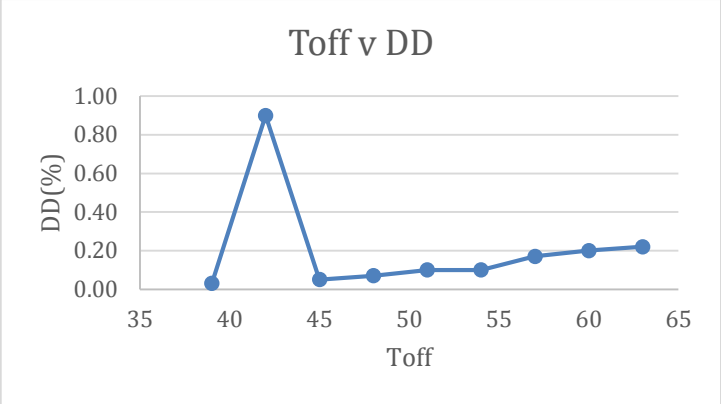

Figure 3.20 Toff vs DD

3.7.4 Influence of Spark Gap Voltage on Performance Characteristics

SV is changed between 5 volts to 80 volts in the increments of 15 volts. The levels of remaining parameters are fixed as Ton = 126 units; Toff = 42 unit; WF = 8 m/min; IP = 230 ampere; WT = 8 units. Table 3.4 represents the results for measurement of performance characteristics. Figure 3.21, 3.22 and 3.23 shows the scatter plots of SV versus different response characteristics. With increase in SV, both cutting rate and surface quality decrease linearly as shown in figure 3.21 & 3.22. For dimensional deviation, it shows decreasing trend up to 50 units and then increases for further values as shown in figure 3.23.

Table 3.4 Performance Characteristics Measurement for Spark Gap Voltage

Sr.No.	Spark Gap Voltage (Volt)	Material Removal Rate(mm^3/min)	Surface Roughness(µm)	Dimensional Deviation (%)
1	5	35.91	4.42	0.22
2	20	32.48	4.15	0.14
3	35	23.33	3.67	0.04
4	50	17.01	3.45	0.02
5	65	14.15	3.42	0.04
6	80	8.97	2.71	0.27

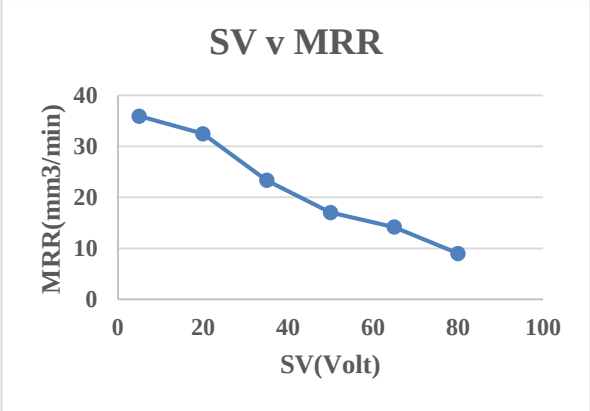

Figure 3.21 SV vs MRR

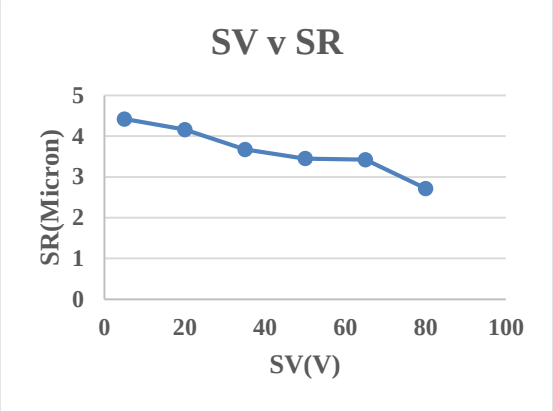

Figure 3.22 SV vs SR

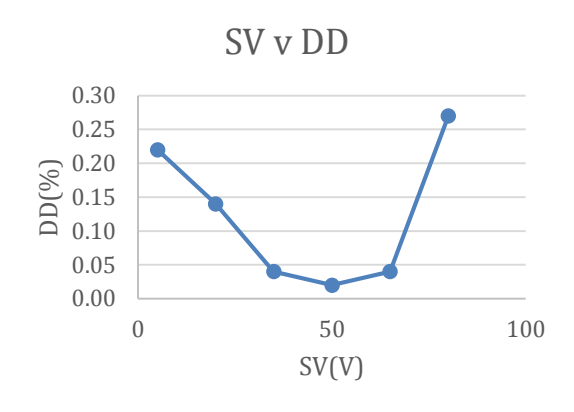

Figure 3.23 SV vs DD

3.7.5 Influence of Peak Current on Performance Characteristics

IP is changed between 50 amperes to 230 amperes in the increment of 30 amperes. The levels of remaining parameters are fixed as Ton = 126 units; Toff = 42 units; SV = 20 volt; WF = 8 m/min; WT = 8 units. Table 3.5 represents the results for measurement of performance characteristics. Figure 3.24, 3.25 and 3.26 represents the graphs of IP versus different response characteristics. From the figure 3.24, the MRR increases w.r.t. IP. for surface roughness, firstly it shows increasing trend with respect to peak current but later on it almost remains flat (figure 3.25). As peak current increases, the dimensional deviation value increases and then almost maintains the consistent results for further values. The dimensional deviation almost remains constant up to 200 Ampere setting as shown in figure 3.26.

Table 3.5 Performance Characteristics Measurement for Peak Current

Sr.No.	Peak Current (Amp)	Material Removal Rate(mm^3/min)	Surface Roughness(µm)	Dimensional Deviation (%)
1	50	12.12	2.16	0.04
2	80	16.91	3.52	0.03
3	110	17.42	2.97	0.01
4	140	17.32	3.76	0.01
5	170	18.41	3.82	0.04
6	200	22.12	3.55	0.00
7	230	25.70	3.66	0.14

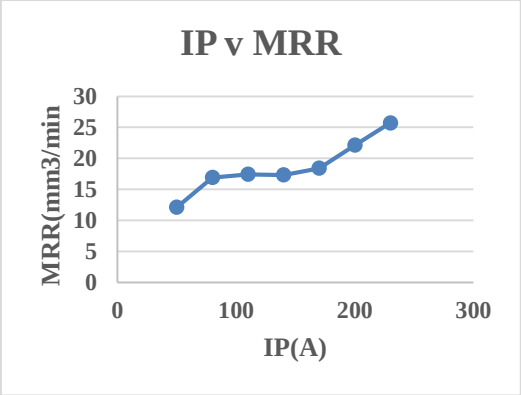

Figure 3.24 IP vs MRR

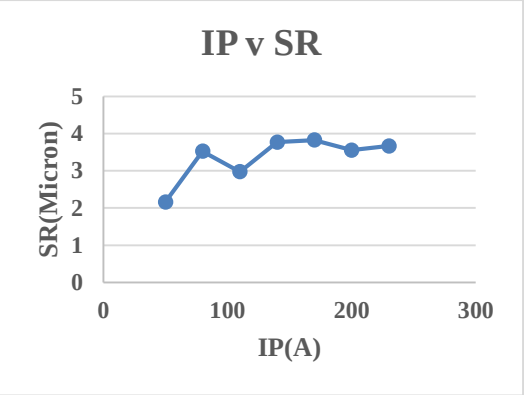

Figure 3.25 IP vs SR

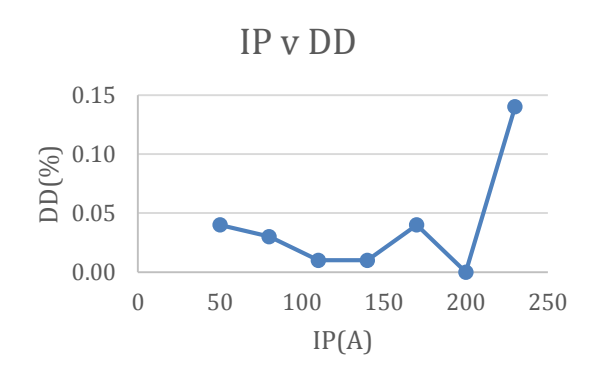

Figure 3.26 IP vs DD

3.7.6 Influence of Wire Feed on Performance Characteristics

The WF is changed between 2 to 12 machine units in the increment of 2 units. The levels of remaining parameters are fixed as Ton = 126 unit; Toff = 42 unit; IP = 230 ampere; SV = 20 volt; WT = 8 unit. Table 3.6 represents the results for measurement of performance characteristics. Figure 3.27, 3.28, 3.29 represents the graphs of WF

versus different response characteristics. From figure 3.27, it can be seen that, the MRR shows down trend up to 6 units and afterwards it shows increasing trend w.r.t. WF. For SR, the curve shows wavy pattern as represented in figure 3.28 and for dimensional deviation (figure 3.29) first it decreases steeply up to 6 units afterwards it remains nearly constant.

Table 3.6 Performance Characteristics Measurement for Wire Feed

Sr.No.	Wire Feed (m/min)	Material Removal Rate(mm^3/min)	Surface Roughness(µm)	Dimensional Deviation (%)
1	2	5.32	4.38	0.14
2	4	4.95	4.44	0.17
3	6	4.44	4.18	0.01
4	8	5.19	4.49	0.10
5	10	5.92	4.26	0.03
6	12	6.76	4.63	0.05

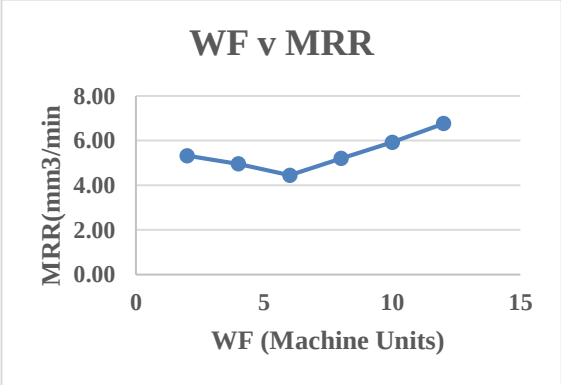

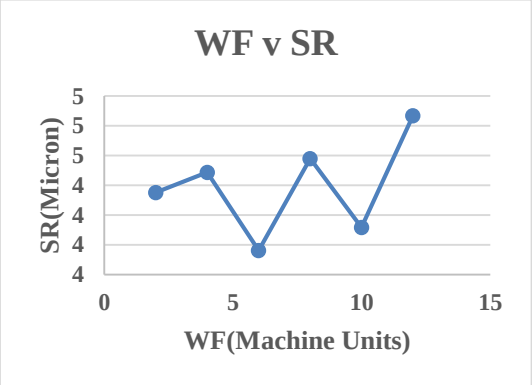

Figure 3.27 WF vs MRR

Figure 3.28 WF vs SR

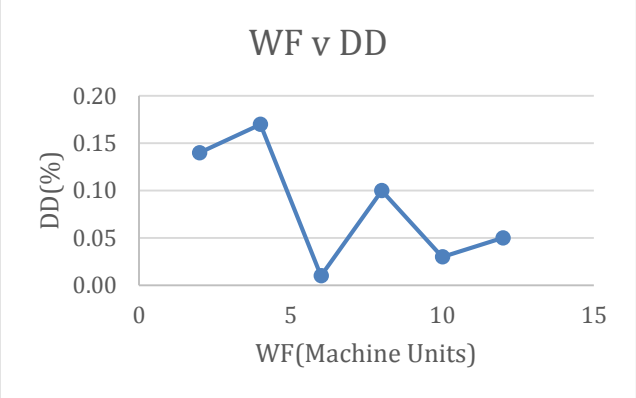

Figure 3.29 WF vs DD

3.7.7 Influence of Wire Tension on Performance Characteristics

WT is changed from 2 to 12 units in the increments of 2 units. The levels of other parameters are kept constant as Ton = 114 units; Toff = 51 units; IP = 230 ampere; WF = 8 m/min; SV = 20 volt. Table 3.7 represents the results for measurement of performance characteristics. Figure 3.30, 3.31, 3.32 shows the graphs of WT versus different response characteristics. From the figure 3.30, it is seen that, the MRR shows almost constant trend up to 8 units and later on it increases. For surface roughness, the graph shows almost a constant value throughout the range (figure 3.31). The dimensional deviation readings initially decrease as WT increases and then increases after 6 units as shown in figure 3.32.

Table 3.7 Performance Characteristics Measurement for Wire Tension

Sr.No.	Wire Tension (Units)	Material Removal Rate(mm^3/min)	Surface Roughness(µm)	Dimensional Deviation (%)
1	2	5.30	4.04	0.12
2	4	6.05	4.52	0.07
3	6	6.14	4.19	0.13
4	8	5.24	4.21	0.14
5	10	5.67	4.03	0.12
6	12	6.70	5.11	0.12

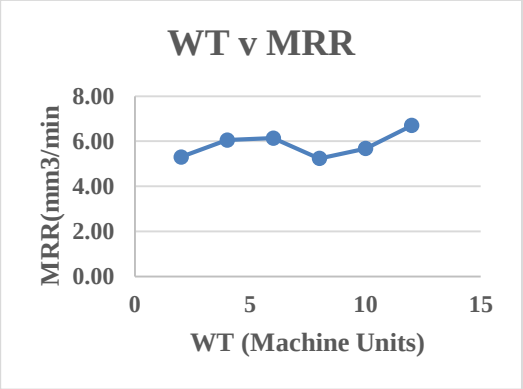

Figure 3.30 WT vs MRR

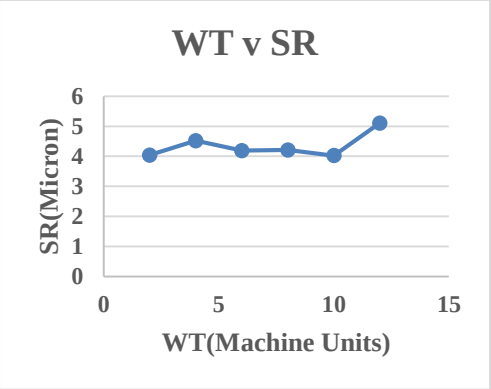

Figure 3.31 WT vs SR

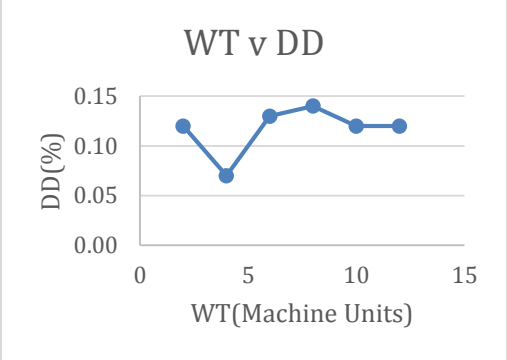

Figure 3.32 WT vs DD

3.8 SELECTION OF INPUT PROCESS PARAMETERS RANGE BASED ON PILOT INVESTIGATION

From the results it is clear that, the wire feed and wire tension doesn't have any significant effect on the quality characteristics. Thus, both these parameters shall be treated as constant parameters for further experimental work. Wire feed is set at 4 m/min and wire tension is set at 8 units. Also, all these parameters don't have a notable effect on the dimensional deviation, hence it is not considered as a response characteristic for further experimentation work. Similarly wire breakage issue is also considered before finalizing the parameter levels. The guidelines from Taguchi are also considered for the selection of parameter levels which are as follows

1. When multiple levels are used, the levels should be equally spaced.
2. Any factor can be made to look insignificant by choosing levels that are too close together and
3. Conversely any factor can be made to look significant by choosing the levels that are too far apart.

Considering above mentioned guidelines, the parameter levels are finalized as follows

Table 3.8 Finalization of parameter levels

Sr.No.	Parameter	Level 1	Level 2	Level 3	Range Available	Unit
1	Pulse on Time (Ton)	105	110	115	100-131	Machine Units
2	Pulse off Time (Toff)	40	50	60	00-63	Machine Units
3	Servo Voltage (SV)	20	40	60	00-99	Volt
4	Peak Current (IP)	70	150	230	10-230	Amp.

The following parameters are considered as constant parameters.

Table 3.9 List of constant parameters

Sr.No.	Parameter	Value	Unit
1	Wire Feed (WF)	4	Machine Units
2	Wire Tension (WT)	8	Machine Units
3	Flushing Pressure	1	Machine Units

3.9 EXPERIMENT DESIGN USING RESPONSE SURFACE METHODOLOGY (RSM)

RSM is implemented to establish the correlation between a response and a number of quantitative process variables or parameters. This approach is helpful when vital few important parameters are already identified and it is necessary to select the optimum parameter settings for optimizing the response. RSM designs are especially chosen when nonlinear behavior of the process is identified.

RSM are used to:

- Find the parameter combination which will yield the best response.
- Find the parameter combination that satisfy operating or process specifications.
- Establish a relationship between response characteristics and the process parameters.

The addition of the squared (Quadratic) terms in the model makes response surface equation different from the equation for a factorial design which makes it useful to:

1. Understand or map a region of a response surface.
2. Model the curvature (non-linearity) in the response.
3. Find the levels of controlled variables which optimizes the response characteristic.
4. Select the operating conditions to meet the desired output.

The most common forms of RSM are low-order polynomials (first or second-order). The first-order model of RSM demonstrates very low predictability, therefore the

second-order model is preferred. Similarly, the second order polynomial must be used to model a system where the non-linearity is present. The second-order model is expressed as

$$y = b_0 + \sum_{i=1}^{n} b_i x_i + \sum_{i=1}^{n} b_{ii}\, x_{i^2} + \sum\sum_{i<j} b_{ij} x_i x_j + \in \qquad \textbf{3.3}$$

Where y is the response variable, x_i are the independent variables, b_i & b_{ij} are the coefficients, $\in$ is the experimental error. This assumed surface y contains linear, squared, and cross-product terms of parameters x_i's to estimate the regression coefficients.

There are two types of response surface designs. Central Composite Design and Box Behnken design.

3.9.1 CENTRAL COMPOSITE DESIGN (CCD)

It is generally used for designing the experiments. CCD are a factorial or fractional factorial designs with center points, augmented with a group of axial points (also called star points) that enables to estimate curvature. The CCD is used to:

1. Efficiently estimate first and second order terms.
2. Model a response variable with curvature by adding center and axial points to a previously done factorial design.

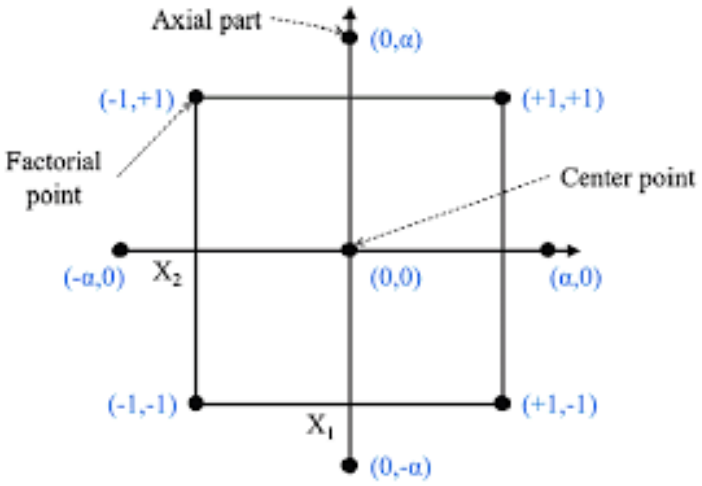

Figure 3.33 Central Composite Design

It is suitable for sequential experiments where by adding the star and center points to previous factorial experiments, the design can be modified or improved.

3.9.2 BOX BEHNKEN DESIGN (BBD)

A BBD is a design that doesn't contain a fractional factorial or an embedded factorial design. BBD have parameter combinations where two levels are the extreme levels and one level is at the mid of these two extreme levels. Also, this design requires minimum three process parameters for creating a designed experiment. Figure 3.34 shows the three factor Box Behnken design. The points in the diagram shows the experimental run combinations.

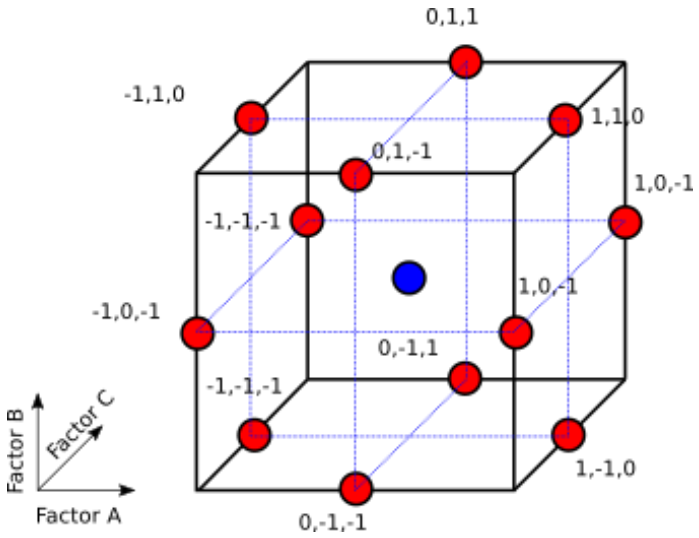

Figure 3.34 Box-Behnken design

This design allows efficient prediction of the first and second order coefficients. Box Behnken designs are less expensive as they have a smaller number of design points than the CCD for the identical number of parameters. However, BBD is not suitable for sequential experiments as it does not have an embedded factorial design. If the safe operational conditions for the process are known, then the Box Behnken design proves to be useful. CCD has axial points lying outside the cube. Sometimes these points are outside the safe operating zone which will make the conduction of experiments impossible or these points might not lie in the area of interest. Box-Behnken designs do not have axial points, therefore, it is confirmed that all the parameter levels fall within the safe operating zone. Also, Box Behnken design ensures that all the factors are not set at their higher levels at the same time.

3.9.3 Why Box Behnken Design?

The primary goal of the RSM studies is to fit the second order model. BBD is especially designed to complete this task. BBD requires 3 levels for each parameter whereas CCD requires five levels to fit the second order (Quadratic) model. Therefore, as compared to CCD, BBD requires a fewer experimental run. The BBD uses a mid-level of parameter between the high and low of the parameter and avoids the extreme axial (star) points as in the CCD. Additionally, the BBD uses face points rather than the corner points in CCD. The inclusion of the middle level point permits the efficient estimation of the coefficients of a second order model.

Therefore, developing a more accurate model is preferred. The model will be more accurate when the dealing with the smaller region as in Box Behnken Design than a wider range in central composite design. And hence the BBD will perhaps provide the better estimation of the model.

For instance, consider the influence of temperature on human comfort as represented in figure 3.35 below,

Comparison between the Central Composite and the Box-Behnken Designs

Design	Axial Low		Low Level		Mid Level		High Level		Axial High	
	°F	°C	°F	°C	°F	°C	°F	°C	°F	°C
Central Composite Design	63.6	17.5	65.0	18.3	72.0	22.2	77.0	25.0	80.5	26.9
Box-Behnken Design			65.0	18.3	72.0	22.2	77.0	25.0		

Figure 3.35 Comparison between CCD & BBD

The high and low level of temperatures are 25^0 C and 18.3^0 C. The temperature of 18.3^0 C is already low for human comfort. In the CCD, the axial points are located farther from the high and low levels. This means that it will be a total waste of resources as the temperature of 17.5^0 C will lead to lower comfort rating. So, it's not essential to study what is already known. On the contrary, in BBD the mid-level of factor is considered in addition to low and high level. Therefore, the investigation is conducted in the expected optimum region.

BBD is more useful when the user already has prior knowledge of the process while the CCD is more useful for investigating relatively unknown process. This is why the central composite design is used more often as most of the studies are conducted to

explore new things. Nevertheless, Box Behnken Design provides more precision for better refinement and optimization.

In this work, twenty-seven experiments were planned based on the Box Behnken design using Minitab 17 statistical software, and the input parameters like pulse on time, pulse off time, peak current, and servo voltage were controlled to determine their influence on the responses. The above mentioned controlled parameters are selected after a thorough literature review. Furthermore, preliminary trials are conducted prior to the main experimentation to ascertain the parametric levels. During preliminary trials, the phenomenon of wire breakage was intensely studied while selecting parametric levels.

Table 3.10 The levels of variables chosen for the Box–Behnken design

Controlled Variable	Coded Variable level		
	-1	0	+1
Pulse on Time (Ton) Machine Units	105	110	115
Pulse off Time (Toff) Machine Units	40	50	60
Peak Current (IP) Amp	70	150	230
Servo Voltage (SV) Volt	20	40	60

The table 3.11 shows the parametric combination of 27 experiments with different levels.

Table 3.11 Parametric combination of factors

Experiment No.	Ton	Toff	IP	SV		Experiment No.	Ton	Toff	IP	SV
1	105	40	150	40		16	110	60	230	40
2	115	40	150	40		17	105	50	70	40
3	105	60	150	40		18	115	50	70	40
4	115	60	150	40		19	105	50	230	40
5	110	50	70	20		20	115	50	230	40
6	110	50	230	20		21	110	40	150	20
7	110	50	70	60		22	110	60	150	20
8	110	50	230	60		23	110	40	150	60
9	105	50	150	20		24	110	60	150	60
10	115	50	150	20		25	110	50	150	40

11	105	50	150	60		26	110	50	150	40
12	115	50	150	60		27	110	50	150	40
13	110	40	70	40						
14	110	60	70	40						
15	110	40	230	40						

Chapter 4 EXPERIMENTAL RESULTS AND ANALYSIS

This chapter covers the analysis of MRR, SR results for 3 types of coated wire electrode materials. The effect wire breakage has been considered during the analysis. The surface morphology analysis and recast layer thickness analysis are also discussed.

4.1 EXPERIMENTAL RESULTS

The following table shows experimental results using 3 different types of wire materials viz. zinc coated brass wire, diffused wire and gamma coated wire.

Table 4.1 Results of experimentation

Experiment No.	Ton	Toff	IP	SV	Zinc-coated Brass Wire		Diffusion Annealed Wire		Gamma Coated Wire	
					MRR (mm^3/min.)	SR (µm)	MRR (mm^3/min.)	SR (µm)	MRR (mm^3/min.)	SR (µm)
1	105	40	150	40	3.07	1.52	1.89	1.61	2.33	1.75
2	115	40	150	40	**Wire Breakage**		3.05	3.07	3.65	3.25
3	105	60	150	40	1.17	1.68	1.15	1.64	1.68	1.66
4	115	60	150	40	3.17	2.07	3.02	2.08	3.87	2.20
5	110	50	70	20	3.69	1.91	2.82	1.81	3.29	2.13
6	110	50	230	20	3.90	2.29	2.94	2.11	3.03	2.24
7	110	50	70	60	1.91	1.74	1.91	1.73	2.89	1.94
8	110	50	230	60	2.58	1.87	2.27	1.60	3.38	1.91
9	105	50	150	20	2.10	1.57	1.72	1.49	2.35	1.74
10	115	50	150	20	**Wire Breakage**		3.19	2.93	3.61	3.39
11	105	50	150	60	1.42	1.64	1.37	1.58	1.74	1.74
12	115	50	150	60	**Wire Breakage**		3.47	2.01	4.74	2.07
13	110	40	70	40	3.78	1.99	2.31	1.89	3.03	1.99
14	110	60	70	40	1.83	1.65	1.69	1.68	2.32	1.82
15	110	40	230	40	3.65	2.11	2.22	1.85	2.71	2.13
16	110	60	230	40	2.05	1.80	2.14	1.62	2.90	2.03
17	105	50	70	40	1.56	1.41	1.55	1.48	2.08	1.64

Experiment No.	Ton	Toff	IP	SV	Zinc-coated Brass Wire		Diffusion Annealed Wire		Gamma Coated Wire	
					MRR (mm^3/min.)	SR (µm)	MRR (mm^3/min.)	SR (µm)	MRR (mm^3/min.)	SR (µm)
18	115	50	70	40	5.23	2.08	4.19	2.27	4.52	2.30
19	105	50	230	40	1.97	1.41	1.88	1.38	2.96	1.71
20	115	50	230	40	**Wire Breakage**		5.35	3.32	4.90	3.24
21	110	40	150	20	2.51	1.78	1.81	1.77	2.44	2.03
22	110	60	150	20	2.48	1.91	2.34	1.77	2.98	2.08
23	110	40	150	60	**Wire Breakage**		4.42	2.11	4.58	2.08
24	110	60	150	60	1.43	1.84	1.36	1.89	2.28	2.03
25	110	50	150	40	3.50	1.91	3.11	1.89	4.00	1.97
26	110	50	150	40	3.38	1.86	3.08	1.73	3.63	1.91
27	110	50	150	40	3.26	1.80	2.93	1.78	3.60	2.02

Average values for MRR & SR are calculated for all the wires. (excluding Experiment No.2,10,12,20,23). Figure 4.1 & 4.2 shows the performance of various wire materials for SR and MRR. Figure 4.1 depicts that the MRR for gamma coated wire is the highest among all the wires. Gamma phase brass is extremely brittle; hence the gamma coating's thickness is usually limited to 5 microns because thicker coatings will crack and peel off after the last drawing process. Due to its brittleness, brass in the Gamma phase completely breaks during the last drawing process, leaving a very uneven surface. This rough surface offers the benefit of speeding up cutting. On the other hand, zinc-coated wire has more MRR compared to diffused wire but the wire breakage issue is observed 5 times for zinc-coated wire whereas for diffused wire no wire breakage was observed hence performance of diffused wire is considered superior to zinc-coated wire. From Figure 4.2 it is clear that the surface quality is getting mainly affected when using the gamma coated wire. As the cutting speed is increasing the amount of energy necessary to remove the material is very high which leads crater formation and discontinuous surfaces. Because of this the surface quality is getting affected for gamma coated wire. For diffused wire and zinc-coated the surface quality almost remains the same.

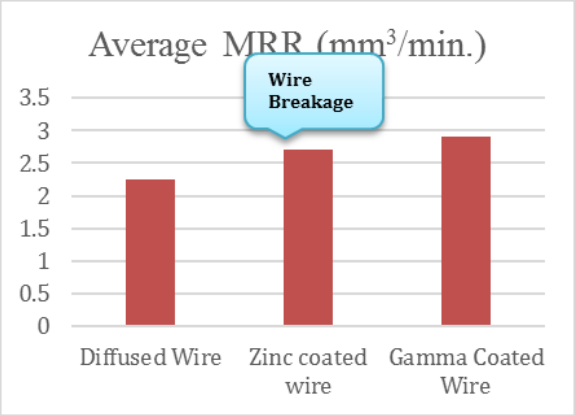

Figure 4.1 Average MRR for different wire materials

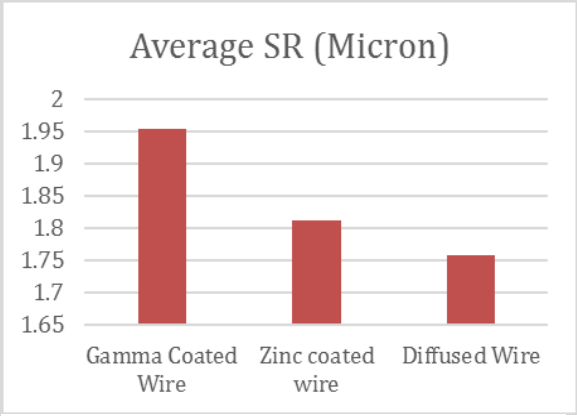

Figure 4.2 Average SR for different wire material

4.2 WIRE BREAKAGE INCIDENCES

As the WEDM process starts, the wire begins to deteriorate, and this process continues as the wire enters the workpiece and exits from the bottom. Due to stress, high temperature, and material transfer throughout the machining, the wire's surface texture and shape changes. Electric sparks contribute to plastic deformation and the vaporization of wire electrode in addition to removing the material from the workpiece. Irrespective of the type of work material, all of these transform the wire's original circular cross-section into an oval shape. The wire undergoes an irreversible distortion because of its interactions with the hostile environment while the material is being removed. (A. Pramanik and A. Basak) [45]

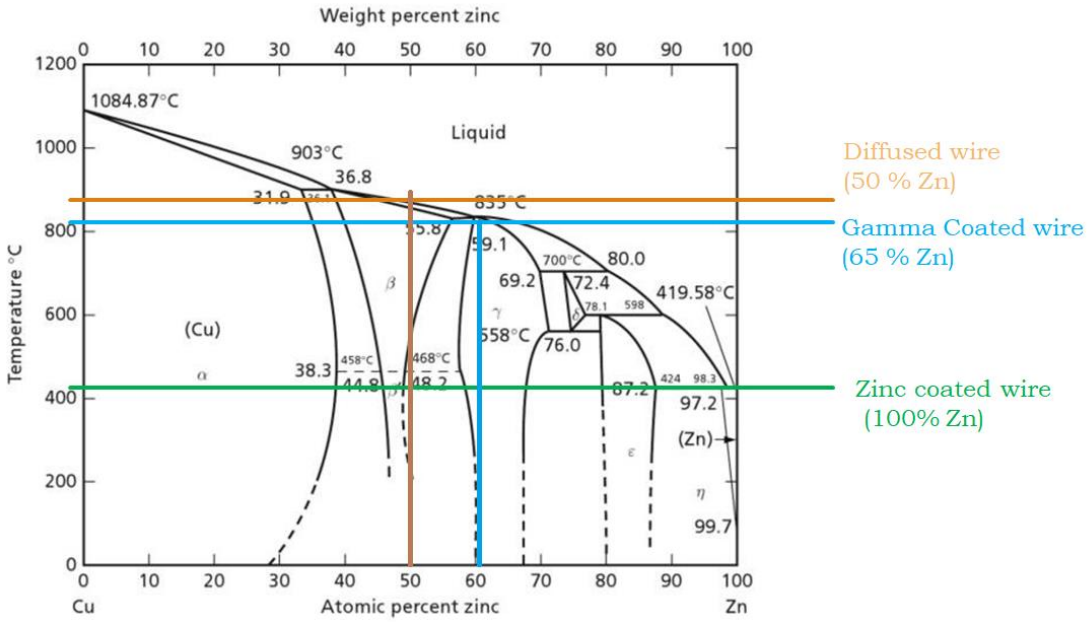

Figure 4.3 Cu Zn Equilibrium Diagram

During the experimentation, wire breakage problem is reported for zinc coated brass wire. Zinc has a low melting point of approximately 419.5 ^{0}C (refer figure 4.3) and it is only plated onto the surface of the core wire. Wire breakage occurs frequently under specific machining circumstances. Majority of the wire breakage occurs at the high value of pulse on time (115 MU) and high value of peak current (150 A). This happens as the larger current's tendency to run continuously for a longer time, which causes the zinc to be blasted off the wire's surface. This exposes the core of the wire to high temperatures. Also, the zinc coated wire has low tensile strength which is not able to withstand the high amount of thermal stress produced during machining process which leads to wire breakage at higher energy levels. For expt.No.4, the Toff setting is 60 (high level) which provides sufficient time for wire electrode to cool down and for expt. No.18, the Ip setting is at 70 (Low level) which means that low amount of thermal energy is produced. Because of these reasons the zinc coated wire has not experienced wire breakage issue for expt.no. 4 & 18. Table 4.2 shows the instances of wire breakage for zinc-coated brass.

Table 4.2 Wire Breakage Incidences

Experiment No.	**Zinc-coated Wire**				**Diffusion Annealed Wire**	**Gamma Coated Wire**
	Ton	**Toff**	**IP**	**SV**		
2	115	40	150	40	No Wire Breakage Observed	No Wire Breakage Observed
10	115	50	150	20		
12	115	50	150	60		
20	115	50	230	40		
23	110	40	150	60		

When wire breakage occurs, the machine stops automatically displaying warning message on the screen as shown in Figure 4.4.

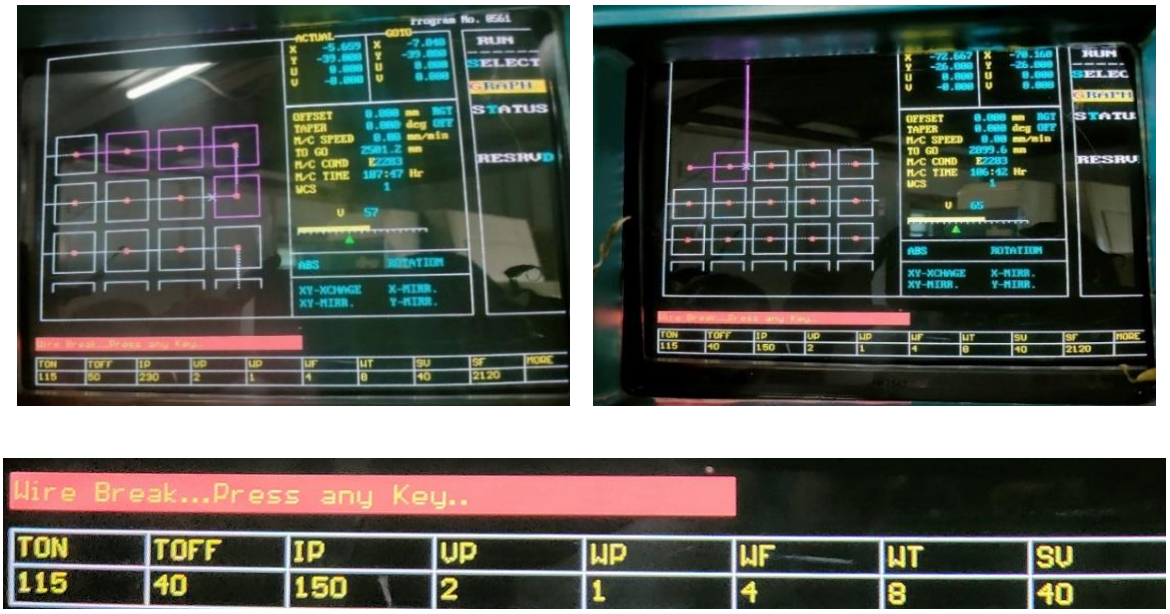

Figure 4.4 Machine display showing wire breakage warning

Whereas for diffused wire and gamma coated wire, the Zn content in the coating is reduced to 50% & 65% respectively which increases the melting point of the coating. The melting point of the coating is ≈ 825 ^{0}C and ≈ 815 ^{0}C respectively for diffused wire and gamma coating. (refer figure 4.3) Also, the coating is metallurgically bonded onto the wire core material. This prevents the exposure of the wire core material to high temperatures. Both these wires possess high tensile strength (≈ 800 Mpa) than zinc coated wire (≈ 490 Mpa). Therefore, these wires are able to withstand the high amount of thermal stress produced during machining process. Therefore, these wires do not experience the wire breakage issue.

4.3 ANALYSIS OF RESULTS:

Analysis of variance is performed for gamma coated wire and diffused wire. There were 5 incidences of wire breakages for zinc coated wire, therefore, the data set is unbalanced and hence ANOVA is not performed.

4.3.1 Analysis of MRR:

It is seen that for gamma coated wire and diffused wire, Ton (p-value <0.05) is the significant factor influencing MRR with 59.47% & 58.18% respectively. The percentage contribution is calculated by dividing the Adj.SS value of the parameter by the total value. Toff (p-value =0.06), IP (p-value = 0.206) & SV (p-value =0.168) are insignificant for both these wires. Here, Ton is the key influential process parameter that controls the length of the electric spark generation and consequently has a notable impact on the performance characteristics. From Table 4.3, the results of the ANOVA analysis help in understanding each parameter's influence and contribution to MRR. It is clear from Table 4.3 that Ton (p-value <0.05) is the important parameter influencing MRR with 59.47%. Toff, IP & SV are found to be insignificant. The R-Square value of the ANOVA models is 91.71%. This shows that the model can efficiently predict the outcomes of the process. The important diagnostic method for evaluating the model's suitability is residual analysis. The residual error measures the dissimilarity in the response left unexplained by the model. The p-value of 0.263 for gamma coated wire is more than 0.05. Hence, it is concluded that the model adequately explains the dissimilarity in the responses.

Table 4.3 ANOVA Results for MRR (Gamma Coated Wire)

Source	DF	Adj SS	Adj MS	F Value	P- Value
Linear	4	13.4643	3.3661	23.57	0.000
TON	1	12.2875	12.2875	86.06	0.000
TOFF	1	0.6138	0.6138	4.30	0.060
IP	1	0.2553	0.2553	1.79	0.206
SV	1	0.3077	0.3077	2.15	0.168
Square	4	2.1366	0.5342	3.74	0.034
TON* TON	1	0.1374	0.1374	0.96	0.346
TOFF*TOFF	1	2.0503	2.0503	14.36	0.003
IP*IP	1	0.2465	0.2465	1.73	0.213

SV*SV	1	0.4876	0.4876	3.41	0.089
2 Way interaction	6	3.3470	0.5578	3.91	0.021
TON*TOFF	1	0.1893	0.1893	1.33	0.272
TON*IP	1	0.0603	0.0603	0.42	0.528
TON*SV	1	0.7485	0.7485	5.24	0.041
TOFF*IP	1	0.2000	0.2000	1.40	0.260
TOFF*SV	1	2.0071	2.0071	14.06	0.003
IP*SV	1	0.1419	0.1419	0.99	0.338
Error	12	1.7134	0.1428		
Lack of Fit	10	1.6118	0.1612	3.17	0.263
Pure Error	2	0.1016	0.0508		
Total	26	20.6614			
Model Summary					
	S	R-sq.	R-sq. (adj)		
	0.377867	91.71%	82.03%		

Table 4.4 ANOVA Results for MRR (Diffused Wire)

Source	DF	Adj SS	Adj MS	F Value	P- Value
Linear	4	15.2515	3.8129	9.18	0.001
TON	1	13.4675	13.4675	32.43	0.000
TOFF	1	1.3337	1.3337	3.21	0.098
IP	1	0.4503	0.4503	1.08	0.318
SV	1	0.0000	0.0000	0.00	0.994
Square	4	2.2635	0.5659	1.36	0.304
TON* TON	1	0.0087	0.0087	0.02	0.887
TOFF*TOFF	1	1.9069	1.9069	4.59	0.053
IP*IP	1	0.0674	0.0674	0.16	0.694
SV*SV	1	0.5442	0.5442	1.31	0.275
2 Way interaction	6	3.7234	0.6206	1.49	0.260
TON*TOFF	1	0.1272	0.1272	0.31	0.590
TON*IP	1	0.1737	0.1737	0.42	0.530
TON*SV	1	0.0990	0.0990	0.24	0.634
TOFF*IP	1	0.0721	0.0721	0.17	0.684
TOFF*SV	1	3.2380	3.2380	7.80	0.016
IP*SV	1	0.0135	0.0135	0.03	0.860
Error	12	4.9836	0.4153		

Lack of Fit	10	4.9641	0.4964	51.14	0.019
Pure Error	2	0.0194	0.0097		
Total	26	26.2219			
Model Summary					
	S	R-sq.	R-sq. (adj)		
	0.6444	80.99 %	58.82 %		

According to the mean effect plot (Figure 4.5 & Figure 4.6), Ton influences the discharge energy. As Ton increases, the ionization occurring at the interface of the workpiece also increases. Ionization of the dielectric medium is crucial for the creation of a conductive path for the electrical discharge to occur. By ionizing the dielectric medium, the electrical conductivity of the fluid increases, allowing for more efficient energy transfer between the wire electrode and the workpiece. Efficient ionization enables the generation of more sparks in a given time period, leading to higher cutting speeds. The Heat Affected Zone (HAZ) also enlarges with increasing Ton because of the temperature increase. This substantial amount of material is flushed out with dielectric fluid during the Ton, raising the MRR. The impact of Toff on MRR is quadratic for both the wires. The MRR is shown to increase from 40 to 50, but it then drops from 50 to 60. When Toff increases, reduction in sparking subsequently reduces the melting and vaporization of workpiece, thus erosion rate diminishes leading to reduced MRR. Also, this is linked to the mobility of the dielectric fluid, which causes cooling around the HAZ as the Toff duration gets longer, the material solidifies once again, and the debris is improperly flushed out, resulting in lower MRR. Increase in IP causes the increase in current intensity, which increases the spark energy, which leads more metal to melt and be ejected from the workpiece. This causes the MRR to increase linearly as IP increases. The servo voltage controls the gap between the wire and the workpiece. The gap between the workpiece and the wire increases as the servo voltage increases resulting in a reduction in the number of sparks. This expanded interelectrode gap causes a higher proportion of pulse energy to be absorbed by the dielectric. Consequently, there is a less efficient utilization of pulse energy, resulting in a decrease in machining speed. This leads to a more stable electric discharge and a slower cutting rate. (K. Natarajan et al.) [1] (K. Mandal et al.) [38] For gamma coated wire, the trend is almost flat. For diffused wire and zinc coated wire the trend is negative.

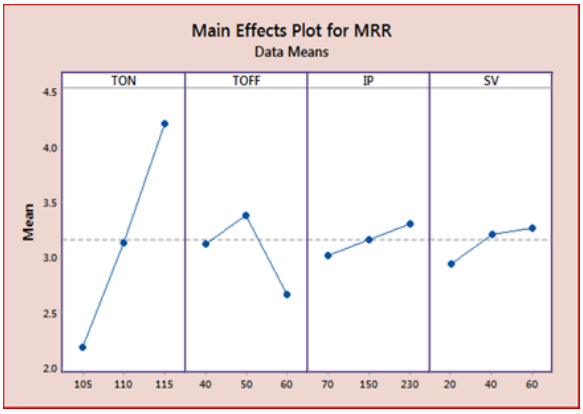

Figure 4.5 Main effect plot for MRR (Gamma Coated Wire)

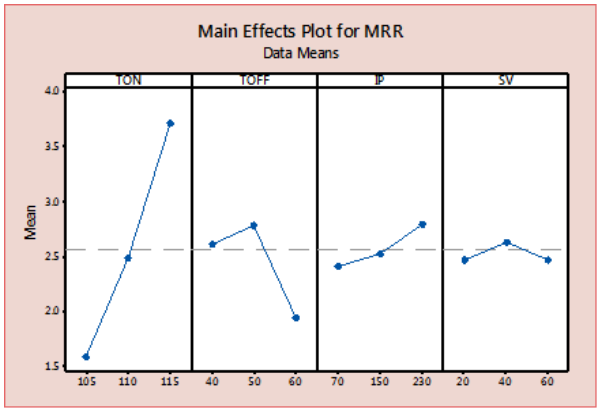

Figure 4.6 Main effect plot for MRR (Diffused Wire)

Figures 4.7 & 4.8 depict the correlation between the input parameters for gamma coated wire and diffused wire. The MRR decreases with a fall in Ton and increasing Toff, because a longer Toff enables the dielectric fluid to remove the debris and spark generation to be ceased. MRR increases along with IP and Ton because the workpiece's excess material is being removed for a longer time using a large amount of spark energy. Additionally, the incorporation of Ton and SV increments has increased MRR. Lower Toff and moderate SV values have shown a notable impact on MRR. This is because moderate SV values will have sufficient energy and lower Toff values will result in shorter spark off times. As a result, more material is removed which increases the MRR. The combination of IP & Toff and SV & IP have a negligible influence on MRR.

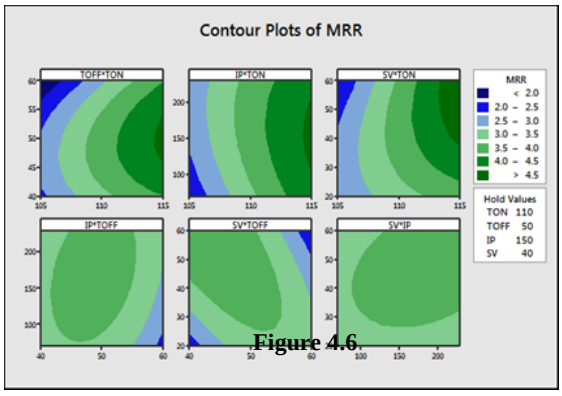

Figure 4.6

Figure 4.7 Contour plot for MRR (Gamma Coated Wire)

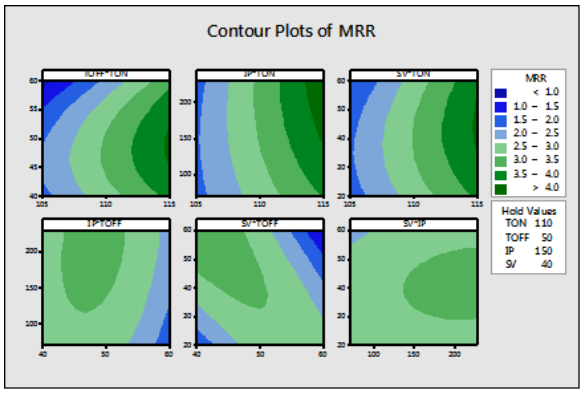

Figure 4.8 Contour plot for MRR (Diffused Wire)

4.3.2 Analysis of SR:

From ANOVA table 4.5, for both gamma coated wire and diffused wire Ton (p-value <0.05) is the most important parameter influencing SR with 58.18% & 59.69 % respectively. The results of Toff, IP, and SV are not significant. The R-Square value of

the ANOVA models is 90.43% & 89.10% respectively. The important diagnostic method for evaluating the model's suitability is residual analysis. The p-value of 0.062 for gamma coated wire and 1.00 for diffused wire is more than 0.05. Hence, it can be inferred that the model adequately explains the variation in the responses.

Table 4.5 ANOVA Results for SR (Gamma Coated Wire)

Source	DF	Adj SS	Adj MS	F Value	P- Value
Linear	4	3.82044	0.95511	21.73	0.000
TON	1	3.20850	3.20850	73.01	0.000
TOFF	1	0.16194	0.16194	3.68	0.079
IP	1	0.16756	0.16756	3.81	0.075
SV	1	0.28244	0.28244	6.43	0.026
Square	4	0.29684	0.07421	1.69	0.217
TON* TON	1	0.26790	0.26790	6.10	0.030
TOFF*TOFF	1	0.00187	0.00187	0.04	0.840
IP*IP	1	0.00258	0.00258	0.06	0.813
SV*SV	1	0.02058	0.02058	0.47	0.507
2 Way interaction	6	0.86294	0.14382	3.27	0.038
TON*TOFF	1	0.22944	0.22944	5.22	0.041
TON*IP	1	0.18792	0.18792	4.28	0.061
TON*SV	1	0.43692	0.43692	9.94	0.008
TOFF*IP	1	0.00116	0.00116	0.03	0.874
TOFF*SV	1	0.00281	0.00281	0.06	0.805
IP*SV	1				
Error	12	0.52734	0.04394		
Lack of Fit	10	0.52058	0.05206	15.40	0.062
Pure Error	2	0.00676	0.00338		
Total	26	5.50756			
Model Summary					
	S	R-sq.	R-sq. (adj)		
	0.209630	90.43%	79.25%		

Table 4.6 ANOVA Results for SR (Diffused Wire)

Source	DF	Adj SS	Adj MS	F Value	P- Value
Linear	4	3.89943	0.97486	18.24	0.000
TON	1	3.5193	3.5193	65.85	0.000
TOFF	1	0.2194	0.2194	4.11	0.066
IP	1	0.8467	0.8467	1.58	0.232
SV	1	0.0759	0.0759	1.42	0.256
Square	4	0.4433	0.1108	2.07	0.147
TON* TON	1	0.3671	0.3671	6.87	0.022
TOFF*TOFF	1	0.0041	0.0041	0.08	0.786
IP*IP	1	0.000	0.000	0.000	0.968
SV*SV	1	0.000	0.000	0.000	0.951
2 Way interaction	6	0.8989	0.1498	2.80	0.061
TON*TOFF	1	0.2557	0.2557	4.78	0.049
TON*IP	1	0.3335	0.3335	6.24	0.028
TON*SV	1	0.2521	0.2521	4.72	0.051
TOFF*IP	1	0.000	0.000	0.000	0.954
TOFF*SV	1	0.0122	0.0122	0.23	0.641
IP*SV	1	0.045	0.045	0.84	0.376
Error	12	0.6413	0.0534		
Lack of Fit	10	0.6278	0.0627	9.34	1.00
Pure Error	2	0.0134	0.00672		
Total	26	5.8830			
Model Summary					
	S	R-sq.	R-sq. (adj)		
	0.2311	89.10%	76.38%		

From Figure 4.9 & 4.10, it is obvious that, the SR value increases as pulse-on time increases for both the wires. During the WEDM process micro cracks, cavities, and craters are formed. With the rise in Ton, discharge energy increases, and the size of these irregularities also increases. Therefore, SR is increasing. Extended pulse duration leads to increased heat energy, which promotes more material to be removed from the workpiece surface. At higher Ton, the ionization is higher. This increase in ionization increases spark generation intensity. With higher spark intensity, the craters created on the workpiece surface become deeper and larger. This increases the SR of the machined surface. Sparks generated at higher Ton values, widens the heat affected zone.

Additionally, intermittent surfaces are created during the flushing process, which lowers the quality of the manufactured parts. At lower Ton, the discharge energy decreases; this reduces the melting of the material. This decreases the cutting rate because of the reduced spark intensity. The craters formed on the workpiece surface at lower spark intensity are smaller and shallower, resulting in lower surface roughness. The surface quality of the machined surface improves when the Toff value goes up for both gamma coated wire and diffused wire. Because the machine won't be in use during Toff, a drop in electric spark generation may be the reason for the reduction in Ra value. Because of the longer flushing time, it is possible to remove the tiny material from the machined work surface and reduce the possibility of localized welding of particles on the machined surface, which may cause reduction in Ra value. The lower SR values also have resulted from the effective debris removal from the workpiece surface with a higher Toff value. The SR value also increases with increase in peak current. The reason for this is that stronger currents generate greater spark energy, which removes more material and forms deep, wide craters with a greater SR value. The SR is found to decrease as the SV increases. As the SV increases, the gap between the wire and workpiece increases. This causes a higher proportion of heat energy to be absorbed by dielectric medium. Therefore, it leads to generation of relatively good surface.

Figure 4.9 Main effect plot for SR (Ra) (Gamma Coated Wire)

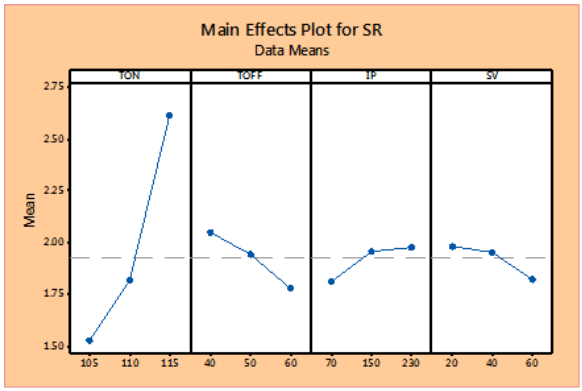

Figure 4.10 Main effect plot for SR (Ra) (Diffused Wire)

The contour plot for both gamma coated wire and diffused wire (Figure 4.11 & 4.12) shows that Ton with a low value and a different Toff value when combined significantly affects SR. This is so that enough time can be provided to clear the debris from the workpiece when the Toff value rises. Combining a high IP level with a high Ton value reveals a decline in workpiece's surface quality since the excessive spark intensity will be removing the material more quickly. As the Ton value decreases, less time will be

available for the large quantity of spark energy to be produced, which will result in less surface wear and tear. This combination of decreasing Ton value and increasing SV value demonstrates very good surface finish quality. Other combinations, such Toff &IP, Toff & SV, and IP & SV, have less of an impact on SR value.

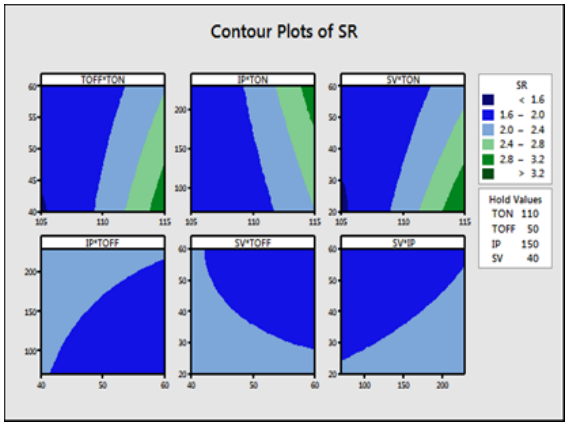

Figure 4.11 Contour plot for SR (Ra) (Gamma Coated Wire)

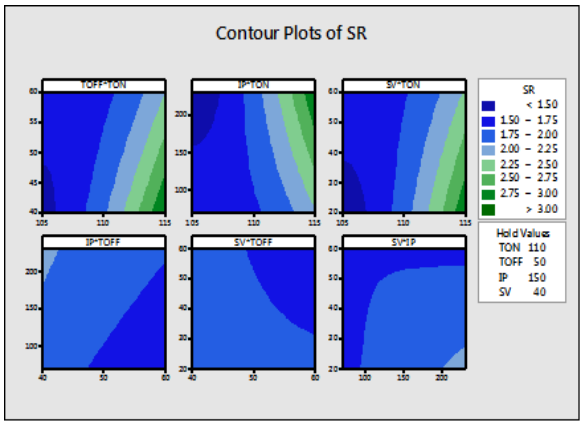

Figure 4.12 Contour plot for SR (Ra) (Diffused Wire)

4.3.3 Surface Morphology Analysis:

After WEDM process, the workpiece surface is inspected using a scanning electron microscope (SEM). Figure 4.13- 4.15 shows the images of the machined workpiece surface using WEDM process. The SEM images are presented for the experiment No. 8 having process parameters Ton (110 MU), Toff (50MU), peak current (230A) & servo voltage (60V). The microstructure shows the formation of globules, craters, re-solidified layer and micro holes. Due to high toughness of Nitronic-30, no micro cracks were observed. Higher levels of pulse-on time (110 MU) and current (230A) result in generation of high discharge energy because of an increase in spark intensity. At this energy level, a pool of molten metal is formed and is overheated. This overheated molten metal gets evaporated leading to the gas bubbles formation. These gas bubbles explode when the discharge ceases, and removes the molten material. The result is the formation of crater. Successive discharges that have a random nature will result in the formation of craters, globules, micro cracks, voids and other surface defects. (P. Sharma et al.) [102]

The diffused wire consists of brass core with coating of 50% Cu & 50% Zn which is the beta phase. With 50% of Zn in the beta phase which is metallurgically bonded, it possesses lesser electrical conductivity. Therefore, the smaller amount of heat energy is produced. This leads to removal of smaller amount of material from the workpiece

surface. The smaller amount molten material is deposited on the workpiece surface. Also, micro globules and craters of very small size as shown in Figure 4.13. For zinc-coated wires, as the zinc coating possesses a low melting point, the high temperature electrical discharges tend to melt and evaporate the zinc coating from the wire core. This exposes the brass core. Since the brass has slightly high electrical conductivity, slightly larger amount of heat energy is generated. This leads to deposition of molten material on workpiece surface as represented in Figure 4.14. The increased MRR is an indication of this phenomenon. Whereas, the gamma coated wire which has discontinuous surface offers higher cutting rate. More molten material is re-deposited on the workpiece surface also, deep and wide craters are produced because of this high amount of energy as shown in Figure 4.15.

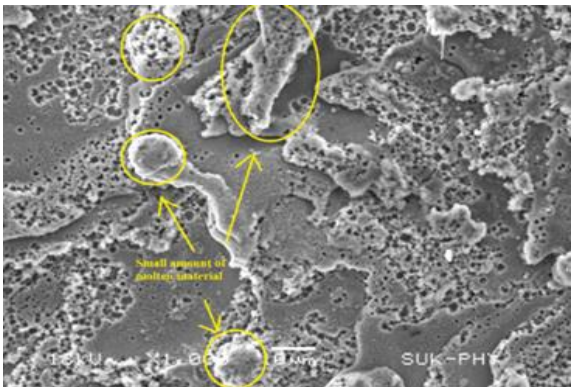

Figure 4.13 SEM image for machined surface using Diffused wire

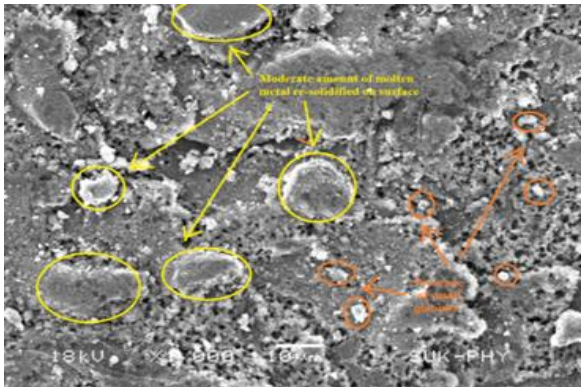

Figure 4.14 SEM image for machined surface using Zinc Coated wire

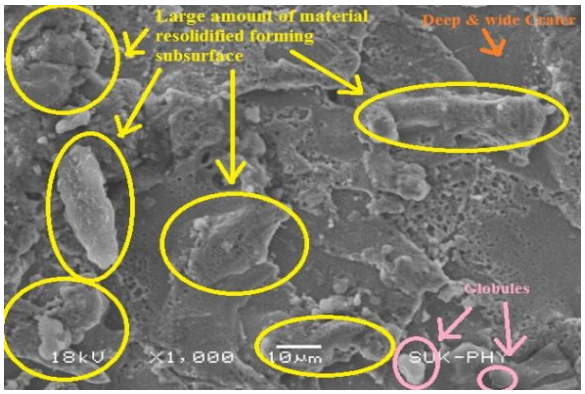

Figure 4.15 SEM image for machined surface using Gamma Coated wire

4.3.4 Analysis of Recast Layer Thickness:

During WEDM process, very high amount temperatures of more than 10000 ^{0}C are generated. This high temperature electrical discharges can easily melt and evaporate the conductive material. The workpiece is exposed to cycles of rapid heating and cooling. Most of the material is flushed away by the pressurized waves while remaining molten metal gets resolidified on the workpiece surface. The thickness of this resolidified layer is called as recast layer thickness. As explained in 4.3.3, For diffused wire, lesser heat energy is generated during WEDM. Therefore, majority of the molten metal gets flushed properly and a small amount molten metal gets re-solidifies on the workpiece surface. Hence, for diffused wire, the recast layer thickness is around 12 µm (Figure 4.16) which is less compared to zinc-coated wire and gamma coated wire. The recast layer thickness increases to approximately to 15 µm for zinc-coated wire this (Figure 4.17) as substantial amount of heat is generated, leading to re-solidification of more molten metal on the surface. For gamma coated wire the recast layer thickness is considerably increased to 20 µm. (Figure 4.18) as very high amount of heat is generated re-depositing high volumes of molten material onto the workpiece surface.

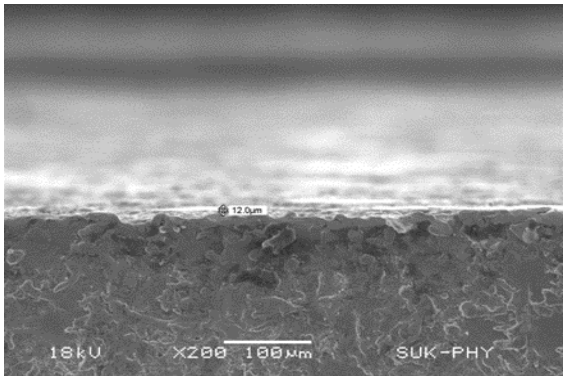

Figure 4.16 Recast layer Thickness measurement for Diffused Wire

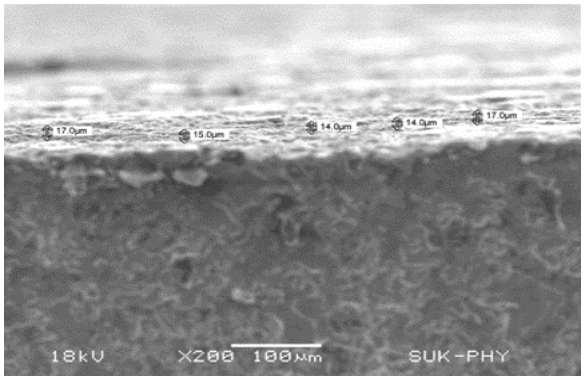

Figure 4.17 Recast layer Thickness measurement for Zinc Coated Wire

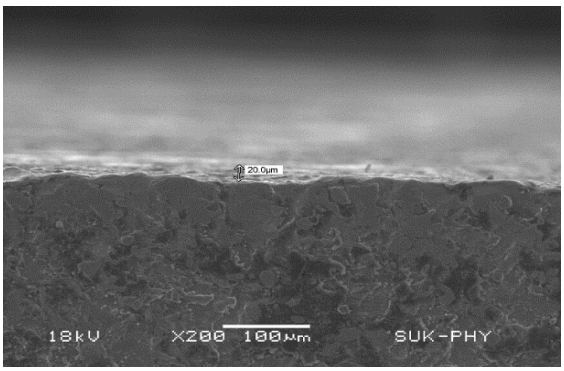

Figure 4.18 Recast layer Thickness measurement for Gamma Coated Wire

Chapter 5 MULTI-RESPONSE OPTIMIZATION USING GREY RELATIONAL ANALYSIS

5.1 GREY RELATIONAL ANALYSIS (GRA)

GRA is very useful technique to optimize a process with multi response characteristics. WEDM is considered as complex process in which the relationship between various factors is unclear. Such systems are often being called grey that give poor, incomplete and uncertain information. To solve such kind of problem, GRA is very useful. Through the GRA, a Grey Relational Grade (GRG) is obtained to estimate the multiple response characteristics. GRA provides an effective solution to the uncertainty in multi-input and discrete data problems for multi-response optimization through the selection of machining parameters. Therefore, optimization of the complex multiple response characteristics can be converted into optimization of a single grey relational grade.

5.2 PROCEDURE FOR GREY RELATIONAL ANALYSIS:

In GRA, the experimental results of the measured response output are normalized between 0 to 1. This is called as 'Grey relational generation'. The Grey Relational Coefficient is then calculated. Overall performance depends upon the computation of Grey Relational Grade (GRG).

From the economic justification mentioned in chapter 7, the performance of gamma coated wire is superior compared to diffused wire. Therefore, the GRA for gamma coated wire is represented in the following section. The following table shows the MRR &SR results for the experiments performed using gamma coated wire.

Table 5.1 MRR & SR Results for Gamma coated wire

Experiment No.	Gamma Coated Wire		Experiment No.	Gamma Coated Wire	
	MRR (mm^3/min.)	SR (µm)		MRR (mm^3/min.)	SR (µm)
1	2.33	1.75	15	2.71	2.13
2	3.65	3.25	16	2.90	2.03
3	1.68	1.66	17	2.08	1.64
4	3.87	2.20	18	4.52	2.30

Experiment No.	Gamma Coated Wire		Experiment No.	Gamma Coated Wire	
	MRR (mm^3/min.)	SR (µm)		MRR (mm^3/min.)	SR (µm)
5	3.29	2.13	19	2.96	1.71
6	3.03	2.24	20	4.90	3.24
7	2.89	1.94	21	2.44	2.03
8	3.38	1.91	22	2.98	2.08
9	2.35	1.74	23	4.58	2.08
10	3.61	3.39	24	2.28	2.03
11	1.74	1.74	25	4.00	1.97
12	4.74	2.07	26	3.63	1.91
13	3.03	1.99	27	3.60	2.02
14	2.32	1.82			

Step 1: Normalization of the data

Normalization in grey relational analysis refers to the process of transforming raw data into a comparable scale or dimensionless form. Normalization is done to make all the values under same range and unit. This step is crucial because since each variable has its own range and unit, therefore comparison of these values is not possible. The values of response characteristics obtained from experimental results are normalized in the range from 0 to 1.

For Material removal rate higher values are desired and for surface roughness lower values are desired therefore the values are normalized using the eq.5.1 & eq.5.2.

For smaller the better:

$$x_i = \frac{(max(y_i) - y_i)}{\left(max(y_i) - min(y_i)\right)} \quad \textbf{5.1}$$

For larger the better:

$$x_i = \frac{\left(y_i - min(y_i)\right)}{\left(max(y_i) - min(y_i)\right)} \quad \textbf{5.2}$$

Where,

X_i = obtained grey relational generation

min (Y_i) = The least value of Y_i for the i^{th} response

max (Y_i) = The highest value of Y_i for the i^{th} response

where i= 1,2,3,4 ……

E.g. The normalized value for MRR of Expt. No.1 is calculated as,

y_i= 2.33, min (y_i) = 1.68, max (y_i) = 4.9

Putting these values in eq. 5.2, we get

$$x_i = \frac{(2.33 - 1.68)}{(4.9 - 1.68)}$$

$$\boldsymbol{x_i = 0.2019}$$

Similarly, the calculations are done for remaining experiments and the normalized values for MRR & SR are shown in following table,

Table 5.2 Normalized values for MRR & SR Results

Expt. No.	MRR	SR	Expt. No.	MRR	SR
1	**0.2019**	0.9372	15	0.3199	0.7220
2	0.6118	0.0839	16	0.3789	0.7763
3	0.0000	0.9880	17	0.1242	1.0000
4	0.6801	0.6815	18	0.8820	0.6210
5	0.5000	0.7180	19	0.3975	0.9635
6	0.4193	0.6587	20	1.0000	0.0896
7	0.3758	0.8288	21	0.2360	0.7785
8	0.5280	0.8476	22	0.4037	0.7483
9	0.2081	0.9418	23	0.9006	0.7471
10	0.5994	0.0000	24	0.1863	0.7774
11	0.0186	0.9412	25	0.7205	0.8116
12	0.9503	0.7540	26	0.6056	0.8487
13	0.4193	0.8031	27	0.5963	0.7825
14	0.1988	0.8961			

Step 2: Calculation of deviation sequence

The deviation sequence $\Delta 0_i\,(k)$ is the absolute difference between the reference sequence $x_0{}^*(k)$ and the comparability sequence $x_i{}^*(k)$after normalization. It is determined using eq.5.3 as:

$$\Delta 0_i\,(k) = |x_0{}^*(k) - x_i{}^*(k)| \qquad \textbf{5.3}$$

For MRR of Expt. No.1

$$x_0{}^*(k) = 1.0000$$

$$x_i{}^*(k) = 0.2019$$

Therefore, eq. 5.3 becomes

$$\Delta 0_i\,(k) = 1.0000 - 0.2019$$

$$\boldsymbol{\Delta 0_i\,(k) = 0.7981}$$

Similarly, the calculations are done for remaining experiments and the deviation sequence values for MRR & SR are shown in following table,

Table 5.3 Deviation Sequence values for MRR & SR Results

Expt. No.	MRR	SR	Expt. No.	MRR	SR
1	**0.7981**	0.0628	15	0.6801	0.2780
2	0.3882	0.9161	16	0.6211	0.2237
3	1.0000	0.0120	17	0.8758	0.0000
4	0.3199	0.3185	18	0.1180	0.3790
5	0.5000	0.2820	19	0.6025	0.0365
6	0.5807	0.3413	20	0.0000	0.9104
7	0.6242	0.1712	21	0.7640	0.2215
8	0.4720	0.1524	22	0.5963	0.2517
9	0.7919	0.0582	23	0.0994	0.2529
10	0.4006	1.0000	24	0.8137	0.2226
11	0.9814	0.0588	25	0.2795	0.1884
12	0.0497	0.2460	26	0.3944	0.1513
13	0.5807	0.1969	27	0.4037	0.2175
14	0.8012	0.1039			

Step 3: Calculation of Grey Relational Coefficient (GRC)

GRC establishes the relationship between the ideal (best) and the normalized response values. The eq.5.4 gives the relation for GRC

$$\gamma(x_0(k), x_i(k)) = \frac{\Delta_{min} + \zeta\, \Delta_{max}}{\Delta_{0i}\,(k) + \zeta\, \Delta_{max}} \qquad \textbf{5.4}$$

where, Δmin is the smallest value of $\Delta 0_i\,(k) = min_{\,i}\; min_{\,k} |x_0^*(k) - x_i^*(k)|$ and Δmax is the largest value of $\Delta 0_i\,(k) = max_{\,i}\; max_{\,k} |x_0^*(k) - x_i^*(k)|$, $x_0^*(k)$ is the ideal normalized S/N ratio, $x_i^*(k)$ is the normalized comparability sequence, and ζ is the objective weight. The procedure for calculation of the value of ζ is explained in detail in section 5.3.

For MRR of Expt. No.1

Δmin = 0, Δmax = 1, ζ =0.65 (refer section 5.3 for more details), $\Delta 0_i\,(k) = 0.7981$

Putting above values in eq. 5.4, we get

$$\gamma(x_0(k), x_i(k)) = \frac{0 + (0.65 * 1)}{0.7981 + (0.65 * 1)}$$

$$\boldsymbol{GRC = \gamma(x_0(k), x_i(k))} = \textbf{0.4489}$$

Similarly, the calculations are done for remaining experiments and the GRC values for MRR & SR are shown in following table,

Table 5.4 GRC values for MRR & SR Results

Expt. No.	MRR	SR	Expt. No.	MRR	SR
1	**0.4489**	0.8479	15	0.4887	0.5574
2	0.6261	0.2764	16	0.5114	0.6100
3	0.3939	0.9669	17	0.4260	1.0000
4	0.6702	0.5236	18	0.8463	0.4801
5	0.5652	0.5538	19	0.5190	0.9055
6	0.5281	0.5063	20	1.0000	0.2777
7	0.5101	0.6715	21	0.4597	0.6125
8	0.5793	0.6967	22	0.5216	0.5817
9	0.4508	0.8574	23	0.8674	0.5806

Expt. No.	MRR	SR	Expt. No.	MRR	SR
10	0.6187	0.2593	24	0.4441	0.6112
11	0.3984	0.8562	25	0.6993	0.6501
12	0.9290	0.5872	26	0.6224	0.6982
13	0.5281	0.6399	27	0.6169	0.6168
14	0.4479	0.7711			

Step 4: Calculation of Grey Relational Grade (GRG)

The GRG decides the overall evaluation of the multiple response characteristics. The average sum of the GRC gives the value for GRG which is given below in eq.5.5.

$$\gamma\ (x_{o,}x_i) = \frac{1}{m} \sum_{i=1}^{m} \gamma(x_0(k), x_i(k)) \qquad \textbf{5.5}$$

GRG is very important number in grey relational analysis. It decides which experiment number gives the parameters, which are close to optimum parameters. The experiment with largest of the GRG is the closest to optimized parameters.

For MRR of Expt. No.1

m= 2 (Number of performance characteristics)

$$\gamma\ (x_{o,}x_i) = \frac{1}{2}\ (0.4489 + 0.8479)$$

$$\boldsymbol{GRG = \gamma\ (x_{o,}x_i)} = \mathbf{0.6484}$$

Similarly, the calculations are done for remaining experiments and the GRG values for MRR & SR are shown in following table,

Table 5.5 GRG values

Expt. No.	GRG	Expt. No.	GRG	Expt. No.	GRG
1	0.6484	10	0.4390	19	0.7122
2	0.4513	11	0.6273	20	0.6388
3	0.6804	**12**	**0.7581**	21	0.5361
4	0.5969	13	0.5840	22	0.5516
5	0.5595	14	0.6095	23	0.7240

Expt. No.	GRG	Expt. No.	GRG	Expt. No.	GRG
6	0.5172	15	0.5230	24	0.5277
7	0.5908	16	0.5607	25	0.6747
8	0.6380	17	0.7130	26	0.6603
9	0.6541	18	0.6632	27	0.6168

Step 5: Determination of Optimum Parametric Combination

For each sequence, the GRG is calculated and is used as a response for the further analysis. The larger-the-better quality characteristic is considered for analyzing the GRG. The parametric combination associated with the highest GRG will give the optimum performance of the process.

Step 6: Prediction of GRG under optimum parameters

Using these optimal parametric combinations, the values of the quality characteristics can be predicted and verified. The estimated GRG by using the optimal level of the process parameters can be calculated as:

$$\hat{\gamma} = \gamma_m + \sum_{i=1}^{n} (\bar{\gamma} - \gamma_m) \qquad \textbf{5.6}$$

where γ_m is the total mean GRG, $\bar{\gamma}$ is the mean GRG at the optimum level, and n is the number of the controlled parameters that affect the response characteristics. The predicted GRG (optimal) is equal to the mean GRG plus the summation of the difference between the overall mean GRG and the mean GRG for each of the parameter at optimum level.

5.3 WEIGHT CALCULATION USING ENTROPY METHOD

Entropy measures the degree of disorder and randomness in the data. The subjective way of weighting the answer variable relies on the decision- maker, who must do so based on his prior experience or level of subject matter expertise. In contrast, the decision maker would have no influence on how the weights are determined in the objective technique.

The weights are determined using an objective method, and the steps are described

below.

Step 1: Following the normalization of the performance indices, project outcomes are calculated.

$$P_{ij} = \frac{X_{ij}}{\sum_{i=1}^{m} X_{ij}} \qquad \textbf{5.7}$$

For MRR of Expt. No.1

$$X_{ij} = 2.33$$

$$\sum_{i=1}^{m} X_{ij} = 85.49$$

Therefore, the eq.5.7 becomes

$$P_{ij} = \frac{2.33}{85.49}$$

$$\boldsymbol{P_{ij} = 0.0273}$$

Similarly, the calculations are done for remaining experiments and the P_{ij} values for MRR & SR are shown in following table,

Table 5.6 P_{ij} values for MRR & SR Results

Expt. No.	MRR	SR	Expt. No.	MRR	SR
1	**0.0273**	0.0307	15	0.0317	0.0373
2	0.0427	0.0569	16	0.0339	0.0357
3	0.0197	0.0292	17	0.0243	0.0288
4	0.0453	0.0386	18	0.0529	0.0404
5	0.0385	0.0374	19	0.0346	0.0299
6	0.0354	0.0393	20	0.0573	0.0568
7	0.0338	0.0340	21	0.0285	0.0356
8	0.0395	0.0335	22	0.0349	0.0365
9	0.0275	0.0306	23	0.0536	0.0366
10	0.0422	0.0595	24	0.0267	0.0356
11	0.0204	0.0306	25	0.0468	0.0346
12	0.0554	0.0363	26	0.0425	0.0334

13	0.0354	0.0348	27	0.0421	0.0355
14	0.0271	0.0320			

Step 2: Entropy measure Calculation:

$$E_j = -k \sum_{i=1}^{m} P_{ij} * \ln P_{ij} \qquad \textbf{5.8}$$

Where, $k = \frac{1}{\ln(m)}$, m= number of experiments =27

For MRR:

$\sum_{i=1}^{m} P_{ij} * \ln P_{ij} = -3.2575, \quad k = \frac{1}{\ln(27)} = 0.3034$

Therefore, eq. 5.8 becomes

$$E_j = -0.3034 * -3.2575$$

$$\boldsymbol{E_j = 0.9883}$$

For SR:

$\sum_{i=1}^{m} P_{ij} * \ln P_{ij} = -3.2752, \quad k = \frac{1}{\ln(27)} = 0.3034$

Therefore, eq. 5.8 becomes

$$E_j = -0.3034 * -3.2752$$

$$\boldsymbol{E_j = 0.9937}$$

Step 3: Objective Weight Calculation:

$$W_j = \frac{1 - E_j}{\sum_{j=1}^{n}(1 - E_j)} \qquad \textbf{5.9}$$

For MRR:

$1 - E_j = 0.0116, \quad \sum_{j=1}^{n}(1 - E_j) = 0.0178$

Therefore, eq. 5.9 becomes

$$W_j = \frac{0.0116}{0.0178}$$

$$W_j = \mathbf{0.65}$$

For SR:

$1 - E_j = 0.0062, \ \sum_{j=1}^{n}(1 - E_j) = 0.0178$

Therefore, eq. 5.9 becomes

$$W_j = \frac{0.0062}{0.0178}$$

$$W_j = \mathbf{0.35}$$

In this study, multi-response analysis based on GRA is used to achieve the highest MRR and lowest Ra from the chosen control parameters. Here, the output responses are normalized using larger the better criteria for MRR and smaller the better criteria for SR, respectively.

Table 5.7 shows the obtained relevant data, where the trial with the highest GRG value indicates the close to optimum parameter combination. According to Table 5.7, the experiment number 12 has the highest ranking. The respective output responses are SR (2.072 μm), and MRR (4.74 mm^3/min). The corresponding levels are Ton (115 Units), Toff (50 Units), IP (150 Amp.), SV (60 Volt). The experiment number 10 has the lowest ranking with corresponding output responses as SR (3.39 μm), and MRR (3.61 mm3/min).

Table 5.7 Grey relation response

Expt.No.	Normalized MRR	NormalizedRa	GRC MRR	GRC Ra	GRG	Rank
1	0.201863	0.937215	0.449	0.848	0.648	10
2	0.611801	0.083904	0.626	0.276	0.451	26
3	0	0.988014	0.394	0.967	0.680	5
4	0.680124	0.681507	0.670	0.524	0.597	16
5	0.5	0.718037	0.565	0.554	0.560	20
6	0.419255	0.658676	0.528	0.506	0.517	25
7	0.375776	0.828767	0.510	0.671	0.591	17
8	0.52795	0.847603	0.579	0.697	0.638	12
9	0.208075	0.941781	0.451	0.857	0.654	9
10	0.599379	0	0.619	0.259	0.439	27

Expt.No.	Normalized MRR	NormalizedRa	GRC MRR	GRC Ra	GRG	Rank
11	0.018634	0.94121	0.398	0.856	0.627	13
12	**0.950311**	**0.753995**	**0.929**	**0.587**	**0.758**	**1**
13	0.419255	0.803082	0.528	0.640	0.584	18
14	0.198758	0.896119	0.448	0.771	0.610	15
15	0.319876	0.722032	0.489	0.557	0.523	24
16	0.378882	0.776256	0.511	0.610	0.561	19
17	0.124224	1	0.426	1.000	0.713	3
18	0.881988	0.621005	0.846	0.480	0.663	7
19	0.397516	0.96347	0.519	0.905	0.712	4
20	1	0.089612	1.000	0.278	0.639	11
21	0.236025	0.778539	0.460	0.612	0.536	22
22	0.403727	0.748288	0.522	0.582	0.552	21
23	0.900621	0.747146	0.867	0.581	0.724	2
24	0.186335	0.777397	0.444	0.611	0.528	23
25	0.720497	0.811644	0.699	0.650	0.675	6
26	0.60559	0.848744	0.622	0.698	0.660	8
27	0.596273	0.782534	0.617	0.617	0.617	14

Response means shown in table 5.8, are used to get the ideal parametric combination for improved output responses. From the table 5.8, it is clear that, the lower levels for pulse on time (Ton) and peak current (IP), medium levels for pulse off time (Toff) and higher levels for Servo voltage (SV), can be considered as optimum levels.

Table 5.8 shows the optimum level for each parameter represented by its highest GRG. The largest value of GRG for a particular setting will give the optimized output responses.

Table 5.8 Response table for GRG means

	Level 1	Level 2	Level 3
TON	**0.67**	0.59	0.59
TOFF	0.58	**0.63**	0.59
IP	**0.62**	0.61	0.60
SV	0.54	0.62	**0.64**

The values for different levels are calculated by taking the average of the MRR values at the particular levels of parameter. The recorded optimal parameter levels are Ton1, Toff2, IP1, and SV3. For optimum settings, the relevant values are Ton 105 (MU), Toff 50 (MU), IP 70 (A), and SV 60. (V).

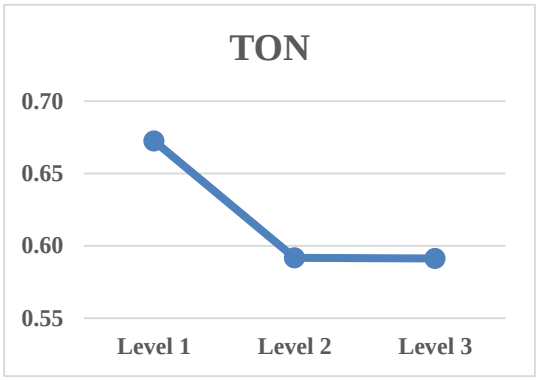

Figure 5.1 GRG plots for Ton

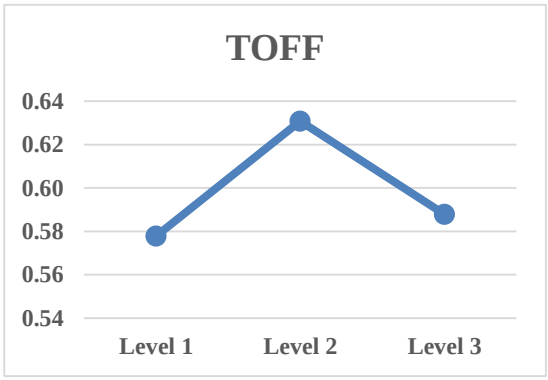

Figure 5.2 GRG plots for Toff

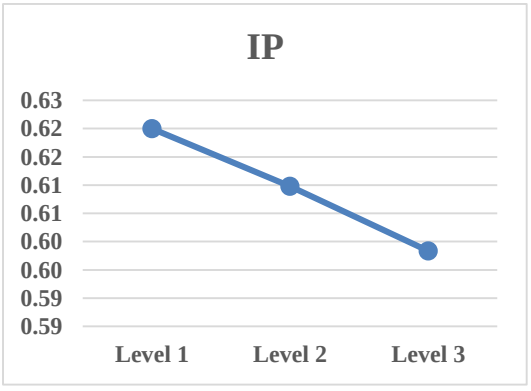

Figure 5.3 GRG plots for IP

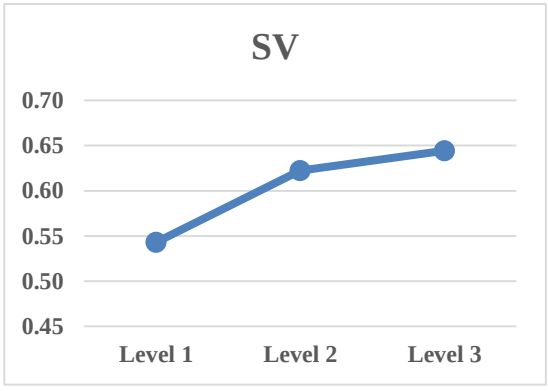

Figure 5.4 GRG plots for SV

5.4 CONFIRMATION TEST:

After selecting the most suitable machining parameters, the analysis is validated using the confirmation test. The estimated GRG is calculated as,

$$\gamma = \gamma_m + \Sigma(\gamma_n - \gamma_m) \quad \textbf{5.10}$$

where,
γ_m = Total mean grey relational grade

γ_n =The mean grey relational grade at optimum level

Table 5.9 GRG comparison with Optimized Parameters

Setting level	**Optimum process parameter combination**	
	Predicted	**Experimental**
	A1B2C1D3	A1B2C1D3
GRG	0.7372	0.6969
Deviation in Grey Relational Grade= 5.78%		

5.5 MATHEMATICAL MODEL DEVELOPMENT USING RESPONSE SURFACE METHODOLOGY

Regression analysis has been used to develop a mathematical model (Eqs. (5.11) and (5.12)) shows the model for gamma coated wire to forecast the output data based on the relationship between the input and output data.

MRR= -79.5 + 1.27 Ton + 0.219 Toff + 0.0270 IP - 0.248 SV - 0.00642 Ton*Ton - 0.00620 TOFF*TOFF - 0.000034 IP*IP - 0.000756 SV*SV + 0.00435 Ton*Toff - 0.000307 Ton*IP + 0.00433 Ton*SV + 0.000279 Toff*IP - 0.003542 Toff*SV + 0.000118 IP*SV **5.11**

$$\boldsymbol{SR} = 68.3 - 1.578\ \text{Ton} + 0.499\ \text{Toff} - 0.0594\ \text{IP} + 0.353\ \text{SV} + 0.00897\ \text{Ton}*\text{Ton} + 0.000187\ \text{Toff}*\text{Toff} + 0.000003\ \text{IP}*\text{IP} + 0.000155\ \text{SV}*\text{SV} - 0.00479\ \text{Ton}*\text{Toff} + 0.000542\ \text{Ton}*\text{IP} - 0.00331\ \text{Ton}*\text{SV} + 0.000021\ \text{Toff}*\text{IP} - 0.000133\ \text{Toff}*\text{SV} - 0.000021\ \text{IP}*\text{SV} \quad \textbf{5.12}$$

The predicted value of the RSM model shows very good agreement with the experimental results. For gamma coated wire, the deviation for MRR results from the experimental results is 6.71 % and for surface roughness this deviation is about 6.03 %.

And, for diffused wire, the deviation for MRR and SR is 13.37 & 6.54% respectively. This shows that the developed mathematical model can predict the output responses with acceptable accuracy. The following graph shows the comparison between the experimental results with predicted results by RSM.

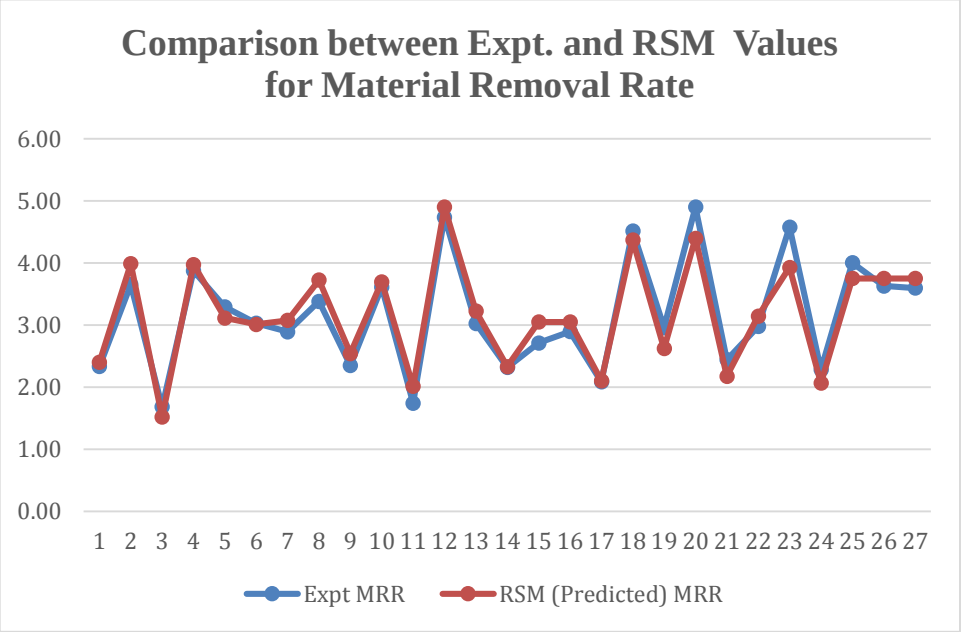

Figure 5.5 Comparison between Expt. and RSM Values for Material Removal Rate for Gamma Coated Wire

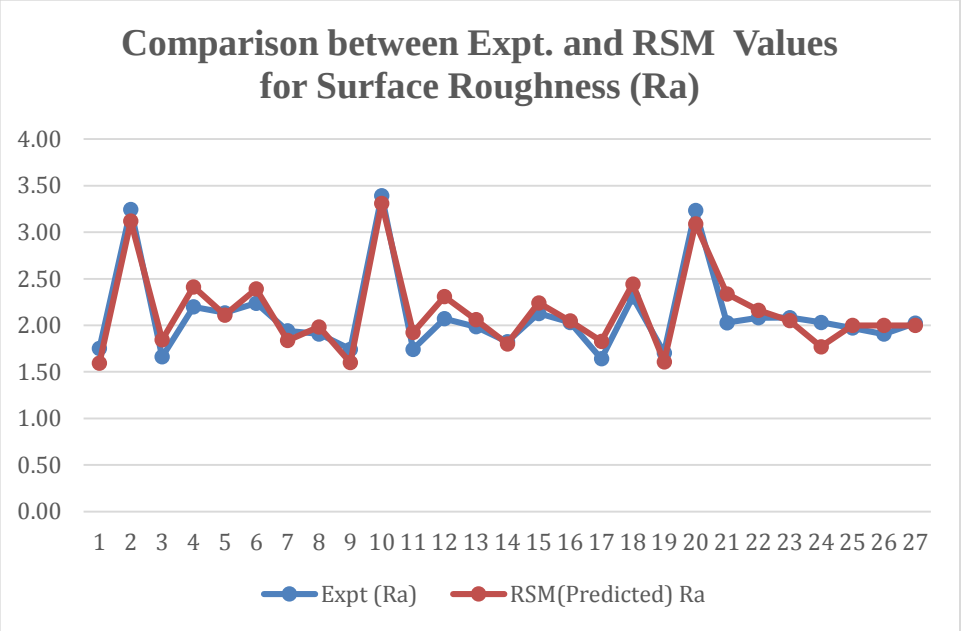

Figure 5.6 Comparison between Expt. and RSM Values for Surface Roughness (Ra) for Gamma Coated Wire

Chapter 6 FINITE ELEMENT MODELING OF TEMPERATURE DISTRIBUTION ON WORKPIECE

The following section explains the detailed procedure of finite element modeling. The results of trials experiments which were performed before the main experimentation work are considered for the comparison purpose. The developed model can be used to predict the temperature distribution profile for any parametric combination.

In present research, efforts are taken to develop a thermal model for WEDM using ANSYS software by incorporating the effect of latent heat of fusion or phase change, calculating exact value of amount of energy absorbed by the workpiece. This investigation will help to achieve more precise temperature distribution profile and material removal rate. The formulation of the thermal model in this research has integrated the aspects of Gaussian heat distribution, energy distribution factor, and latent heat of fusion to predict temperature distribution profile and the material removal rate. From the literature review, it is noticed that few researchers have addressed the WEDM process using finite element and simulation approach. Thus to study the behavior of this thermoelectric process using appropriate software and assuming proper assumptions is of prime importance.

Assumptions

1. The model is developed for single spark.
2. The workpiece material and wire material is considered homogenous, isotropic.
3. The heat transfer takes place only through conduction.
4. The workpiece geometry is axisymmetric about z- axis.
5. Gaussian heat source distribution is considered.
6. Plasma flushing efficiency is considered 100%.

6.1 TEMPERATURE MODEL

6.1.1 Governing Equation:

Heating of workpiece due to a single spark is governed by differential equation which is used by many researchers like S. Karidkar and U. Dabade [78], M. Kalajahi et al. [103], S. Joshi and S. Pande [104], H. Kansal et al. [105], S. Saha et al. [5], U. Vishwakarma et al. [106], M. Shabgard et al. [107], M. Singh et al. [70], J. Kumar et al. [108] is given as follows,

$$\rho C \frac{\partial T}{\partial r} = \frac{1}{r} * \frac{\partial}{\partial r}\left(K * \frac{\partial T}{\partial r}\right) + \frac{\partial}{\partial z}\left(K * \frac{\partial T}{\partial z}\right) \qquad \textbf{6.1}$$

6.1.2 Heat distribution:

The accuracy of model depends on selection of appropriate heat source. When plasma channel incidents on the workpiece surface, it causes temperature rise on the workpiece surface. The plasma channel distribution may be of the distributed heat source or point heat source but in actual these models are not realistic as the energy density of the spark radius varies with radius of plasma channel.

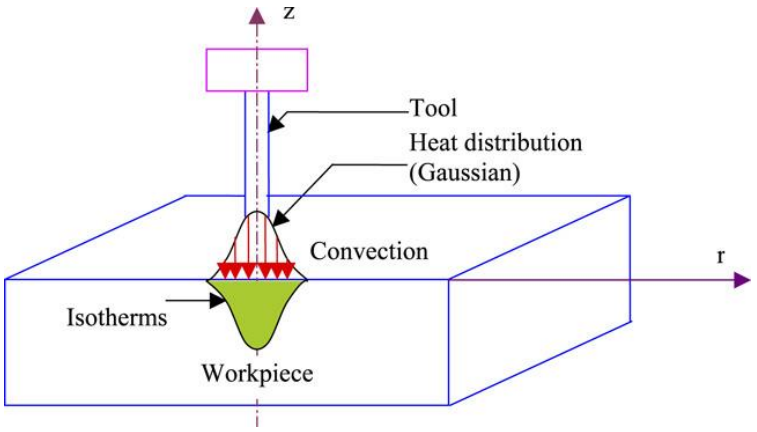

Figure 6.1 Gaussian Heat Distribution

In this work Gaussian heat distribution is considered which is more realistic and precise, also the Gaussian heat distribution is used by most of the researchers for modeling purpose. (S. Karidkar and U. Dabade [78], M. Kalajahi et al. [103], S. Joshi and S. Pande [104], U. Vishwakarma et al [106], M. Shabgard et al. [107])

6.1.3 Boundary Conditions:

Figure 6.2 shows the thermal model with boundary conditions.

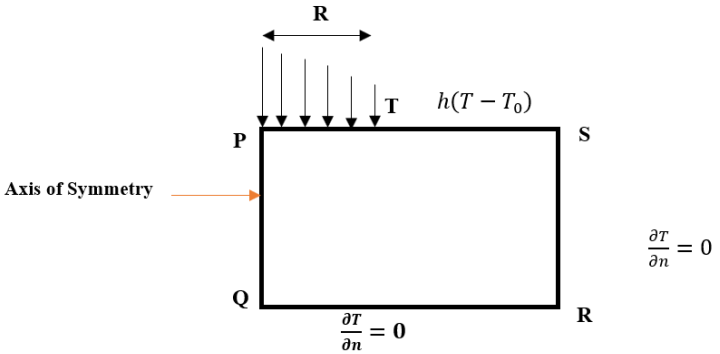

Figure 6.2 An axisymmetric thermal model

From figure 6.2 it is clear that maximum heat flux is applied at point ‘P’ and minimum heat flux is applied towards the end of plasma radius ‘R’ at point ‘T’. Therefore maximum temperature is applied at ‘P’ and minimum at point ‘T’. Area PQRS is considered for thermal analysis. On the surface PT heat is transferred due to Gaussian heat distribution and through conduction only. Beyond ‘T’ heat is transferred takes due to convection. As SR and QR are away from the applied heat flux, no heat transfer is considered. For boundary PQ, the heat transfer is zero as it is an axis of symmetry. (S. Karidkar and U. Dabade) [78]

Therefore the boundary conditions are ,

1. $K\frac{\partial T}{\partial z} = Q(r)$……..for r<R for surface PS
2. $K\frac{\partial T}{\partial z} = hc(T - T_0)$……for r≥R for surface PS
3. $\frac{\partial T}{\partial n} = 0$……at boundary RS,QR & PQ

6.1.4 Heat flux:

The spark generated in the WEDM process follows Gaussian heat distribution and the heat flux is given by M. Kalajahi et al. [103],

$$Q(r) = \frac{4.57\ F_C VI}{\pi R^2} * \ e^{-4.5\left(\frac{r^2}{R^2}\right)} \qquad \textbf{6.2}$$

Where, Fc = Energy distribution factor (%), V = Voltage (volt) , I = Current (Amp.), r = radial distance (µm), R = Spark Radius (µm)

6.1.5 Spark radius:

Spark radius (R) depends on pulse on time and current which is calculated by using the equation given by M. Shabgard et al. [107],

$$R = (2.04 * I^{0.43} * Ton^{0.44}) \qquad \textbf{6.3}$$

Where, I = Peak current (Amp), Ton= pulse on time

6.1.6 Energy distribution factor:

Large amount of heat energy is discharged once the current is supplied, out of which substantial amount of energy is absorbed by the workpiece which is partly utilized for melting and evaporation of the material and partly will be carried away by the dielectric

fluid through convection. The energy distribution factor (Fc) is percentage amount of energy absorbed by the workpiece. The researchers have suggested different values for Fc. (M. Kalajahi et al.) [103] Different materials exhibit various values of Fc as the capability of material to absorb energy is different, therefore the value of Fc cannot be generalized. For the current work, the value of 60% is considered for the analysis.

6.1.7 Phase Change:

The energy discharged during WEDM process generates sufficient amount of heat so that workpiece is melted, vaporized. Also, it generates the latent heat during martensitic transformation and solidification. The increase in heat capacity because of this latent heat change during phase change can be incorporated in the form of an equation as given by M. Kalajahi et al. [103]

$$\boldsymbol{C_{Peff.} = C_p + \frac{CH}{\Delta T}} \qquad \textbf{6.4}$$

Where,

C_{peff} = Effective specific heat capacity

CH (J/Kg) = latent heat of fusion (the amount of energy required to convert 1 Kg of solid material into liquid form)

The value for CH is considered as 283 KJ/Kg. K

$\Delta T = T_m - T_0$

T_m= Melting temperature of material (1813.15 ^{0}K)

$T_{0=}$ Dielectric temperature at the beginning of machining process (299.15 ^{0}K)

Therefore, from Eq. 6.4

$$C_{peff} = 813 + \frac{283 * 10^3}{(1813.15 - 299.15)}$$

$$C_{peff} = 1000 \frac{J}{Kg}.K$$

The table 6.1 shows the parameter levels for the trial experimentation work which were performed before the main experimentation work.

Table 6.1 Parameter levels for experimentation

Expt.No.	Parameter levels		
	Pulse on Time (Machine Unit)	**Pulse off Time (Machine Unit)**	**Peak Current (Amp)**
1	110	40	70
2	**110**	**45**	**150**
3	110	50	230
4	115	40	230
5	115	45	70
6	115	50	150
7	120	40	150
8	120	45	230
9	120	50	70

Table 6.2 Experiment values for MRR

Experiment no.	Kw (mm)	Vc (mm/min)	Mt (mm)	MRR(Exp) (mm^3/min)
1	0.273	2.86	7.5	5.85585
2	0.283	3.03	7.5	6.431175
3	0.291	2.31	7.5	5.041575
4	0.283	3.67	7.5	7.789575
5	0.286	4.09	7.5	8.77305
6	0.27	2.59	7.5	5.24475
7	0.273	2.99	7.5	6.122025
8	0.277	3.93	7.5	8.164575
9	0.276	4.2	7.5	8.694

6.2 FINITE ELEMENT MODELING PROCEDURE

The following section explains the step-by-step procedure followed to complete the finite element analysis. ANSYS 16.2 is used to perform the analysis. Sample calculations are also included for experiment no.2. The detailed steps are as follows.

6.2.1 Choice of element:

Two-dimensional quadrilateral axisymmetric model with size equal to 1mm*1mm is considered for each experiment.

6.2.2 Defining material properties:

The material properties used are as follows,

Density (ρ) $= 8100\ kg/m^3$

Specific heat(C) = 813 J/kg. k …. (Without latent heat)

Specific heat(C) = 1000 J/kg. k … (Considering latent heat)

Thermal conductivity (K) = 25.5 W/mk

6.2.3 Geometry:

In this step, an axisymmetric model of size 1mm*1mm is created and the mesh size= 1/10* plasma radius is considered.

6.2.4 Heat flux Calculation:

Heat flux on each element is computed by varying the radial distance. For node no.1, radial distance is zero, for node no. 2 it is equal 1/10* plasma radius and for node no.11 it is equal to plasma radius. As a result, the heat flux values for ten elements and for eleven nodes are obtained which covers the entire plasma radius.

6.2.5 Calculation of temperature on each node:

The temperature at each node is calculated using a formula given by S. Karidkar and U. Dabade [78] as follows:

$$T_f = T_i + \frac{Q}{\Delta z * \rho * C_p}\left[\frac{e^{-\frac{Uy^2}{4\alpha x}}}{(4\pi v \alpha x)^{0.5}}\right] \qquad \textbf{6.5}$$

Where,

T_f = Temperature at the node (^{0}K)

T_i = Initial Temperature (^{0}K)

Δz = Workpiece Thickness (µm)

ρ = Density (kg/m^3)

C_p = Specific Heat (J/Kg. K)

U = Wire feed (µm/ µs)

y = Element Size (µm)

α = Thermal Diffusivity (µm^2/ µs)

x = Spark Gap (µm)

v = Wire Speed (µm/ µs)

The temperature distribution profile is obtained by applying temperature to respective nodes on the workpiece.

6.3 DETERMINATION OF MRR USING ANSYS

The elements which are having temperature greater than or equal to melting temperature of material are selected from the temperature distribution profile obtained from ANSYS.(Refer figure 6.3) These elements are responsible for the material removal from workpiece surface.

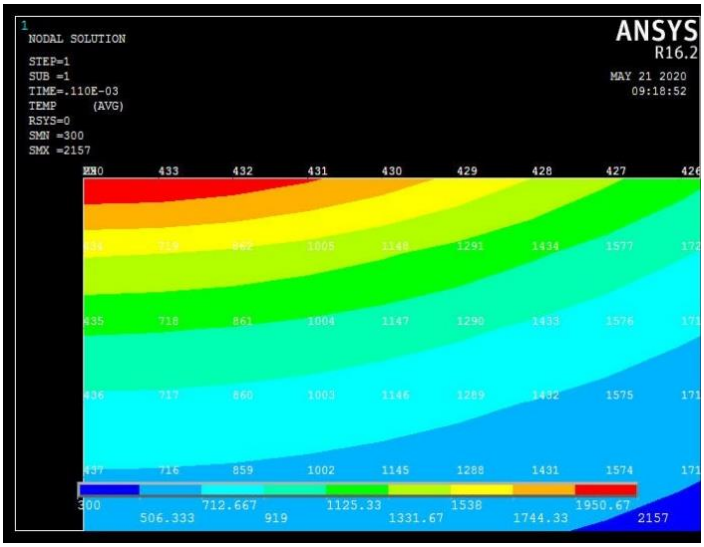

Figure 6.3 Temperature distribution profile for Ton=110 µs, Toff=45 µs and I=150A

Crater formed in single discharge are assumed to have circular parabolic geometry because the temperature distribution on the line PS & PQ are decreasing in nature and when the temperature profile is revolved about line PQ, it will produce a circular parabolic geometry and similar observations are reported by M. Shabgard et al. [107], U. Vishwakarma et al [106] S. Joshi and S. Pande [104] as shown in figure 6.4.

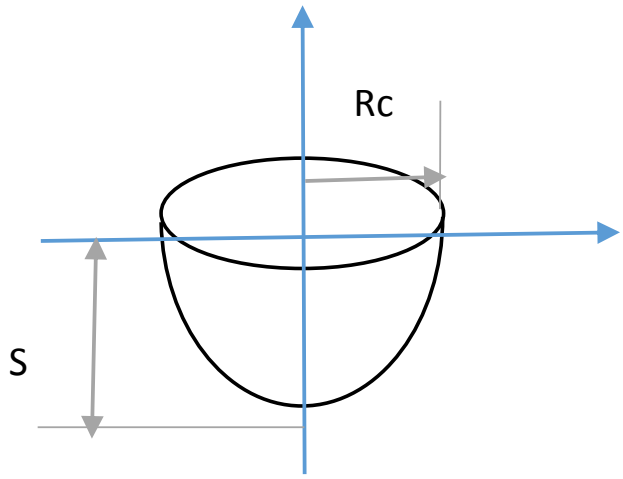

Figure 6.4 Geometry of the crater formed in single spark

Theoretical crater volume/pulse is given by,

$$Vc = \frac{1}{2} * \pi * S * Rc^2 \qquad \textbf{6.6}$$

Where,

S= depth of crater (µm), R_c= Radius of crater (µm)

Now, the total number of pulses are calculated using the equation,

$$NOP = \frac{T_{machining}}{T_{on} + T_{off}} \qquad \textbf{6.7}$$

Therefore, the theoretical MRR can be calculated as,

$$MRR = \frac{Vc * NOP}{T_{machining}} \qquad \textbf{6.8}$$

Sample Calculation of MRR for Expt. No.2:

$$Vc = \frac{1}{2} * \pi * 6 * (35)^2$$

$$\boldsymbol{Vc = 1.15\, e^{-5}\, mm^3}$$

The total number of pulses are calculated by,

$$NOP = \frac{14.41 * 60 * 10^6}{110 + 45}$$

$$\boldsymbol{NOP = 5.6e^6}$$

Finally, the MRR is calculated by,

$$MRR = \frac{1.15\, e^{-5} * 5.6e^{6}}{14.41}$$

$$\boldsymbol{MRR = 4.46\ \frac{mm^3}{min}}$$

The following tables shows the ANSYS MRR for the experiments.

Table 6.3 ANSYS MRR (Without Latent Heat)

Expt No.	S (micron)	Rc (Micron)	Vc (mm^3)	Tmachining (Min)	Ton (MU)	Toff (MU)	No. of Pulses	MRR (mm^3/min)
1	8	30	1.13E-05	14.38	110	40	5.8E+06	4.5216
2	6	35	1.154E-05	14.41	110	45	5.6E+06	4.466903226
3	5	37	1.075E-05	18	110	50	6.8E+06	4.02999375
4	6	34	1.089E-05	11.47	115	40	4.4E+06	4.215298065
5	8	31	1.207E-05	10.14	115	45	3.8E+06	4.52631
6	8	31	1.207E-05	16	115	50	5.8E+06	4.389149091
7	9	29	1.188E-05	10.4	120	50	3.7E+06	4.194116471
8	8	39	1.91E-05	9.57	120	45	3.5E+06	6.946821818
9	7	38	1.587E-05	13.49	120	50	4.8E+06	5.601021176

Table 6.4 ANSYS MRR (With Latent Heat)

Expt No.	S (micron)	Rc (Micron)	Vc(mm^3)	Tmachining (Min)	Ton (MU)	Toff (MU)	No. of Pulses	MRR (mm^3/min)
1	8	35	1.539E-05	14.38	110	40	5.8E+06	6.1544
2	6.95	41	1.834E-05	14.41	110	45	5.6E+06	7.100218645
3	8	40	2.01E-05	18	110	50	6.8E+06	7.536
4	7	42	1.939E-05	11.47	115	40	4.4E+06	7.504397419
5	7	50	2.748E-05	10.14	115	45	3.8E+06	10.303125
6	9	35	1.731E-05	16	115	50	5.8E+06	6.294272727
7	9	37	1.934E-05	10.4	120	50	3.7E+06	6.827283529
8	7	51	2.858E-05	9.57	120	45	3.5E+06	10.39454182
9	9	46	2.99E-05	13.49	120	50	4.8E+06	10.55261647

6.4 VALIDATION OF RESULTS

The investigation is conducted by considering the effect of latent heat of fusion or phase change. As anticipated, the temperature is maximum at beginning of spark radius where maximum heat flux is applied and gradually decreases as radial distance increases. (Figure 6.3)

It is also evident from the results that, considering the latent heat of fusion results in reasonable agreement between experimental MRR and ANSYS MRR. The results obtained after applying the latent heat of fusion in the model are significantly closer to the experimental MRR as shown in figure 6.5.

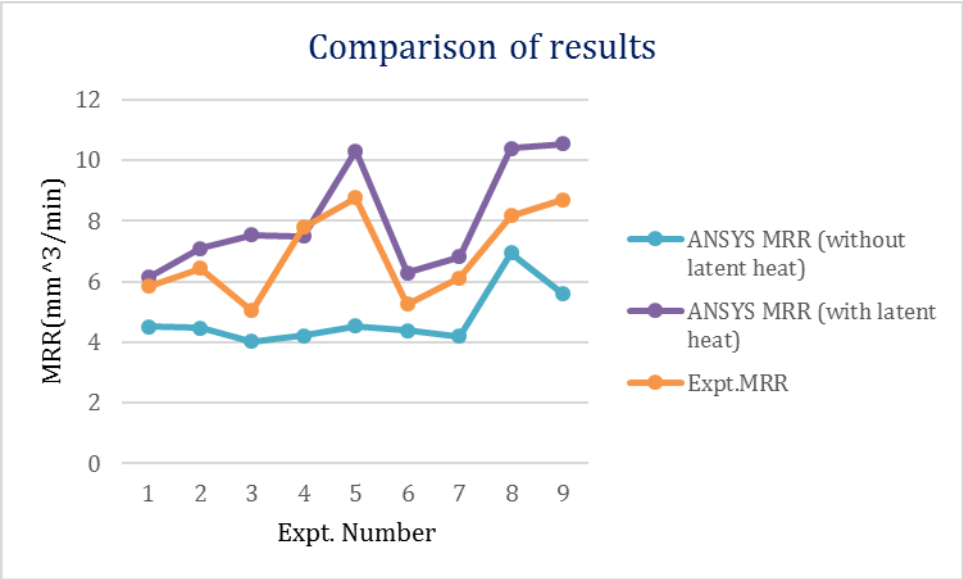

Figure 6.5 Comparison of experimental MRR with ANSYS MRR

ANSYS MRR predicted by proposed model is validated with experimental results. The ANSYS results shows good agreement with experimental results with some variation. It is seen from the results that, average % deviation from experimental MRR is about 30% without considering latent heat whereas it reduces to 18% when the effect of latent heat is considered. The variation in the results may be due to some simplified assumptions like no deposition of recast layer, 100% flushing efficiency as in actual practice the melted material is not fully flushed away but some amount of melted material again solidifies forms the recast layer. Also, calculating the exact value for energy distribution factor is a difficult task as different materials possesses different capability of energy absorption.

Chapter 7 ECONOMIC JUSTIFICATION

To understand the practical benefits of using gamma coated wires, a comprehensive economic analysis was conducted. This analysis deliberately excluded zinc-coated wire due to its high incidence of wire breakage, which renders it unsuitable for machining Nitronic-30. Instead, the focus was placed on comparing diffused wire and gamma coated wire, evaluating factors such as wire cost, machining cost, and overall operational cost. Table 7.1 provides a detailed comparison, revealing that while gamma coated wire initially appears more expensive than diffused wire, the actual cost of used wire is nearly identical for both types. This is primarily because the consumption rate of gamma coated wire is significantly lower due to its superior cutting speeds. Consequently, the efficiency of gamma coated wire translates into a notable reduction in machining time 22% less than that of diffused wire.

This reduction in machining time directly impacts the overall machining cost, leading to substantial savings. Specifically, the total operational cost is reduced by Rs. 82.04, which equates to approximately 19% cost savings. Such a significant reduction underscores the economic advantage of gamma coated wire.

The economic justification presented not only highlights the cost-effectiveness of gamma coated wire but also supports its practical applicability in industrial use. By opting for gamma coated wire, industries can achieve enhanced efficiency and substantial cost savings, making it a superior choice for machining applications.

Table 7.1 Economic Justification

Input Data	**Unit**	**Diffused Wire**	**Gamma Coated Wire**
Price	Rs. /Kg.	970	1250
Hourly Rate	Rs.	500	500
Time required to cut 100 mm length	Minutes	44.24	34.36
Used Weight of Wire	Kg.	0.068	0.053
Used Wire Cost (A)	Rs.	65.96	66.25
Machining Cost (B)	Rs.	368.66	286.33
Overall Cost (A+B)	Rs.	434.62	352.58
Savings	Rs.	82.04	
% Cost Saving using Gamma Coated Wire		**18.87%**	

Chapter 8 CONCLUSIONS AND FUTURE SCOPE

8.1 CONCLUSIONS

The current research work investigates the effects of various wire electrode materials when machining Nitronic-30 in an effort to increase the productivity of the WEDM process. The outcomes of this research would be useful for the readers, WEDM service providers / business owners to understand the benefits of using gamma coated wires as compared to other types of coated wires. It will also help them to grow their business with improved productivity and sustainability. Based on the outcomes of current research following inferences can be made.

8.1.1 Investigation on Parameters affecting the WEDM performance

- From the results of pilot experiments, it has been observed that wire feed and wire tension have no significant effect on the process.
- The results show that pulse on time is the most significant parameter affecting both material removal rate and surface roughness.
- It has been found that pulse off time, peak current and servo voltage have negligible effect on the performance characteristics.

8.1.2 Investigation on Material Removal Rate

During the study, the MRR is calculated by using machine speed, thickness of the workpiece and kerf width. Kerf width is measured by using optical microscope and the readings for machining speed are taken from the display unit of the controller. Some of the significant findings for MRR are listed below.

- It is observed that for both gamma coated wire and diffused wire Ton (p-value <0.05) is the most significant parameter influencing MRR with 59.47% & 58.18% respectively.
- For Ton, the MRR increases linearly from 105 MU to 115 MU and the slope of the curve indicates that it has considerable effect on the MRR.
- It has been found that Toff, IP & SV have negligible effect on MRR.
- Gamma coated wire shows significant improvement in MRR. The MRR obtained using gamma coated wire is 28.84% more compared to diffused wire.

8.1.3 Investigation on Surface Roughness

During this investigation, the SR measurement is done using a Mitutoyo SJ-210 portable roughness tester. From the results following conclusions can be drawn.

- It is observed that for both gamma coated wire and diffused wire Ton (p-value <0.05) is the most important parameter influencing SR with 58.18% & 59.69 % respectively.
- For Ton, the SR value increases with increase in Ton value from 105 MU to 115 MU and the slope of the curve indicates that it has significant effect on the SR.
- The results of Toff, IP, and SV are not significant.
- Diffused wire shows promising results for SR. The SR is 10.05% less compared to gamma coated wire.

8.1.4 Investigation on surface integrity

For this investigation, the Scanning Electron Microscope is used to inspect the surface integrity of the machined component. The high-resolution images are taken for the samples machined using zinc-coated wire, diffused wire and gamma coated wire.

- The quality of machined surface can attribute to material removal rate. More the material removal rate, poorer will be the surface quality.
- For gamma coated wire, the formation of large craters, globules, micro cracks are observed which leads to poor surface quality.
- For zinc-coated wire the surface quality gets slightly improved and for zinc-coated wire the surface quality is best.
- Recast layer thickness also contributes towards the surface integrity. The thickness of the recast layer is minimum for diffused wire (Approximately 12 µm). It increases for zinc-coated wire to (Approximately 16 µm) and for gamma coated wire, the thickness is the highest (Approximately 20 µm).

8.1.5 Investigation on Multi- Response Optimization

GRA is employed to perform multi-response optimization. The entropy method is employed to calculate the weight for each response characteristics. The following conclusions can be made based on the study.

- GRA is very useful technique to solve optimization problems where the machining processes deals with multiple responses.

- GRA indicates that Ton is very important parameter during WEDM of Nitronic-30
- The optimized parameters obtained from GRA are Ton 105 (MU), Toff 50 (MU), IP 70 (A), and SV 60 (V) which yields optimum responses as SR 1.51 μm, and MRR 1.18 mm^3/min.

8.1.6 Investigation on development of mathematical model

- The developed mathematical model shows very good agreement with the experimental results.
- For gamma coated wire, the deviation for MRR results from the experimental results is 6.71% and for surface roughness this deviation is about 6.03 %.
- For diffused wire, the deviation for MRR and SR is 13.37 & 6.54% respectively.

8.1.7 Investigation on Finite Element Modeling

In the investigation, finite element modeling is performed using ANSYS software to determine the temperature distribution on the workpiece. The modeling has been done by considering important aspects such as energy distribution factor, Gaussian heat distribution and latent heat of fusion. Following are some important conclusions of this study.

- It is seen from the results that, average % deviation from experimental MRR is about 30% without considering latent heat whereas % deviation reduces to 18% when the effect of latent heat is considered.
- MRR predicted by ANSYS shows very good agreement with the experimental results.

8.1.8 Investigation on electrode wire material

During the investigation three types of wire materials are used viz. zinc-coated wire, diffused wire and gamma coated wire. Based on the experimental results, following conclusions are made

- Use of zinc-coated wire is not recommended because of multiple wire breakage incidences which leads to increased energy consumption with lowered productivity.

- Gamma coated wire shows significant improvement in MRR. The MRR is 7.38% more compared to zinc-coated wire and 28.84% more compared to diffused wire.
- Diffused wire shows very good results for SR. The SR is 2.96% less compared to zinc-coated wire and 10.05% less compared to gamma coated wire.
- Percentage cost saving using gamma coated wire is 18.87 % as compared to diffused wire.
- The use of Gamma coated wire is recommended for machining Nitronic-30 on the basis of economic justification.

8.2 SUGGESTIONS FOR FUTURE WORK

Considering the excellent performance of gamma coated wire for material removal rate, there is a potential research area to explore development of gamma coated wire with varying coating thicknesses to enhance the surface quality.

References

[1] K. Natarajan, H. Ramakrishnan, A. Gacem, V. Vijayan, K. Karthiga, H. Ali, B. Prakash and A. Mekonnen, "Study on optimization of WEDM process parameters on stainless steel," *Journal of Nanomaterials,* vol. 2022, pp. 1-7, 2022.

[2] J. Wang, J. Sanchez, B. Izquierdo and I. Ayesta, "Effect of discharge accumulation on wire breakage in WEDM process," *The International Journal of Advanced Manufacturing Technology,* vol. 125, pp. 1343-1353, 2023.

[3] J. Gamage and A. Desilva, "Effect of wire breakage on the process energy utilisation of EDM," *Procedia CIRP,* vol. 42, pp. 586–590, 2016.

[4] A. Kumar, V. Kumar and J. Kumar, "Parametric effect on wire breakage frequency and surface topography in WEDM of pure titanium," *Journal of Mechanical Engineering and Technology,* vol. 1, pp. 51–56, 2013.

[5] S. Saha, M. Pachon, A. Ghoshal and M. Schulz, "Finite element modeling and optimization to prevent wire breakage in electro-discharge machining," *Mechanics Research Communications,* vol. 31, pp. 451–463, 2004.

[6] N. Tosun, C. Cogun and T. Tosun, "A study on kerf and material removal rate in wire electrical discharge machining based on Taguchi method.," *Journal of Materials Processing Technology,* vol. 152, pp. 316-322, 2004.

[7] I. Maher, A. Sarhan and M. Hamdi, "Review of improvements in wire electrode properties for longer working time and utilization in wire EDM machining," *The International Journal of Advanced Manufacturing Technology,* vol. 76, pp. 329–351, 2015.

[8] R. Rajendran and S. Vendan, "Single Discharge Finite Element Simulation of EDM Process," *Journal of Advanced Manufacturing Systems,* vol. 14, no. 2, pp. 75-89, 2015.

[9] "Injection systems," Aubert & Duval, [Online]. Available: https://www.aubertduval.com/markets/transportation/injection-systems-metals/.

[10] R. Panchal and P. Umrigar, "Evaluation on Failure Analysis of an Automobile Differential Pinion Assembly," *International Journal for Innovative Research in Science & Technology,* vol. 1, pp. 311-317, 2015.

[11] L.Alvarez, C.Luis and I.Puertas, "Analysis of the influence of chemical composition on the mechanical and metallurgical properties of engine cylinder blocks in grey cast iron," *Journal of Materials Processing Technology,* Vol. 153-154, pp. 1039-1044, 2004.

[12] A. Ktari, N.Haddar and H. Ayedi, "Fatigue fracture expertise of train engine crankshafts," *Engineering Failure Analysis,* vol. 18, pp. 1085-1093, 2011.

[13] M. Bassey, A. Ikpe and V. David, "Failure Analysis of Vehicular Camshaft Component with Variable Materials Subjected to Multi-translated Non-proportional Loading Conditions in its Duty Cycle," in *International Conference on Mathematics*, Buenos Aires, Argentina, 2023.

[14] C. Juarez, F. Rumiche, A. Rozas, J. Cuisano and P. Lean, "Failure analysis of a diesel generator connecting rod," *Case Studies in Engineering Failure Analysis*, vol. 7, pp. 24-31, 2016.

[15] "Fuel Pump Housing," Cirex, [Online]. Available: https://cirexfonderie.fr/producten/fuel-pump-housing/.

[16] R. Couturier and C. Escaravage , "High temperature alloys for the HTGR Gas Turbine: Required properties and development needs.," France, 2001.

[17] "Continental Supplies World's First Turbocharger with Aluminum Turbine Housing in Cars," Continental, 2014. [Online]. Available: https://www.continental.com/en/press/press-releases/2014-07-15-turbocharger/.

[18] S. Krawiec and Ł. Krawczyk, "Microstructural investigations of cracks in turbine wheels in car engine turbochargers," *Solid State Phenomena*, vol. 231, pp. 133-138, 2015.

[19] "Nitronic-30," AK Steel, Ohio.

[20] "High Temperature Characteristics of Stainless Steel," American Iron and Steel Institue.

[21] "An Introduction to Grey Iron," AZOM Materials, 2001. [Online]. Available: https://www.azom.com/properties.aspx?ArticleID=783.

[22] "AISI 4130 Alloy Steel (UNS G41300)," AZO Materials, 2012. [Online]. Available: https://www.azom.com/article.aspx?ArticleID=6742.

[23] "AISI 4340 Alloy Steel (UNS G43400)," AZO materials, 2012. [Online]. Available: https://www.azom.com/article.aspx?ArticleID=6772.

[24] "Engineering Properties of ALLOY 713C".

[25] A. Yadav, "A parametric optimization & experimental analysis of Wire-EDM on Hastelloy-C22 by Taguchi method," in *3rd International Conference on Recent Development in Engineering Sciences, Humanities and Management. 2017*, 2017.

[26] D. Mahto and N. Singh, "Experimental study of process parameters through dissimilar form of electrodes in EDM machining," *SSRN Electronic Journal*, vol. 1, pp. 1-31, 2017.

[27] A. Kumar, V. Kumar and J. Kumar, "Experimental investigation on material transfer mechanism in WEDM of pure titanium (Grade-2)," *Advances in Materials Science and Engineering*, vol. 2013, pp. 1-20, 2013.

[28] G. Lakshmikanth, N. Murali, G. Arunkumar and S. Santhanakrishnan, "Investigation on optimization of machining parameters in wire EDM using

Taguchi technique," *International Journal for Scientific Research and Development, 1 (9),* vol. 1, pp. 1772–1774, 2013.

[29] S. Kumar, S. Dhanabalan and C. Narayanan, "Application of ANFIS and GRA for multi-objective optimization of optimal wire-EDM parameters while machining Ti–6Al–4V alloy," *SN Applied Sciences,* vol. 1, pp. 1–12, 2019.

[30] U. Dabade and S. Karidkar, "Analysis of response variables in WEDM of Inconel 718 using Taguchi technique," *Procedia CIRP,* vol. 41, pp. 886–891, 2016.

[31] A. Goyal, "Investigation of material removal rate and surface roughness during wire electrical discharge machining (WEDM) of Inconel 625 super alloy by cryogenic treated tool electrode," *Journal of King Saud University-Science,* vol. 29, pp. 528–535, 2017.

[32] D. Kashid and S. Bhatwadekar, "Effect of Process Parameters on Material Removal Rate of WEDM for AISI D7 Tool Steel.," *International Journal of Mechanical and ProductionEngineering Research and Development,* vol. 4, pp. 99-106, 2014.

[33] R. Chalisgaonkar and J. Kumar, "Multi-response optimization and modeling of trim cut WEDM operation of commercially pure titanium (CPTi) considering multiple user's preferences," *Engineering Science and Technology, an International Journal,* vol. 18, pp. 125–134, 2015.

[34] B. Lodhi and S. Agarwal, "Optimization of machining parameters in WEDM of AISI D3 Steel using Taguchi Technique," *Procedia CIRP,* vol. 14, pp. 194–199, 2014.

[35] F. Kausar, S. Kumar, M. Azam, S. Suman, A. Sharma and A. Sethi, "Optimization of machining parameter for surface roughness on WEDM of En36 alloy steel," *Journal of Mechanical and Civil Engineering,* Vol. 12, pp. 101–104, 2015.

[36] J. Saedon, N. Jaafar, M. Yahaya, N. Saad and M. Kasim, "Multi-objective optimization of titanium alloy through orthogonal array and grey relational analysis in WEDM," *Procedia Technology,* vol. 15, pp. 832–840, 2014.

[37] S. Sherdual and S. Dahake, "Parametric optimization on graphite plate by WEDM," *International Research Journal of Engineering and Technology,* vol. 2, pp. 2473–2479, 2015.

[38] K. Mandal, D. Bose, S. Mitra and S. Sarkar, "Experimental investigation of process parameters in WEDM of Al 7075 alloy," *Manufacturing Review,* vol. 7, pp. 1-9, 2020.

[39] T. Chaudhary, A. Siddiquee and A. Chanda, "Effect of wire tension on different output responses during wire electric discharge machining on AISI 304 stainless steel," *Defence Technology,* vol. 15, pp. 541–544, 2019.

[40] K. Ishfaq, S. Anwar, M. Ali, M. Raza, M. Farooq, S. Ahmad, C. Pruncu, M. Saleh and B. Salah, "Optimization of WEDM for precise machining of novel

developed Al6061-7.5% SiC squeeze-casted composite," *The International Journal of Advanced Manufacturing Technology,* vol. 111, pp. 2031–2049, 2020.

[41] T. Muthuramalingam, R. Annamalai, K. Moiduddin and others, "Enhancing the surface quality of micro titanium alloy specimen in WEDM process by adopting TGRA-Based optimization," *Materials,* vol. 13, pp. 1-13, 2020.

[42] K. Ishfaq, S. Zahoor, S. A. Khan, M. Rehman, A. Alfaify and S. Anwar, "Minimizing the corner errors (top and bottom) at optimized cutting rate and surface finish during WEDM of Al6061," *Engineering Science and Technology, an International Journal,* vol. 24, pp. 1027–1041, 2021.

[43] N. Tosun and C. Cogun, "An investigation on wire wear in WEDM.," *Journal of Materials Processing Technology,* vol. 134, pp. 273-278, 2003.

[44] W. Dekeyser, R. Snoeys and M. Jennes, "A thermal model to investigate the wire rupture phenomenon for improving performance in EDM wire cutting," *Journal of Manufacturing Systems,* vol. 4, pp. 179–190, 1985.

[45] A. Pramanik and A. Basak, "Sustainability in wire electrical discharge machining of titanium alloy: understanding wire rupture," *Journal of Cleaner Production,* vol. 198, pp. 472–479, 2018.

[46] B. Ranganath, K. Sudhakar and A. Srikantappa, "Wire failure analysis in wire-EDM process," in *International Conference on Mechanical Engineering,* 2003.

[47] M. Selvam and P. Kumar, "Optimization Kerf width and surface roughness in wire cut electrical discharge machining using brass wire," *Mechanics and Mechanical Engineering,* vol. 21, pp. 37–55, 2017.

[48] R. Bobbili, V. Madhu and A. Gogia, "Modelling and analysis of material removal rate and surface roughness in wire-cut EDM of armour materials," *Engineering Science and Technology, an International Journal,* vol. 18, pp. 664–668, 2015.

[49] S. Shahane and S. Pande, "Development of a Thermo-Physical Model for Multi-spark Wire EDM Process," *Procedia Manufacturing,* vol. 5, pp. 205-219, 2016.

[50] T. Ebisu, A. Kawata, Y. Okamoto, A. Okada and H. Kurihara, "Influence of jet flushing on corner shape accuracy in wire EDM," *Procedia CIRP,* vol. 68, pp. 104–108, 2018.

[51] D. Sudhakara and G. Prasanthi, "Application of Taguchi method for determining optimum surface roughness in wire electric discharge machining of P/M cold worked tool steel (Vanadis-4E)," *Procedia Engineering,* vol. 97, pp. 1565–1576, 2014.

[52] K. Zakaria, Z. Ismail, N. Redzuan and K. Dalgarno, "Effect of wire EDM cutting parameters for evaluating of Additive Manufacturing Hybrid Metal Material," *Procedia Manufacturing,* vol. 2, pp. 532–537, 2015.

[53] J. Saliya, "Comparative Study for the effect of Powder mixed dielectric on Performance of Wire EDM," *International Journal of Engineering Development and Research,* vol. 2, pp. 3671–3673, 2014.

[54] A. Goswami and J. Kumar, "Investigation of surface integrity, material removal rate and wire wear ratio for WEDM of Nimonic 80A alloy using GRA and Taguchi method," *Engineering Science and Technology, an International Journal,* vol. 17, pp. 173–184, 2014.

[55] N. Sharma, R. Khanna and R. Gupta, "Multi quality characteristics of WEDM process parameters with RSM," *Procedia Engineering,* vol. 64, pp. 710–719, 2013.

[56] N. Sharma, R. Khanna and R. D. Gupta, "WEDM process variables investigation for HSLA by response surface methodology and genetic algorithm," *Engineering Science and Technology, an International Journal,* vol. 18, pp. 171–177, 2015.

[57] A. Conde, J. Sanchez, S. Plaza and J. Ramos, "On the influence of wire-lag on the WEDM of low-radius free-form geometries," *Procedia CIRP,* vol. 42, pp. 274–279, 2016.

[58] N. Sharma, A. Singh, R. Sharma and others, "Modelling the WEDM process parameters for cryogenic treated D-2 tool steel by integrated RSM and GA," *Procedia Engineering,* vol. 97, pp. 1609–1617, 2014.

[59] J. Liu, L. Li and Y. Guo, "Surface integrity evolution from main cut to finish trim cut in W-EDM of shape memory alloy," *Procedia CIRP,* vol. 13, pp. 137–142, 2014.

[60] M. Galindo-Fernandez, C. Diver and W. Leahy, "The prediction of surface finish and cutting speed for wire electro-discharge machining of Polycrystalline Diamond," *Procedia CIRP,* vol. 42, pp. 297–304, 2016.

[61] Y. Zhu, T. Liang, L. Gu and W. Zhao, "Machining of micro rotational parts with wire EDM machine," *Procedia Manufacturing,* vol. 5, pp. 849–856, 2016.

[62] Z. Chen, J. Moverare, R. Peng and S. Johansson, "Surface integrity and fatigue performance of Inconel 718 in wire electrical discharge machining," *Procedia CIRP,* vol. 45, pp. 307–310, 2016.

[63] P. Singh, A. Chaudhary, T. Singh and A. Rana, "Experimental investigation of wire EDM to optimize dimensional deviation of EN8 steel through Taguchi's technique," *International Research Journal of Engineering and Technology (IRJET),* vol. 2, pp. 1753–1757, 2015.

[64] K. Mohapatra, V. Shaibu and S. Sahoo, "Modeling and analysis of Wire EDM in a Gear Cutting process for a 2D Model," *Materials Today: Proceedings,* vol. 5, pp. 4793–4802, 2018.

[65] F. Vogeler, A. Migdal, B. Lauwers and E. Ferraris, "The effect of wire-edm processing on the flexural strength of large scale ZrO2-TiN," *Procedia CIRP,* vol. 45, pp. 179–182, 2016.

[66] O. Guven, U. Esme, I. Kaya, Y. Kazancoglu, M. Kulekci and C. Boga, "Comparative modeling of wire electrical discharge machining (Wedm) process using Back propagation (BPN) and general regression neural networks (GRNN)," *Materials and Technology*, vol. 44, pp. 147–152, 2010.

[67] R. Ramakrishnan and L. Karunamoorthy, "Modeling and multi-response optimization of Inconel 718 on machining of CNC WEDM process," *Journal of Materials Processing Technology*, vol. 207, pp. 343–349, 2008.

[68] M. Sadeghi, H. Razavi, A. Esmaeilzadeh and F. Kolahan, "Optimization of cutting conditions in WEDM process using regression modelling and Tabu-search algorithm," *Proceedings of the Institution of Mechanical Engineers, Part B: Journal of Engineering Manufacture*, vol. 225, pp. 1825–1834, 2011.

[69] K. Manikandan, K. Palanikumar and others, "Machinability evaluation and comparison of Incoloy 825, Inconel 603 XL, Monel K400 and Inconel 600 super alloys in wire electrical discharge machining," *Journal of Materials Research and Technology*, vol. 9, pp. 12260–12272, 2020.

[70] M Singh, K Das and D Sarma , "Thermal simulation of machining of alumina with wire electrical discharge," *Journal of Mechanical Science and Technology*, vol. 32, pp. 333-343, 2018.

[71] H. Majumder and K. Maity, "Prediction and optimization of surface roughness and micro-hardness using grnn and MOORA-fuzzy-a MCDM approach for nitinol in WEDM," *Measurement*, vol. 118, pp. 1–13, 2018.

[72] T. Sibalija, S. Kumar, G. Patel and Jagadish, "A soft computing-based study on WEDM optimization in processing Inconel 625," *Neural Computing and Applications*, vol. 33, pp. 11985–12006, 2021.

[73] V. Sharma, N. Sharma, G. Singh, M. Gupta and G. Singh, "Optimization of WEDM Parameters While Machining Biomedical Materials Using EDAS-PSO," *Materials*, vol. 16, pp. 114, 2023.

[74] S. Wang, J. Wu, H. Gunawan and R.Tu, "Optimization of Machining Parameters for Corner Accuracy Improvement for WEDM Processing," *Applied Sciences*, vol. 12, pp. 10324, 2022.

[75] R. Ravi, S. Rachit and A. Mandal, "Analysis of Wire Wear in WEDM," *Indian Journal of Science and Technology*, vol. 9, pp. 1-6, 2016.

[76] S. Jarin, T. Saleh, M. Rana, A. Muthalif and M. Ali, "An experimental investigation on the effect of nanopowder for micro-wire electro discharge machining of gold coated silicon," *Procedia engineering*, vol. 184, pp. 171–177, 2017.

[77] C. Cao, X. Zhang, X. Zha and C. Dong, "Surface integrity of tool steels multi-cut by wire electrical discharge machining," *Procedia Engineering*, vol. 81, pp. 1945–1951, 2014.

[78] S. Karidkar and U. Dabade, "Finite Element Modeling and Simulation of Inconel 718 Using WEDM," in *ASME International Mechanical Engineering Congress and Exposition*, Arizona, 2016.

[79] M. Priyadarshini, C. Biswas and A. Behera, "Machining of sub-cooled low carbon tool steel by wire-EDM," *Materials and Manufacturing Processes,* vol. 34, pp. 1316–1325, 2019.

[80] A. Mori, M. Kunieda and K. Abe, "Clarification of gap phenomena in wire EDM using transparent electrodes," *Procedia CIRP,* vol. 42, pp. 601–605, 2016.

[81] P. Rao, K. Ramji and B. Satyanarayana, "Effect of wire EDM conditions on generation of residual stresses in machining of aluminum 2014 T6 alloy," *Alexandria Engineering Journal,* vol. 55, pp. 1077–1084, 2016.

[82] A. Takale and N. Chougule, "Effect of wire electro discharge machining process parameters on surface integrity of Ti49. 4Ni50. 6 shape memory alloy for orthopedic implant application," *Materials Science and Engineering: C,* vol. 97, pp. 264–274, 2019.

[83] P. Reddy, C. Kumar and K. Reddy, "Modeling of wire EDM process using back propagation (BPN) and General Regression Neural Networks (GRNN)," in *Frontiers in Automobile and Mechanical Engineering-2010*, 2010.

[84] R. Abdallah, S. Soo and R. Hood, "The influence of cut direction and process parameters in wire electrical discharge machining of carbon fibre–reinforced plastic composites," *The International Journal of Advanced Manufacturing Technology,* vol. 113, pp. 1699–1716, 2021.

[85] L. Prasad, M. Upreti, A. Yadav, R. Patel, V. Kumar and A. Kumar, "Optimization of process parameters during WEDM of EN-42 spring steel," *SN Applied Sciences,* vol. 2, pp. 1–11, 2020.

[86] V. Aggarwal, C. I. Pruncu, J. Singh, S. Sharma and D. Pimenov, "Empirical investigations during WEDM of Ni-27Cu-3.15 Al-2Fe-1.5 Mn based superalloy for high temperature corrosion resistance applications," *Materials,* vol. 13, pp. 1-6, 2020.

[87] C. He, "Dynamic distribution of discharge products influenced by composition of dielectric in WEDM narrow slit were observed and exploration of its mechanism," *Procedia CIRP,* vol. 42, pp. 591–595, 2016.

[88] C. Naresh, P. Bose and C. Rao, "Artificial neural networks and adaptive neuro-fuzzy models for predicting WEDM machining responses of Nitinol alloy: Comparative study," *SN Applied Sciences,* vol. 2, pp. 1–23, 2020.

[89] R. Chaudhari, J. Vora, V. Patel, L. Lacalle and D. Parikh, "Effect of WEDM process parameters on surface morphology of nitinol shape memory alloy," *Materials,* vol. 13, pp. 4943, 2020.

[90] T. Kamei, A. Okada and Y. Okamoto, "High-speed observation of thin wire movement in fine wire EDM," *Procedia CIRP,* vol. 42, pp. 596–600, 2016.

[91] M. Hewidy, T. El-Taweel and M. El-Safty, "Modelling the machining parameters of wire electrical discharge machining of Inconel 601 using RSM," *Journal of Materials Processing Technology,* vol. 169, pp. 328–336, 2005.

[92] S. Datta and S. Mahapatra, "Modeling, simulation and parametric optimization of wire EDM process using response surface methodology coupled with grey-Taguchi technique," *International Journal of Engineering, Science and Technology,* vol. 2, pp. 162–183, 2010.

[93] J. Oberholzer, G. Oosthuizen and P. Wet, "Optimal machine parameters to maximize the accuracy of producing aluminum dovetails using WEDM," *Procedia Manufacturing,* vol. 7, pp. 472–477, 2017.

[94] K. Raju, M. Balakrishnan, D. Prasad, V. Nagalakshmi, P. Patil, S. Kaliappan, B. Arulmurugan, K. Radhakrishnan, B. Velusamy, P. Paramasivam and others, "Optimization of WEDM Process Parameters in Al2024-Li-Si3N4 MMC," *Journal of Nanomaterials,* vol. 2022, pp. 1-12, 2022.

[95] V. Shukla, R. Kumar and B. Singh, "Evaluation of machining performance and multi criteria optimization of novel metal-Nimonic 80A using EDM," *SN Applied Sciences,* vol. 3, pp. 1–10, 2021.

[96] R. Soundararajan, A. Ramesh, N. Mohanraj and N. Parthasarathi, "An investigation of material removal rate and surface roughness of squeeze casted A413 alloy on WEDM by multi response optimization using RSM," *Journal Of Alloys And Compounds,* vol. 685, pp. 533–545, 2016.

[97] Y. Kuo and T. Yang, "The use of gray relational analysis in solving multi attribute decision making problems," *Engineering Optimization,* vol. 40, pp. 517-528, 2008.

[98] V. Kavimani, K. Prakash and T. Thankachan, "Multi-objective optimization in WEDM process of graphene–SiC-magnesium composite through hybrid techniques," *Measurement,* vol. 145, pp. 335–349, 2019.

[99] A. Raj, J. Misra, D. Khanduja, K. Saxena and V. Malik, "Design, modeling and parametric optimization of WEDM of Inconel 690 using RSM-GRA approach," *International Journal on Interactive Design and Manufacturing,* vol. 18, pp. 2107-2117, 224.

[100] A. Goyal, H. Rahman and S. Ghani, "Experimental investigation & optimisation of wire electrical discharge machining process parameters for Ni49Ti51 shape memory alloy," *Journal of King Saud University-Engineering Sciences,* vol. 33, pp. 129–135, 2021.

[101] S. Singh Nain, R. Sai, P. Sihag, S. Vambol and V. Vambol, "Use of machine learning algorithm for the better prediction of SR peculiarities of WEDM of Nimonic-90 superalloy," *Archives of Materials Science and Engineering,* vol. 95, pp. 12-19, 2019.

[102] P. Sharma, D. Chakradhar and S. Narendranath, "Effect of wire diameter on surface integrity of wire electrical discharge machined Inconel 706 for gas

turbine application," *Journal of Manufacturing Processes,* vol. 24, pp. 170-178, 2016.

[103] M. Kalajahi, S. Ahmadi and S. Oliaei, "Experimental and finite element analysis of EDM process and investigation of material removal rate by response surface methodology," *The International Journal of Advanced Manufacturing Technology,* vol. 69, pp. 687–704, 2013.

[104] S. Joshi and S. Pande, "Thermo-physical modeling of die-sinking EDM process," *Journal of Manufacturing Processes,* vol. 12, pp. 45–56, 2010.

[105] H. Kansal, S. Singh and P. Kumar, "Numerical simulation of powder mixed electric discharge machining (PMEDM) using finite element method," *Mathematical and Computer Modelling,* vol. 47, pp. 1217–1237, 2008.

[106] U. Vishwakarma, A. Dvivedi and P. Kumar, "FEA modeling of material removal rate in electrical discharge machining of Al6063/SiC composites," *International Journal of Mechanical and Aerospace Engineering,* vol. 6, pp. 398–403, 2012.

[107] M. Shabgard, M. Seyedzavvar, S. Oliaei and A. Ivanov, "A numerical method for predicting depth of heat affected zone in EDM process for AISI H13 tool steel," *Journal of Scientific & Industrial Research,* vol. 70, pp. 493-499, 2011.

[108] J. Kumar, S. Das and S. Joshi, "Three-Dimensional Numerical Modelling of Temperature Profiles on theWire Electrode During Wire Electric Discharge Machining Process," in *International Conference on Recent Innovations and Developments in Mechanical Engineering,* Meghalaya, 2020.

LIST OF PUBLICATIONS

1. Nilesh T. Mohite, Geetanjali V.Patil, Anupama N. Kallol, **"The use of entropy-based GRA approach to analyze and optimize the wire electrical discharge machining process for Nitronic-30"**, Materials Today: Proceedings, Elseveir, Volume No. 49, Page No. 1426-1430, 2022.
   DOI: https://doi.org/10.1016/j.matpr.2021.07.133

2. Nilesh T. Mohite, Geetanjali V. Patil, Anupama N. Kallol **"Performance enhancement in WEDM of nitronic-30 using latent heat energy"**, Sadhana, Springer, Volume No. 4, Issue No.2, Article No.75, 2022.
   DOI: https://doi.org/10.1007/s12046-022-01852-z

3. Nilesh T. Mohite, Geetanjali V. Patil, **" Comparative Analysis of WEDM Performance of Nitronic-30 Using Different Wire Electrode Materials"**, International Journal of Machining and Machinability, Volume No.25, Issue No.3/4, Page No.375-407, 2023.
   DOI: 10.1504/IJMMM.2023.10060601